

Masterarbeit

Magnetic Human Hand Motion Reconstruction

Daniel Müller

07.03.2016

Albert-Ludwigs-Universität Freiburg im Breisgau
Technische Fakultät
Embedded Systems Engineering

Eingereichte Masterarbeit gemäß den Bestimmungen der Prüfungsordnung der Albert-Ludwigs-Universität Freiburg für den Studiengang Master of Science (M. Sc.) Embedded Systems Engineering vom 3. 6. 2014.

Bearbeitungszeitraum

07. 09. 2015 – 07. 03. 2016

Gutachter

Prof. Dr. Kristof Van Laerhoven

Prof. Dr. Christoph Scholl

Betreuer

Prof. Dr. Kristof Van Laerhoven

Dipl. Inf. Philipp M. Scholl

Erklärung

Hiermit erkläre ich, dass ich diese Abschlussarbeit selbständig verfasst habe, keine anderen als die angegebenen Quellen/Hilfsmittel verwendet habe und alle Stellen, die wörtlich oder sinngemäß aus veröffentlichten Schriften entnommen wurden, als solche kenntlich gemacht habe. Darüber hinaus erkläre ich, dass diese Abschlussarbeit nicht, auch nicht auszugsweise, bereits für eine andere Prüfung angefertigt wurde.

Ort, Datum

Daniel Müller

Abstract

The tracking and reconstruction of human hand motion can be used for modern human-machine interaction or as support for medical rehabilitation. State of the art motion tracking systems adopted for this purpose introduce often bulky constructions. The underlying work presents an approach for the reconstruction of human hand motion by measuring the magnetic field, induced by permanent magnets on the fingertips. When the fingers move, the cumulative sum of the magnetic flux density, excited by the magnets, is recorded with a sensor array, consisting of four measurement units. This data is used to estimate the finger poses, based on a kinematic hand model.

The magnetic sensors are placed inside a bracket to be worn on the back of the hand. The recorded data is transferred via Bluetooth Low Energy to a host PC, where the actual state estimation is executed. The finger postures are estimated, by solving an optimization problem. The underlying human hand model is represented as a kinematic chain and uses the joint angles to describe finger postures. The thumb is neglected, for simplicity reasons.

The performance of the developed system is highly dependent on several parameters. The most critical factor is the exact determination of the anatomic hand dimensions and the positions of the sensors. Those parameters have a nonlinear contribution to the model equations and build the base for the state estimation. However, they can only be measured by hand with a calliper, which is very error-prone. Furthermore, the dynamic elimination of the surrounding earth magnetic field is not possible. Therefore, the system is only usable in static hand positions. To overcome those nonlinear and highly critical distortion factors, a scaling of the sensor values to the model parameters is adopted. The scaling factors are determined by a predefined fitting gesture.

Several datasets were recorded with the magnetic system and the estimated states were compared to data provided by a commercially available vision based approach. The individual motions of multiple fingers cannot be tracked by the developed system. However, equipping a single finger with a magnet and estimating its pose can be done almost reliable and leads to reasonable results. The smallest predicted difference for this case to the vision system is $0.467\text{rad} \pm 0.027$ ($=26.757^\circ \pm 1.547$).

Zusammenfassung

Die Beobachtung und Rekonstruktion von Bewegungen der menschlichen Hand kann für Mensch-Computer-Interaktionen oder für die Unterstützung medizinischer Therapien eingesetzt werden. Moderne Systeme zur Bewegungsverfolgung, die für diesen Zweck angepasst sind, bringen oft sperrige Geräte mit sich. Die vorliegende Arbeit präsentiert einen Ansatz zur Rekonstruktion von Handbewegungen, indem das Magnetfeld gemessen wird, welches von Permanentmagneten, die sich auf den Fingerspitzen befinden, erzeugt wird. Wenn sich die Finger bewegen, ändert sich die von den Magneten hervorgerufene magnetische Flussdichte, was von dem aus vier Sensoren bestehenden Sensorarray gemessen werden kann. Diese Daten werden benutzt, um die Fingerpositionen auf der Basis eines kinematischen Handmodels zu schätzen.

Die Magnetsensoren werden in einem Gestell platziert, welches am Handrücken getragen werden kann. Die Sensordaten werden über Bluetooth Low Energy zu einem PC gesendet, auf dem die eigentliche Zustandsschätzung durchgeführt wird. Die Fingerpositionen werden durch die Lösung eines Optimierungsproblems vorausgesagt. Das zugrunde liegende Modell zur Darstellung der menschlichen Hand beschreibt die Fingerpositionen durch die Angabe der Gelenkwinkel. Der Daumen wird zur Vereinfachung nicht beachtet.

Die Qualität des entwickelten Systems hängt von mehreren Faktoren ab. Der kritischste ist hierbei die exakte Bestimmung der anatomischen Gegebenheiten und der Sensorpositionen. Diese Parameter haben einen nichtlinearen Einfluss auf die Modellgleichungen, welche die Grundlage für die Zustandsschätzung bilden. Diese Werte können jedoch nur per Hand mit einem Messschieber gemessen werden, woraus Messfehler resultieren können. Weiterhin ist die dynamische Eliminierung des Erdmagnetfeldes nicht möglich. Deshalb ist das System nur benutzbar, wenn auch die Hand ruhig gehalten wird. Um diese nichtlinearen und höchst kritischen Einflussfaktoren zu umgehen, werden die Sensorwerte an die Modellgleichungen angepasst. Diese Skalierungsfaktoren werden über eine vorbestimmte Initialisierungsgeste bestimmt.

Mehrere Datensets wurden mit dem magnetischen System aufgenommen. Die Resultate der Zustandsschätzung wurden mit einem bestehenden kamerabasierten System verglichen. Einzelne Bewegungen von mehreren Fingern können mit dem entwickelten System nicht nachverfolgt werden. Jedoch ist die Schätzung eines einzelnen Fingers relativ zuverlässig und führt zu nachvollziehbaren Ergebnissen. Für diesen Fall beträgt der kleinste beobachtete Unterschied zum Kamerasytem $0.467\text{rad} \pm 0.027$ ($=26.757^\circ \pm 1.547$).

Contents

Abstract	5
List of Figures	iii
1 Introduction	1
2 Related Work	3
2.1 Approaches for Hand Motion Reconstruction	3
2.1.1 Camera Based	3
2.1.2 IMU based	9
2.1.3 Flexion based	10
2.1.4 Magnetic based	12
2.1.5 Other approaches	13
2.2 Fields for Applications	16
2.2.1 Human Computer Interface (HCI)	16
2.2.2 Therapeutic	17
2.2.3 Activity and Gesture tracking	18
3 Foundations	21
3.1 Anatomy of the Human Hand	21
3.2 Magnetic	23
4 System Design and Implementation	29
4.1 System Design	29
4.2 Human Hand Model	31
4.3 Sensor Design and Data Acquisition	34
4.4 Calibration and Preprocessing of Sensor Data	35
4.4.1 Calibration for Hard and Soft-Iron Coefficients	35
4.4.2 Cancellation of the Surrounding Earth Magnetic Field	37
4.5 Magnetic Field Interpretation Towards Finger Pose Reconstruction	38
4.6 Hand State Estimation	39
4.7 Visualization	41
5 Results	43
5.1 Sensor Behaviour	43
5.2 Quality of Calibration Procedures	45
5.2.1 Calibration for Hard and Soft-Iron Effects	45

5.2.2	Elimination of Earth Magnetic Field	48
5.3	Evaluation of the Magnetic Field Models	50
5.4	Evaluation of the Human Hand Model	52
5.5	Expectable Magnetic Flux Densities	54
5.6	Pose Estimation	57
5.6.1	Identification of the Minimization Process	57
5.6.1.1	Utilized Minimization Methods	57
5.6.1.2	Classifying the Methods with Simulated Data	58
5.6.2	Results for Recorded Datasets	69
5.6.2.1	Recording Procedure	69
5.6.2.2	Evaluation, Discussion and Comparison to Leap Motion and Video Data	70
5.6.2.3	Influence of Different System Parameters	83
5.6.2.4	Concluding Observations	86
6	Conclusion and Future Work	87
Bibliography		89

List of Figures

2.1	Vision based hand tracking systems	8
2.2	Glove systems using IMUs	10
2.3	Flexion based glove systems	12
2.4	Magnetic hand tracking systems.	13
2.5	Collection of various approaches for hand motion reconstruction	15
3.1	Bone and joint definitions of the human hand.	23
3.2	Magnetic field lines, excited by a dipole.	25
3.3	Cylindrical bar magnet with infinitesimal slice dz	25
3.4	Cylindrical coordinate frame	27
4.1	Magnetic system, developed by Ma et al.	29
4.2	Self designed system parts	31
4.3	The introduced hand model.	33
4.4	Breakout board of sensor unit	35
4.5	Calibrated and uncalibrated sensor data	36
4.6	Screenshots of the visual representation with Blender	42
5.1	Clipping behaviour of sensor	44
5.2	Timing behaviour of sensor system	45
5.3	2D representation of the raw calibration measurements	47
5.4	Deviation of the calibrated measurements to the perfect centered sphere	48
5.5	Quality of earth cancellation	49
5.6	Comparing the models and sensor measurements for flat movement .	51
5.7	Influence of erroneous hand dimensions on model predictions	53
5.8	Simulating the magnetic field for various finger movements	56
5.9	Introduced movement pattern for index finger estimation	60
5.10	Estimated states vs. perfect states for using one magnet, one sensor.	62
5.11	Introduced movement pattern for four finger estimation	65
5.12	Estimated states of four sensors and four magnets	67
5.13	Measurement setup	70
5.14	Estimating the motion of four fingers	75
5.15	Comparison of estimated states, which fit best to Leap data	78
5.16	Relationship between θ_{PIP} and θ_{DIP} observed by Leap Motion	80
5.17	Occurrence of wrong estimated states for θ_{MCP}	82
5.18	Measured magnetic flux densities for various initialization gestures . .	84

Acronyms

BFGS Broyden-Fletcher-Goldfarb-Shanno

BLE Bluetooth Low Energy

CEL complete elliptical integral

CGS Centimetre-Gram-Second

CMC Carpometacarpal

CT Computed Tomography

DIP Distal interphalangeal

DOF Degree of Freedom

EKF Extended Kalman Filter

EMG Electromyography

FEM Finite Element Method

FFT Fast Fourier Transform

GATT Generic Attribute Profile

HCI Human Computer Interface

IMU Inertial Measurement Unit

IR Infra Red

LSB Least Significant Bit

MCP Metacarpophalangeal

PCB Printed Circuit Board

PIP proximal Interphalangeal

ROI Region of Interest

ROM Range of Movement

SDK Software Development Kit

SLSQP Sequential Least SQuares Programming

TM Trapeziometacarpal

1 Introduction

The human hand is one of the most important parts of the body for object interaction and communication. The five fingers show a broad range of motions and can perform powerful gestures, such as grasping, as well as sensitive and accurate movements like painting. In order to examine the natural behaviour of the human hand, some special motion tracking systems, capable of the complex finger movements, have been developed until now. Those systems can be used for medical treatment of hand injuries or movement impairment, caused for example by an accident or stroke. Another novel field of application would be the interpretation towards HCI, to establish a natural way of interacting with devices. Motion tracking of the human body as a whole is not a new feature, although a lot of research is going on in this area. For hand and finger tracking however, those general approaches have to be adjusted, since the granular but also complex finger motions are often performed only within a small movement range and therefore need a system with a higher resolution. Traditionally the developed hand tracking methods use standard motion capture approaches, such as cameras or Inertial Measurement Units (IMUs) to identify and reconstruct various movements. In order to make them capable for hand pose reconstruction, those solutions are often bulky and introduce external components. Those systems seem not to stand in a relationship to the small and neat hand. One approach, that uses the limited region of interest for hand state estimation, has received only little attention until now. The measuring of magnetic fields, excited by permanent neodymium magnets attached to the fingertips. This approach would decrease the number of sensors and external components for finger state estimation. Since the decrease of the magnetic field excited by a static magnet decreases with the distance, this method is poorly suited for body tracking. The human hand however, comprises not so big dimensions and the overall measurable magnetic flux density can be adjusted by choosing suitable magnets. This approach seems promising for the purpose.

The aim of this thesis is to develop a system for the reconstruction of finger joint angles, by measuring the magnetic flux densities, excited by artificial magnets on the fingertips. The system should present a new approach accompanied by less bulky and complex components as the ones so far developed. Therefore, the system size and usability is desired to be small and simple. The thesis starts with a general review of related work on hand motion reconstruction and the possible fields of applications. After introducing the general anatomic and magnetic foundations, the hardware and software components of the developed approach will be described. A model will be evaluated to describe the magnetic flux densities, measurable by

the deployed sensors for each finger pose. From that, a reconstruction algorithm mapping the measured superimposed magnetic field to the joint angles of the hand will be implemented. The results of the developed system for the estimated finger poses will be evaluated against the values of a commercially available camera based approach. Therefore, the overall performance of the magnetic system regarding the physical resolution and accuracy of joint angle reconstruction will be determined.

2 Related Work

2.1 Approaches for Hand Motion Reconstruction

In the following sections, several methods for hand motion reconstruction are presented. The benefits and drawbacks of the different approaches are named and discussed, to get an insight to the challenges the movement of the hand brings in. Camera based systems are known to show high accuracy and are therefore often stated as ground truth. Datagloves, using IMUs or flexion sensors reflect commonly adopted mobile systems. The estimation of hand postures by using active or passive magnets has received little attention until now. To conclude this overview, some interesting and unusual systems are presented in the following sections.

2.1.1 Camera Based

Vision based motion capturing systems are widely used. They consist of one or more cameras, arranged in a certain configuration, to generate an almost exact replica of the desired trackable object. Nowadays, those systems are not only used for tracking and analyzing the motion of humans. The systems and applications range from general purpose devices for entertainment, like interacting with video games to examining the movement of athletes [Zha12], [BGT12]. Hence, it is no surprise that some groups decided to use a vision based system for hand motion reconstruction, even though those movements bring in some challenging aspects to consider. However, the quality of the results of such vision based systems is very high and is often classified as ground truth for motion estimation of fingers. The Optotrak system, which is used by several groups, for example has an accuracy of up to 0.1 mm with an resolution of 0.01 mm [201a]. It is very hard to manually reconstruct and measure the real values of finger angles and hand motion, since one can not see bones without an x-ray.

No matter what kind of vision based motion tracking system is used, to extract the actual hand pose and movement from an image or video stream, the following steps need to be performed:

1. Image acquisition, fusion (if more than one camera is used) and preprocessing
2. Image processing, to receive a focus on the relevant sections (Region of Interest (ROI))

3. Pose estimation, to extract and calculate the actual body, respectively hand pose from the image

A fundamental part for these steps is providing a proper three dimensional object model. No matter whether one tracks the entire body or only a small part like the hand, the more detailed the outcome of the system should be, the more detailed the model needs to be. The model uses a mesh of triangles and vertices and applies (anatomical) constraints on them. After extracting the relevant sections from the camera image, the model calculates and maps the actual positions and relations between the joints and bones. This step can consume much computation time, if the result is to be very detailed. Yun et al. for example solved this problem, by combining a system identification stage, which uses the hand model, with a state estimation stage where an Extended Kalman Filter (EKF) is used [YAD13].

For a reconstructing of the hand motion with a vision based system, two approaches mainly appear in literature: The tracking of markers, placed on the hand or a textile glove and the markerless detection of palm and fingers. At first a short overview on the marker based systems is presented.

Supuk et al. [SBZ08] and Metcalf et al. [MNC⁺08] use passive reflective markers attached to the hand. While the Optotrak system [201a], used by Supuk et al., only needs one camera instance, the Vicon system [VMSL] consists of at least two and can handle up to six cameras for more accuracy. Comparing the effort and capabilities of those systems, measuring only the movement of small hands seems to break the relations. The accuracy of the outcome is directly dependent on the number and positions of used markers. Unfortunately there are no exact numbers given about the achieved accuracy of the vision systems. Metcalf et al. modeled the movement of wrist, hand, fingers and thumb. Therefore, they compare the results of different people's tests, each equipped with 26 markers in total for one hand. The passive stickers are placed at the three knuckles of each finger, the fingertips and on the back of the hand and lower forearm to guarantee a tracking of the whole hand motion and not only of the fingers (see Figure 2.1a). It is very important, to place the markers for each person on the same anatomical positions. Attaching the reflectors statically on a textile glove would make the system more flexible and easier to use, but this would also lead to a degradation of the results. Every person's hand varies not only in size, but also in the position and length of the individual bones and knuckles. Consequently, a general purpose glove is very hard to construct. One additional issue that Metcalf et al. found out is, that the size of the surface has to be taken into account, too. The hands of children, for example will not have the surface to place all markers properly in the desired positions. The placement of the stickers took them between three and five minutes each time. In fact, the aim of their study was to show that people perform specific tasks in their own way, but that one can still observe similarities. Supuk et al. used the camera system more or less only as ground truth, to validate the data from a flexion based Data Glove. They used 19 passive markers, placed in a similar shape as the other group. Yun et al. were using active LED markers. Their paper emphasizes on an effective system

identification algorithm and filtering method. They estimated one index finger with seven markers on it, recording it with a system from Phasespace Inc. The accuracy of the measurements was verified by comparing the results to an optimized kinematic model. Here again, no exact numbers about the accuracy are provided.

Wang et al. uses a multi-colored glove for finger identification. Their glove is printed with a special color pattern, to simplify the pose estimation problem. This allows them to use a single general purpose color camera, which is much cheaper than the motion capturing systems mentioned beforehand. A setup of their system is shown in Figure 2.1b. The pose estimation is done on the basis of a database, containing the glove in different articulations. The image is processed to extract the colors clearly, and the pose is found by a nearest neighbors approach, in comparison to the database. To penalize the difference between the image and the matched pose from the database, they tune the result by applying inverse kinematics. In the end their system works reliably. But it is only applicable for one glove size and the results are based on a single test person.

For all the above approaches it is very important to place the markers at the correct anatomical positions, to achieve good and reliable results. So the system presumes that the user knows how to attach the stickers or wear the glove and which mistakes can be made. In order to facilitate this process and make it less fault-prone, a markerless approach would be a better choice. By realizing such a variant however, the region of interest, so to say the actual position of the hand, is not directly given. Furthermore, the orientation and alignment of the test person has to be interpreted. For image acquisition Ionescu et al. use a gray scale camera and filter the image for the biggest white region. To get the best results they mention that one has to hold the hand in front of a black surface. In the end, they only try to detect certain hand gestures and not a whole motion or single fingers. The images are compared to a pre-learned training set in order to recognize the poses. So this group doesn't use any models.

Metcalf et al. and Sharp et al. use the Microsoft Kinect. This system defines anatomic landmarks, to identify certain points of the hand. Actually the system is designed for declaring landmarks on the whole body, so for tracking a petite hand this identification process has to be adopted. Metcalf et al. use the binary depth image and define the landmarks by searching for reasonable maxima and minima in combination with a 3D hand model. Possible poses of the hand are simulated with the model and adopted to the image. In the end their approach led to an overall accuracy of 78 %. A marker based system served as a comparison. The approach of Metcalf et al. was only tested with persons sitting on a table, so it is designed for a front-facing close-range scenario. Sharp et al. goes one step further and brings the system to a universal surrounding. They are able to extract the hand posture and movement from an arbitrary image, no matter at which distance the hand is or what the background looks like. The approach is to introduce a robust reinitializer to handle typical vision based problems like occlusion and image loss. In combination with a fast and effective comparison to a 3D hand model and a learned training data set, the movement and pose of the hand can be estimated very reliably, inde-

pendent from the person or the environmental circumstances.

John et al. use two high resolution color cameras from Sony. To reconstruct the motion of the extracted human hand, the system compares the images to data from the 3d hand model. By matching the model to the input pictures, the position and configuration of the hand is estimated in real time.

The commercially available Leap Motion system [LM] includes two IR cameras and three IR emitters and is particularly constructed for hand motion reconstruction. The small controller just has to be put under your hands, like shown in Figure 2.1d. The Leap Motion Inc. provides a well documented API and software tools for Windows and Mac to use their device for basic interaction with a PC. The system directly outputs hand- and fingerpositions. It can also detect whether one is holding a pen or specific tools. Via the API one can directly access the absolute positions of the hand and joints. Also specific gestures, like swiping or drawing a circle with a finger gets directly detected. The accuracy and robustness of the Leap system is analyzed in [WBRF13]. Different motions and positions were examined. To ensure a reliable “test person” the group chose an industrial robot with a position accuracy of 0.2 mm. The overall error of the system for dynamic motions was below 0.7 mm, which is better than the Microsoft Kinect system.

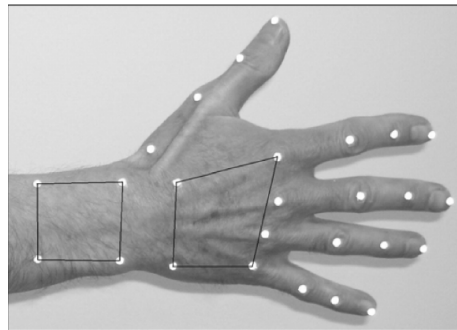
While the so far mentioned systems are all bounded to a certain environment, the Digits system, developed by Chang et al. is a more wearable and mobile realization. It uses a wrist wearable Infra Red (IR) sensor [Cha] and consists of an IR laser line generator, a ring of modulated IR LEDs, a IR camera, and an IMU (see Figure 2.1e). The system collects on the one hand a single 3D point for each finger from the line generator and on the other hand a uniformly illuminated image of the hand, produced by the modulated IR LEDs. With those informations and by using inverse kinematics of the underlying human hand model, the group can robustly reconstruct inward hand and finger movements. The IMU can track the alignment and movement of the whole forearm. The overall angular error of the system is $\leq 9^\circ$ for the joint angles. This value varies with the fingers, since the thumb has a more complex movement and is smaller than the index finger for example. However these values satisfy the clinical standards for joint measurement.

Concluding the presented techniques for hand motion reconstruction by vision based systems, the following basic characteristics of such systems can be asserted. (The impact or applicability of each point varies with the system, of course):

- The quality and stability of the tracking is limited to light conditions.
- Occlusion of unseen fingers, for example by crossing or making a fist, can occur. Also clothes or body parts, held in front of the camera can hide parts of the hand.
- The proposed systems are usually quite big or even need multiple cameras.
- This induces that the installation has to be static (like depicted in 2.1c) and is only capable of localisation based tracking.

2.1 Approaches for Hand Motion Reconstruction

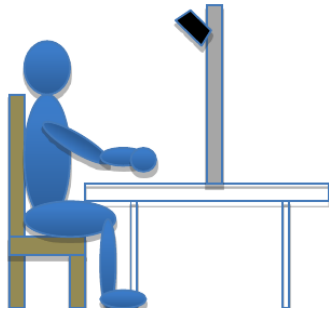
- A three dimensional model of the human hand gets adopted to the images.
- The algorithms for motion tracking are quite complex and are running on an external PC.
- For marker based systems: the placement of the markers is crucial.



(a) The positions of the markers, used in [MNC⁺08]



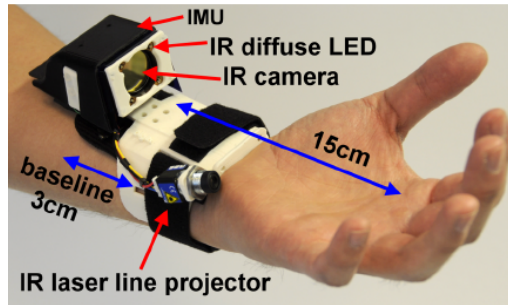
(b) The Color glove with the used camera setup [WP09]



(c) Example for a static camera - subject setup, used by [MRM⁺13]



(d) The Leap Motion system [LM]. The hands can directly be visualized on the screen.



(e) The Digits system [Cha] with the relevant parts.

Figure 2.1: Some examples of the described vision based systems.

2.1.2 IMU based

Another concept of motion tracking consists of using IMUs. Those sensors measure the angular rate, acceleration and magnetic field for three dimensions in space. They are also called 9-Degree of Freedom (DOF) sensors. With existing suitable algorithms, like a Madgwick filter [Mad10] the absolute orientation of the sensor can be calculated, relative to the earth's magnetic field, from the sensor data, making the orientation of a sensor unit instantaneously trackable. Therefore, it is no surprise that those sensors are commonly used for motion tracking applications in general. The Dutch company Xsens Technologies, for example is specialized on motion tracking using IMUs and develops several suits to track the whole body motion. Kortier et al. use a self designed IMU system, consisting of 18 sensor units in total. The sensors are placed on the bare hand, like depicted in Figure 2.2a. The units are a gyroscope-accelerometer combination and placed on each proximal, intermediate and distal phalanges of each finger (for a detailed explanation of the bones, see section 3.1). For additional information three units are placed on the back of the hand. The PCBs on the fingertips and on the dorsal side are additionally equipped with a magnetometer, to get a more accurate estimation about the orientation of the hand. To filter, estimate and map the raw sensor data to an adequate biomechanical hand model the group uses an EKF framework. They achieved an adequate repeatability. By comparing their approach to a vision based one, a maximum error of 12.4 mm was achieved. This value seems pretty high, but they claim that it is because of an misalignment between the optical and their own chosen coordinate frame. This shows once again, that the calibration plays an important role for vision based systems and is not so easy to manage.

Fang et al. uses a similar method than Kortier et al. 16 IMUs, which are all full 9-DOF units, are placed on the three bones of each finger. For the palmar movement they use only one sensor. The processing of the data is also done "on-hand" with the self designed processor-board. For data filtering and position estimation they also use a Kalman Filter and a hand model. The characteristic of the approach lies in the evaluation of the sensor values. Because the hand is composed of rotational joints, they assume that either all sensors are in rotation or none. So they neglect the measurements of the gyroscope, if the hand is held still and only take the accelerometer and magnetometer data into account to track the finger movement. However when the hand is moving, the measurements of the accelerometer and magnetometer have lower dynamics and they use the values of the gyroscope. Furthermore, they first estimate the pose of the palm, then the attitude of the proximal finger bones, then the angles of the joints. Finally they calculate the full hand pose, based on the intermediate results. In the end they achieved the intended requirements and point out that the efficiency of their method is almost twice as high as that of the original EKF. Unfortunately they don't provide exact numbers.

There also exist some commercially available IMU based glove systems. The company Synertial [SLU] or Anthrotronix [Ant] for example provide ready to use gloves. The IGS-Glove from Synertial comes in various editions (two of them shown in

Figure 2.2b), differing in the number of sensors. It is available with 7, 12 or even 15 IMUs, mounted on the easy to wear glove, delivering you the desired accuracy. Anthrotronix however equip their “Acceleglove” with 6 IMUs. Both deliver their systems with a SDK to have direct access to the raw sensor data but also to pre-calculated motion and gesture data.

Again, all the presented systems show some similarities. The following points summarize these:

- The IMUs are mounted on a textile cloth
- A unified cloth, that fits every human hand is difficult to produce
- The accuracy varies with the number, position and measurement range of the sensors.
- The more sensors are used, the more wires are needed. Also the data traffic and processing time increases with the number of units.
- A calibration procedure is needed, to increase the accuracy.
- IMUs are cheap and available in a large variety



Figure 2.2: Examples of glove systems, using IMUs

2.1.3 Flexion based

Another approach of measuring the hand movement is to monitor the flexion of fingers. There are different kinds of flexion sensors out there and many researchers use them for finger tracking. For example in 1977 Thomas de Fanti and Daniel Sandin developed one of the first data glove prototypes at the Massachusetts Institute of Technology (MIT). The Sayre Glove [SZ94]. They equipped a glove with flexible tubes for each finger. At one end of each tube, they put a LED as light source and at the other a photocell. The amount of light, arriving at the sensor varies with the

flexion and extension of the finger. The more the finger is bent, the less light will arrive at the sensor.

Ten years later, in 1987 Visual Programming Language Research, Inc. rolled out some kind of successor to the Sayre Glove. Their device is equipped with five to ten flexion sensors, based on optical fibre [Zim85]. For more accuracy they place a sensor unit on each joint, to measure its angle. They even proposed a system with more sensors, to measure abduction and adduction between adjacent fingers.

Another way to measure the flexion are resistive or capacitive bend sensors. These devices can be printed with resistive ink and are therefore highly customizable in shape and size. Resistive bend sensors are used for example by O'Flynn et al., Zecca et al. or by the company 5DT (for representative pictures see Figure 2.3) [OSA⁺13], [ZEI⁺07], [Fif]. The Didjiglove in contrast is based on capacitive bend sensors [SZ94].

The Italian company Gloreha [Glo16] follows a more application specific approach. Their rehabilitative glove system consists of mechanical cables for each finger. With it, the extent of how much a finger is bent can be measured by the amount of extended wire. On the other hand the patient can be supported by extending or contracting the wire mechanically. This system is big, unhandy and looks more like an exoskeleton, than an unimpressive wearable. Of course, it is constructed for rehabilitation and aimed to support specific motions of a patient and not for general purpose measuring of flexion and extension in every day life (more about it in subsection 2.2.2). However it still shows a mentionable approach.

In the end, one can say that flexion based hand tracking has the following characteristics:

- The sensors are mounted on the joints. Most groups therefore use a textile glove.
- The output of the system is dependent on the positions of the sensors. Ideally this should not change by user. However each human hand is slightly different and there is not a universal glove size and sensor positioning, which would fit for all.
- One way to improve this is to calibrate the glove system for each user.
- The accuracy of the reconstructed finger positions or gestures is limited to the number and the measurement range of the used sensors. With one bend sensor per finger, one could at most only reconstruct the intention of the user's gesture or distinguish between several postures. However by introducing multiple sensors per finger, ideally more than one per joint, acceptable results can be achieved. [ZEI⁺07] used 15 bend sensors on a flexible PCB and reached an average error of 7.1° compared to a camera system.
- Only the bending of a joint or finger is measured. In order to reconstruct a relative or absolute position of the finger additional calculations have to be made.

- It is a simple and highly customizable system.
- Easy applications can be realized with only a few sensors



(a) The flexible PCB, used in [OSA⁺13]



(b) The glove system, developed in [ZEI⁺07].



(c) The Gloreha system for rehabilitation.

Figure 2.3: Examples of glove systems, using flexion based approaches

2.1.4 Magnetic based

Another approach is the use of measuring active and passive magnetic fields. Hashi et al. are using an active, resonator based approach, described in [HTY⁺06] and [HTHK14]. Their system consists of a driving coil, a pick up coil array and resonant LC markers. The desk-like environment can be seen in 2.4b. The markers, consisting of an inductive coil and a chip capacitor, are placed on the fingertips and have different resonant frequencies. The exciting coil modulates several signals and sends them out. An electromagnetic field is generated around the coil. Holding a marker inside this field, the electromagnetic circuit begins to oscillate and generates its own resonant electromagnetic field. This can be measured by the pick up coil array. Each marker has a unique excitation frequency. By modulating the received signals via Fast Fourier Transform (FFT), the markers can be identified. Furthermore, the measured amplitude of the signal represents the intensity of the magnetic field. The group assumes that the excited field of the marker behaves like a magnetic dipole field. By using this magnetic model (also further explained in section 3.2) the position and orientation of each marker can be calculated uniquely. They tested their approach and came up with a position accuracy up to 2 mm, for

2.1 Approaches for Hand Motion Reconstruction

locations up to 100 mm away from the pick up coil array. Increasing the distance further, the results get worse. Schaffelhofer et al. tested the commercially available system of Northern Digital [201b], which is comparable to the afore mentioned, only with primates instead of humans as test subjects. They achieved an overall accuracy of $2.41^\circ \pm 3.36^\circ$ for the tracking of dynamic movements. However the system, consisting of very complex and bulky components is not so well suited for mobile or general purpose use.

Ma et al. take the approach of determining the position of a passive cylindrical bar magnet by approximating it with the magnetic dipole field. They try to reconstruct the movement of the fingers, by placing neodymium magnets on the fingertips and measuring the magnetic field. A draft of the system can be seen in 2.4a. Like the active approaches, they use the model for the magnetic dipole, to estimate the position and orientation of the passive magnets. To conclude from those estimated values to the actual finger position, they use inverse kinematics with an underlying human hand model. For verification of this approach they equipped a test person with one magnet on the index fingertip and six sensors on a wristband. The proband was asked to perform several flexion and extension tasks of his finger. The results for the estimated finger positions and orientations were consistent with the data recorded by a Vicon system. Exact accuracy values are not provided by the group.

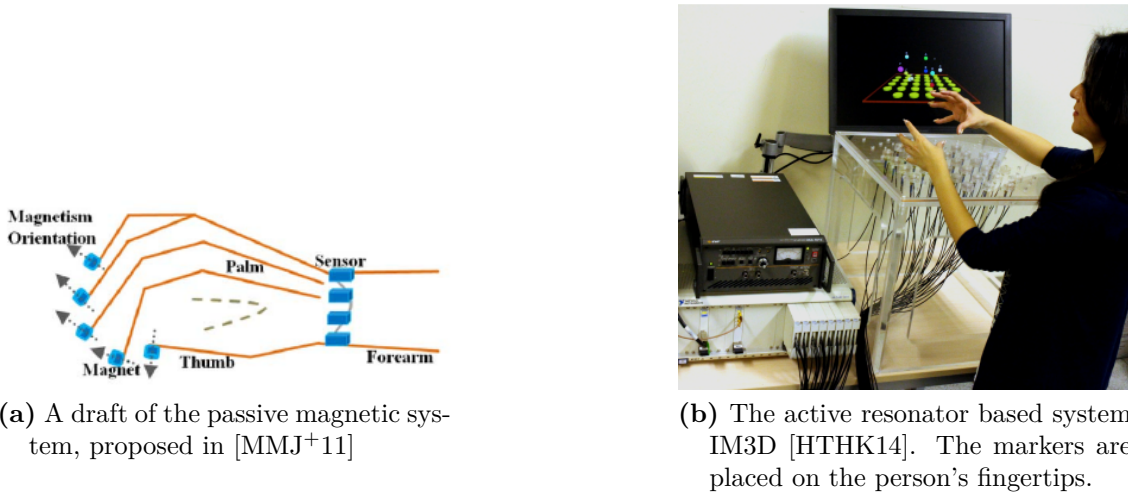


Figure 2.4: Examples of hand tracking systems, using magnetic/electromagnetic approaches

2.1.5 Other approaches

As is clearly visible, there is a lot of research happen in the area of motion estimation for the human hand. The focus of the so far presented approaches was based on general purpose devices, designed for trying to track reliable and accurate the whole

range of motions. Due to the wide range of possible applications (see section 2.2) there are also some more specialised varieties in reconstructing gestures or movements. This section introduces some of them.

The Pinch Gloves, visualized in 2.5a, designed by Fakespacelabs represents an input device [BWCL01]. The system consists of a glove and conductive elements, sewn into the tips of each of the fingers. When two or more fingers are pinched together, the conductive parts come into contact and generate an individual signal. This signal can easily be interpreted by a computer and therefore serve as an input. There is also the possibility to attach a position tracker and add the motion of the hand as an input possibility. The system is used for virtual environment interaction. In [BWCL01] a more elaborated interaction technique with this simple system is presented. They developed an environment to navigate through menus or to type on a virtual keyboard.

The eRing, developed by Wilhelm et al. is another kind of gesture interaction device. It consists of a ring, enclosed by capacitive foils (a first prototype is presented in 2.5b). The capacity of the system is related to the conductive environment. The human body has an influence on the magnitude of capacity, which changes by moving the fingers around the ring. This change in capacity can be measured, by determining the rise time τ of the RC circuit. In their paper the group describes that the system is able to detect static and dynamic gestures, as long as the neighbouring fingers are not too far away from the ring. For recognizing the gestures they use a 1-nearest neighbour approach on a pre learned dataset.

The Rutgers master II represents an exoskeleton like approach [BBPB02]. It consists of four pistons with rings on the ends, to attach them to the thumb, index, middle and ring finger (see 2.5c). The movement of the pinky finger is neglected. The abduction and adduction of the fingers is measured by Hall-effect sensors, the flexion and extension via infrared sensors. From the piston movement the finger angles can be calculated via a kinematic hand model. The pistons are inside an air cylinder to reduce friction in the system. This glove can provide force-feedback to the fingers, since the pistons can be controlled externally. Its main application area is therefore the rehabilitation and learning of hand movements. However the exoskeleton structure restricts the range of movement. Only 55 % of the natural grasping motion can be performed with this system. The accuracy of the system was evaluated to 0.75° for the adduction/abduction and 0.5 mm for the piston position. A similar system is the CyberGrasp haptic glove [Sys]. It is slightly more accurate (resolution of 0.5°) but also heavier and even more cumbersome.

An interesting approach is mentioned by Mascaro et al. They introduce a sensor placed onto the fingernail, measuring emitted light. LEDs are placed on top of the nail, emitting light with different wave lengths and measure the response from the nailbed. This technique is called reflectance photoplethysmography. If there is a force applied to the fingertip, the color of the skin beneath the nail changes. This behaviour can also be obtained when moving the finger. Those, often very small and not clearly visible, changes in color can be detected by their system. However there

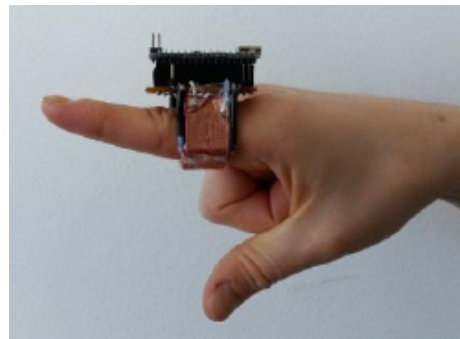
2.1 Approaches for Hand Motion Reconstruction

are many factors to take into account like skin color, blood flow in the fingers, texture of skin and so on, which complicate the reconstruction of motion. Hence they are only able to measure forces with this system [MA⁺01]. The draft of Figure 2.5d illustrates their approach.

Another approach for recognizing gestures is by measuring the electric potential of forearm muscles [KMA08] By performing gestures with the hand, the electromyographic potential especially in the forearm changes. This can be recorded by so called Electromyography (EMG). This approach is based on a learning data set, recorded for one person and by recognizing those gestures in real time. Zhang et al. [ZCL⁺11] designed a framework for this, also taking the data of an accelerometer into account.



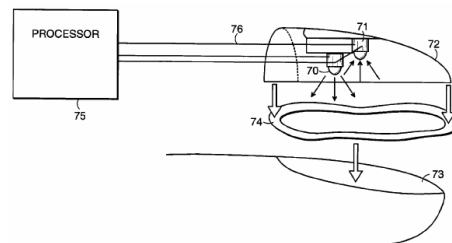
(a) Pinchglove system, used in [BWCL01]



(b) First prototype of the eRing [WKTA15]



(c) The Rutgers Master II [BBPB02]



(d) The photoplethysmography sensor approach of [MA⁺01]

Figure 2.5: Collection of various approaches for hand motion reconstruction

2.2 Fields for Applications

The desired performance of the motion reconstruction is always dependent on the focused application of the system. The following sections provide an overview on three fields and their demand regarding the accuracy, usability and reliability of the extracted hand motion.

2.2.1 HCI

The way we interact with electronic devices becomes more and more natural and is still changing. In the recent years touch input became ubiquitous, for example. Gaming consoles already bring the possibility to physically interact with them. The Kinect camera for Xbox or the Nintendo Wii controller are just two of such haptic systems. Hand motion based systems could be one way to bring the human computer interaction to the next level. Commercially available devices like the Leap Motion or the Myo wristband allow a broad gesture based interaction with the computer or smartphone. The Leap controller for example enables you to play games or interact with 3D graphics in a natural way [LM]. The benefit of such small and portable hand tracking devices is, that you don't need a big camera set up and don't have to leave your desk position. You just place the device in front of you or wear it, perform the desired gesture and the system behaves as you want. For example by swiping, a window gets closed or the field of view gets enlarged by pinching two fingers. For the interaction with mobile devices, such as smartphones, the system has to be wearable, like presented in [Cha]. Also the evolving field of virtual reality environments serves as a base for hand motion interaction. For the Leap Motion again, there exists a mount to combine it with the Oculus Rift system. Also creative tasks can be performed by a hand motion tracking system, for example drawing and designing a 3D object with your fingers on a virtual canvas.

Another, a bit more serious, way for HCI is the control of robotic machines, especially arm like devices. Such an application could be safety critical, so the interpretation of the hand motion has to be accurate and reliable, like the system proposed by Sharp et al. [SKR⁺15]. Dependent on the application, those devices should be able to track the whole finger movement and not only react on predefined gestures. Examples could be controlling robots in space [DSD08] or in dangerous environments like military territory or for bomb disposal [Gre96]. Also the execution of surgical tasks could be one field of application. Nowadays invasive operations should be performed in no time and leave very small scars. For that a lot of endoscopic surgery is done with remote controlled catheters. However, most of those invasive devices have very low functionality, often limited to cutting or exhausting something. The devices are controlled by the surgeon often by a simple mechanical system. Giving the practitioners the ability to use a more sensitive and complex method of interaction, would not only reduce the time needed for the intervention and the risks for the patient, but also enlarge the possibilities of interventions.

2.2.2 Therapeutic

The exact measurement of finger joints, called goniometry, is still a time consuming and error-prone task. Therapists and doctors have to measure patient's Range of Movement (ROM) in case of hand immobility diseases like arthritis, rheumatism [OSA⁺13] or parkinson's disease [SAG⁺03], or after a hand operation and fractures. Till now they use mechanical goniometers [WPC⁰⁰] to measure static angle positions, dynamic measurements are not possible to evaluate. A more accurate and reliable method would ease their life tremendously. This is where the hand motion reconstruction comes in. As described in section 2.1 there are already systems which can measure the ROM of fingers very accurate. Williams et al. [WPC⁰⁰] verified their flexion based glove as clinically admitted and can even measure adduction-abduction more exactly than with goniometers. The group of O'Flynn et al. [OSA⁺13] developed a flexion and IMU based glove with a very detailed interface for doctors. They can record and visualize raw sensor data, like the bending angle or movement velocity, as well as a 3D hand, miming the actions of the user. The interface can also provide information about former measurements and can therefore monitor the development of the patients rehabilitation process. The diagnosis and measurements for Parkinson's disease are also critical. Till now the diagnosis relies on objective observations by the doctor and patients. This induces that the illness is often detected very late in an advanced stage. Su et al. [SAG⁺03] developed a system especially to detect this neurological disease [SAG⁺03]. With the help of an electromagnetic based glove, several experiments which could indicate Parkinson were carried out. In the end they compared the results for ill and healthy patients and could clarify significant differences in the execution of the tasks.

Another possibility to support especially the work of therapists is the home-based rehabilitation or telemedicine [MRM⁺13]. This means that the patients have a suitable guidance system at home and can perform the exercises with it. The paper of Durfee et al. [DSW07] validated that such systems can return the same results as clinical tests and could therefore save the patients time and effort. The system could for example detect over- or under-exertion while performing a presented task. Furthermore, by providing an attractive interface like a virtual-reality environment, the patients are much more motivated to execute the training on their own [PBBH00]. Such an interface doesn't have to be complex. The patient could see for example virtual objects on a screen and try to interact with them. The environment, consisting of a PC and the glove system, records not only the performed motions but also takes a video of the exercise session which can automatically be transmitted to the therapist. This ensures a constant verification and interaction with the clinic personal. That such a system can improve the work of therapists is validated by Heuser et al. [HKW⁰⁷]. In their study five postsurgery subjects suffering from Carpal tunnel syndrome were trained to perform tasks. The effects in hand function improvement was tremendous for all subjects. The strength for grip and pinch movement increased up to 150 %. Such therapeutic systems can benefit from approaches with force feedback. The Rutgers Master II, CyberGrasp or the Gloreha approaches,

all mentioned beforehand, are such systems. Force feedback systems are often more bulky than the motion tracking ones, in 2.3c the exoskeleton like Gloreha system is pictured. Popescu et al. [PBBH00] for example developed a system for the hand, using the Rutgers Master II.

However, for such a telemedicine system the accuracy has to be exact and reliable, also the data has to be processed in real time. One of the most important requirement is however the usability. The system has to be easy to set up and able to detect false focuses or attitudes. A glove based system for example brings in difficulties in donning and doffing [MRM⁺13], other systems are cumbersome or have fragile parts like wires [BBPB02], which could complicate the usage. For camera based systems the focus, illumination and the background of the image are critical points [ICLB05].

Till now only the mentioned studies and systems, described in [HKW⁺07] and [PBBH00] where performed, but certainly there will be more investigation in the near future.

2.2.3 Activity and Gesture tracking

As already depicted in subsection 2.2.1, the reconstruction of human hand motion can be used for gesture recognition. Activity recognition is mainly based on using a training data set for the gestures and an algorithm, to compare the actual movement with this database to finally judge whether the gesture has been performed or not. But this feature can not only be used for HCI. Having a wearable system, one can detect specific gestures ubiquitously, which can be used to produce a diary like tracking of hand gestures. Such a monitoring system could be a support again for therapists, trying to analyse the daily routines of their patients. It is possible to detect a grasp intention [SBZ08], [ZCL⁺11] and also the strength of a grasp [EK05]. By downsizing the systems and making them wearable one could get a detailed logbook about hand activities. The eRing [WKTA15] could be such a system. With an unimposing data glove system, like the one of 5DT or Synertial, one could even track the whole hand motion. Because of the mentioned reasons to use such a system in a ubiquitous environment, vision based systems are not so well suited for this application field. Apart from the Digits [Cha] system, most of the other developments use a bigger and stationary camera system.

Another possible application field concerning the recognition of gestures is the understanding and translation of sign language. Deaf persons are using the sign language to communicate with the outside world. However, most of the “talking” persons do not know this complicated alphabet, which is based on specific hand gestures and poses, such that it can be very tiring for a deaf person to interact with others. Several groups have done research in this field like presented in [MK02], [FH93] or [DSD08]. Again, a wearable and mobile system is better suited for this task than a static, camera based approach. As the sign language has a lot, but sometimes similar looking gestures, the training data set and the corresponding classification

algorithm have to be fast and reliable. In the end such a hand tracking system has to be reliable, accurate, and able to track the movement of the whole hand. As a classification algorithm Fels et al. propose to use neural networks. The detected letters or words can then be visualized on a display or directly made audible by speakers [FH93]. To ensure a natural behaviour, the gestures have to be interpreted and visualized in real time. Fels et al. used a fibre optic data glove with 11 sensors, including an IMU to track the orientation of the hand. In the end they achieved an accuracy of about 99 % for words and only about 5 % of the attempts resulted in no detection. Mehdi et al. use only one flexion sensor per finger and two IMUs to track the orientation of the hand. They only achieved an accuracy of 88 % and some gestures could not be detected, because the movement of the forearm was not tracked. To improve their systems, the two groups state to investigate more on the algorithm and to use gloves with a higher reliability and accuracy.

3 Foundations

The following two sections provide further information about the anatomy of the human hand and the description of permanent magnets. A basic insight to those two fields will be provided, to better understand the upcoming parts about the developed hand model and the formulation of the finger state estimation.

3.1 Anatomy of the Human Hand

The anatomy and the motion of the human hand is very complex. Describing the whole interaction of tendons, muscles and bones would go beyond the scope of this thesis. This section will focus on the kinematic structure and relevant components of the hand for describing motion. The goal is to understand and derive a model to reliably reconstruct the human hand motion.

Bullock et al. [BBD12] and Lin et al. [LWH00] give a good and application oriented introduction to the anatomic structure. A Computed Tomography (CT) scanned image of the hand with explanations is provided in Figure 3.1. The metacarpals are enclosed by muscles and tendons and form the palm. Those parts are in principle static and only slight movements of flexion-extension are possible. During strong motions, like grasping, the metacarpals can move slightly, such that a maximum flexion-extension of 20° around the Carpometacarpal (CMC) joints is possible. Since this movement is not very natural and common, the skeletal palm is often seen as static. For this reason it directly follows that also the positions of the Metacarpophalangeal (MCP) joints lie in the same plane and their positions are also static. This means that the center of rotation for the movement of a finger stays the same. Anatomically seen this is a simplification, since the joint axes are only fixed within 1.5 mm during a full flexion-extension of the MCP. Each MCP shows two DOF. One is represented by the lateral movement of abduction-adduction, which is possible within a range of around -15° to 15° . The second is the flexion-extension of approximately 90° . Strictly speaking one also has to consider axial rotation of the MCP, but since this small amount of movement can only be performed by applying external forces it is neglected here. Next to the MCP comes the proximal phalanges with the proximal Interphalangeal (PIP) joint, the intermediate phalanges with the Distal interphalangeal (DIP) joint and the distal phalanges. The PIP and DIP joints show one DOF each, since only flexion-extension is possible. The maximum range of movement for the PIP will be assumed as 110° and for the DIP as 90° . One could assume that the three bones (proximal, intermediate and distal phalanges)

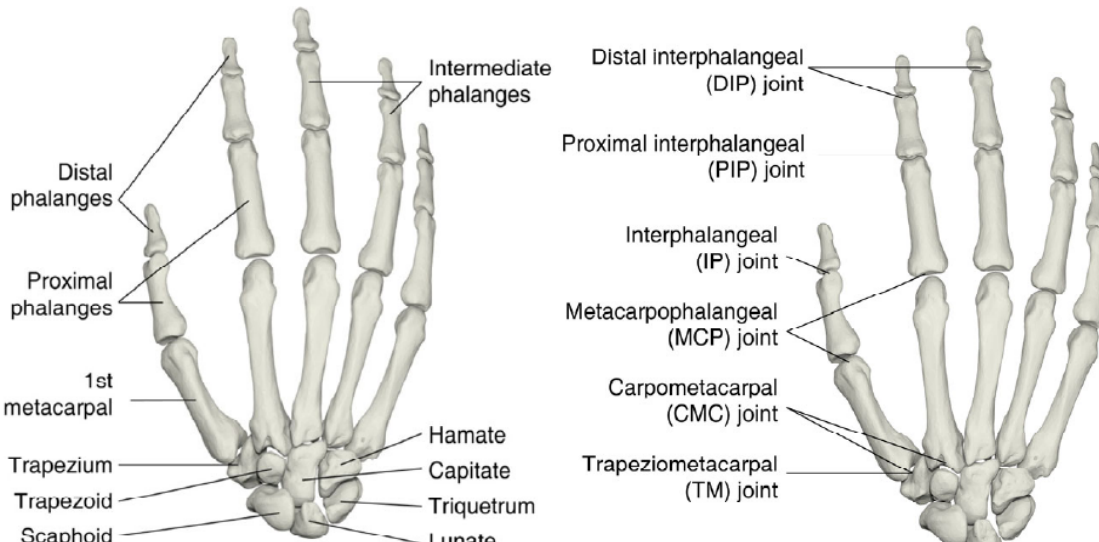
representing a finger move in one plane, relative to the first joint (MCP). In other words, that the flexion-extension axes of the three joints (MCP, PIP and DIP) are all parallel to each other. From an anatomical view, this is not totally right, but since this shift is only small it can be neglected for a simpler but still representable model. So in total one finger comes with 4 DOFs.

When it comes to modelling and simplifying the anatomy of the human hand, one can make some general assumptions. As already stated above, the small movement of the CMC is negligible, and so it is assumed that all MCP joints lie in the same plane. Lin et al. propose to introduce an intra-finger constraint, concerning the movement of the PIP and DIP joints. In order to bend the DIP joint, the PIP must also be bended. The relation between those two joints is commonly approximated as $\theta_{\text{DIP}} = \frac{2}{3}\theta_{\text{PIP}}$. This reduces the overall DOF for one finger from four to three. The thumb was not described till now. This special finger of the human hand, being the most important for powerful and helpful interactions induces even more complexity. Its flexibility allows reaching and touching the other fingertips. Like the ones before, it has three joints, however comprising more DOF in total. The MCP has two DOF as well as the Trapeziometacarpal (TM). In total the thumb has therefore five DOF. To obtain an easier model, the movement of the thumb is neglected.

For analysing the speed and naturalness of hand motions, Ingram et al. [IKHW08] examined six healthy male subjects in a study. The probands were equipped with resistive CyberGloves and asked to wear them for a certain time at a day, in order to become an insight in the natural range of movement. Regarding the angular velocity, they observed a mean value of $10^\circ/\text{s}$. The overall velocity of all joints was always less than $100^\circ/\text{s}$.

The following points summarize the proposed assumptions and simplifications, applied to the model:

- Only movements without applying external forces are modeled.
- Knuckles are modeled as a combination of ideal revolute joints
- Bones serve as perfect rigid bodies.
- The movement of the thumb is neglected for simplicity reasons.
- The flexion-extension of metacarpals is neglected, this means the palm is assumed as a rigid plane which comprises a fixed positions for the MCPs.
- The flexion-extension of one finger is planar
- MCP has 2 DOF with flexion-extension angle: $0^\circ \leq \theta_{\text{MCP}} \leq 90^\circ$ and adduction/abduction angle: $-15^\circ \leq \phi_{\text{MCP}} \leq 15^\circ$
- DIP and PIP have 1 DOF with the following ranges for the flexion-extension angle: $0^\circ \leq \theta_{\text{DIP}} \leq 90^\circ$ and $0^\circ \leq \theta_{\text{PIP}} \leq 110^\circ$
- Dynamic constraint between $\theta_{\text{DIP}} = \frac{2}{3}\theta_{\text{PIP}}$



(a) Bone structure of the right hand.

(b) Joints of the right hand.

Figure 3.1: Skeletal representation for the bones and joints of the right human hand. The view is from the dorsal side.[BBD12]

- So each finger has 3 DOF in total.
- A local frame is used for motion reconstruction, so one can represent a pose by describing the joint angles.
- A mean angular velocity of $10^\circ/\text{s}$ is assumed.

The introduced assumptions try to restrict the human hand in a useful meaning, without loosing too much generality. Utilizing those statements, the fingers of the human hand can be modelled as kinematic chain, which is fully described by the joint angles. The application specific restrictions, applied to the model used for this work are further depicted in section 4.2.

3.2 Magnetic

Permanent magnets are widely used nowadays. Their constant magnetic characteristics are used for example in electric engines, CT or by interacting with other ferro-, para- or diamagnetic materials. In the simplest case they are used for holding things at a dedicated place. The underlying principle is the excitation of a magnetic field. It is commonly known that only magnetic dipoles exist, meaning that a magnetic north pole never comes without its respective south pole. The shape of the magnetic field lines is commonly known and part of undergraduate physics. However, when it comes to the physical description of the magnetic field lines of a permanent magnet, the subject gets more complex. In the following two mathematical models for describing the magnetic field, excited by a permanent cylindrical

neodymium bar magnet of length $2b$ and radius a will be presented. The strength of the magnetic field, or in other words the magnetic flux density is denoted as B . Its corresponding SI-Unit is called Tesla ($1 \text{ T} = 1 \frac{\text{kg}}{\text{As}^2} = 1 \frac{\text{N}}{\text{Am}}$). However, it exists a second unit to describe this strength, called Gauss, which is used by the Centimetre-Gram-Second (CGS)-system ($1 \text{Gs} = 10^{-4} \text{T}$).

At first, one has to mention that a current carrying loop also excites a magnetic field. This is described among others by the Biot-Savart law. The law is valid for the approximation of static magnetic fields. The representation as magnetic dipole by a single current loop or a pair of contrary poles, and the description of its field lines is the base for the ongoing derivation and a common method [DO10]. Accordingly the literature often treats the magnetic field as if it is excited by electric current. The electromagnetic equivalent to a cylindrical bar magnet would be a tightly wound solenoid with a number of turns n per unit length, carrying a current I .

An approximation for describing the magnetic field of a permanent magnet can be done by describing it as a magnetic dipole. This approximation is used by Ma et al. [MJL⁺10]. As briefly mentioned beforehand there are only magnetic dipoles, represented by a pair of a (positive) north pole and a (negative) south pole. The field lines are oriented along the direction of the magnetic dipole moment \vec{m} and go from south to north (see Figure 3.2). The dipole moment can be interpreted as a measure for the orientation and the strength of the bar magnet. If one shrinks the distance of two contemporary charges to a point and keeps the orientation of the magnetic moment constant, the field strength B can be described by the following formula:

$$B(\vec{r}, \vec{m}) = \frac{\mu_0}{4\pi|\vec{r}|^2} \left(\frac{3\vec{r}(\vec{m} \cdot \vec{r}) - \vec{m}|\vec{r}|^2}{|\vec{r}|^3} \right) \quad (3.1)$$

with

$$\vec{m} = \vec{h} \cdot \frac{B_r V}{\mu_0}$$

\vec{r} represents the distance from the magnetic source, which is located at the origin of a Cartesian coordinate frame. For a bar magnet, this means that its center is located at the origin. The constant μ_0 is the vacuum magnetic susceptibility [CS13] and has a value of $4\pi \cdot 10^{-7} \frac{\text{N}}{\text{A}^2}$. The factor B_r represents the Remanence field of the magnetic material. For the used neodymium magnet this value is in between 1.26-1.29 T (for the ongoing calculations it is assumed to be 1.29 T). \vec{h} is the normalised orientation in space of the magnet. One thing that can be observed by this formula is the relationship of the magnetic field at a distance \vec{r} . The field decreases by a cubic magnitude with the distance. So roughly spoken the field strength $B \sim \frac{1}{|\vec{r}|^3}$. Another point is, that due to the dot product between \vec{m} and \vec{r} the model gets nonlinear.

Since this is an approximation for the behaviour of the magnetic field of a bar magnet, Camacho et al. [CS13] follow a more detailed way, by taking the shape of the cylindrical permanent magnet into account. They also state that for a homogeneous,

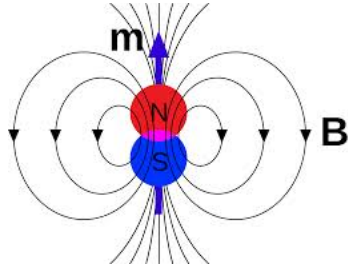


Figure 3.2: The shape of the magnetic field lines is visualized, excited by a magnetic dipole. The magnetic moment is denoted as \vec{m} and represents the orientation of the magnet.

constantly magnetized body the distribution and orientation of magnetic dipoles inside a volume dV of this body is constant and has the magnetic dipole moment $d\vec{m} = \vec{M}dV$. Where \vec{M} is the volume magnetization of the object. Moreover it holds for a permanent magnet that the magnetization does not change for any external fields, they are supposed to be hard. Using this for the cylindrical bar magnet, which is assumed to be magnetized along its symmetry axis, the following can be applied: It is assumed that the bar magnet is centered at the origin of a Cartesian coordinated system and aligned, such that the symmetry axis is oriented in z direction, like shown in Figure 3.3. The magnet is sliced into infinitesimal small discs with height dz , such that one element dV is defined by the radius a and the height dz . The

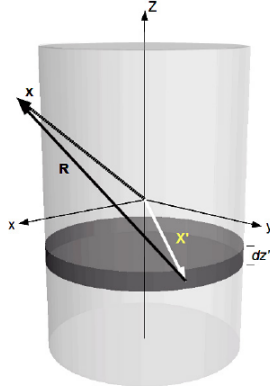


Figure 3.3: A cylindrical magnet, aligned along its magnetization axis in z direction. A infinitesimal piece dz is sketched. The vector R to a dedicated measurement point is visualized [DO10].

magnetic flux along the symmetry axis of such an infinitesimal element dV is given by Equation 3.1. In order to calculate B_z for the whole magnet, one has to integrate these contributions over the entire volume. In the end one gets the following formula for the magnetic field of a bar magnet along its magnetization axis(for a detailed

derivation, please have a look at [CS13], [DO10]):

$$B_z(z) = \frac{B_r}{2} \left(\frac{z+b}{\sqrt{(z+b)^2 + a^2}} - \frac{z-b}{\sqrt{(z-b)^2 + a^2}} \right) \quad (3.2)$$

Remind, that the solenoid has a length of $2b$ and radius r .

For deriving the mentioned equation there exist several methods. As shortly depicted, an integral over the whole surface has to be derived. Those integrals with a cylindrical symmetry are usually quite complex. However, for the symmetrical case along the z axis, one can use some mathematical properties to ease and obtain the Equation 3.2 in the end. However, if one wants not only to describe the magnetic field along the magnetization axis, those properties and therefore the presented equation does not hold any more. Derby et al. [DO10] propose to overcome this problem, by solving a complete elliptical integral (CEL). The generalized form of this is the following:

$$C(k_c, p, c, s) = \int_0^{\frac{\pi}{2}} \frac{c \cos^2 \varphi + s \sin^2 \varphi}{(\cos^2 \varphi + p \sin^2 \varphi) \sqrt{\cos^2 \varphi + k_c^2 \sin^2 \varphi}} d\varphi \quad (3.3)$$

A cylindrical coordinate system is introduced, which makes sense, since one tries to describe a cylindrical shape. The corresponding structure and naming of axes is shown in Figure 3.4. With the help of this cylindrical representation, the general magnetic field components can be expressed by

$$B_\rho = B_o [\alpha_+ C(k_+, 1, 1, -1) - \alpha_- C(k_-, 1, 1, -1)] \quad (3.4)$$

for the radial magnetic component along ρ . And

$$B_z = \frac{B_o a}{a + \rho} [\beta_+ C(k_+, \gamma^2, 1, \gamma) - \beta_- C(k_-, \gamma^2, 1, \gamma)] \quad (3.5)$$

for the axial magnetic component along the z axis. Along with the following introduced variables, which are dependent on the cylindrical position (ρ, φ, z) of the dedicated point in space.

$$B_o = \frac{\mu_0 n I}{\pi} = \frac{B_r}{\pi}$$

$$z_\pm = z_\pm b$$

$$\alpha_\pm = \frac{a}{\sqrt{z_\pm^2 + (\rho + a)^2}}$$

$$\beta_{\pm} = \frac{z_{\pm}}{\sqrt{z_{\pm}^2 + (\rho + a)^2}}$$

$$\gamma = \frac{a - \rho}{a + \rho}$$

$$k_{\pm} = \sqrt{\frac{z_{\pm}^2 + (a - \rho)^2}{z_{\pm}^2 + (a + \rho)^2}}$$

The azimuthal component φ can be neglected, since the magnetic field does not change, by moving along a circle which is aligned perpendicular to the z axis. In order to derive the equation Equation 3.2 from Equation 3.4 and Equation 3.5, one just has to set the radial component ρ to 0 and $z > b$

The presented CEL are not easy to solve, therefore numerical methods are used to find a solution. However, trying to find an exact solution with software like *Mathematica* or *Maple* failed [CS13]. Since CELs are not only restricted to cylindrical bar magnets, some research is going on in this field. For the finally used method and further information about CEL, please look at [DO10]. Another method consists in using numerics, like Finite Element Method (FEM). This can lead to satisfying results [MA09].

The two presented models represent the basis for describing the magnetic flux at a certain position in space, relative to a permanent magnet. They both assume the

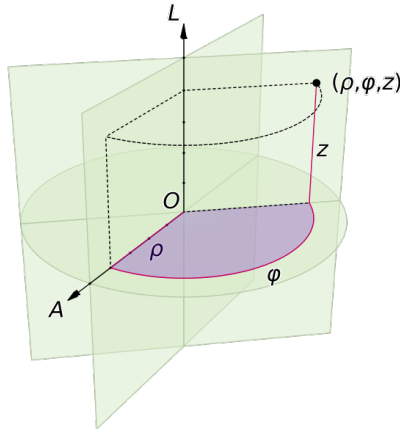


Figure 3.4: Representation of the cylindrical coordinate system frame. The height is denoted by the z axis, the radial component ρ is the euclidean distance from the z axis, the azimuth φ describes the angle between the reference direction and the chosen plane. [DO10]

absence of any additional, static magnetic fields, as for example the one produced by the earth. Both are used in the further evaluation. The equation, describing the magnetic field as an ideal dipole is refereed as the **dipole model** and represents a full nonlinear mathematical equation. The model approximating the cylindrical shape of the bar magnet is refereed to as the **cylindrical model**. Since a numerical algorithmic evaluation method is used for this model, mathematical operations like differentiation or integration is not applicable. A comparison between the two methods with real measurements and its effects on the finger pose reconstruction is done in chapter 5.

4 System Design and Implementation

4.1 System Design

Ma et al. [MJL⁺10] describe in their work an approach for hand pose estimation, using permanent magnets and sensors. Since this group is the only one using static magnets for hand state estimation, the design developed in this thesis relies partly on theirs. However, until now the group only presented results for reconstructing the motion of a single finger with six sensors. An image of their setup is shown in Figure 4.1. The presented system is constructed to estimate the pose of four hu-

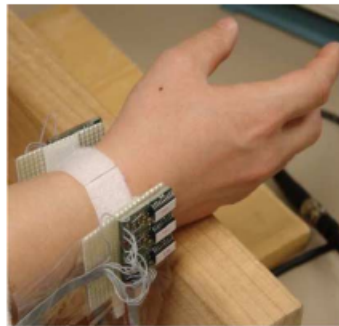


Figure 4.1: The System for estimating the movement of one finger with 6 sensors, used by Ma et al. [MJL⁺10]

man fingers, neglecting the thumb (for details about the underlying hand model, see section 4.2). For this, four cylindrical permanent magnets are used. Their dimensional and magnetic characteristics are shown in Table 4.1. Those components have

Length	15 mm
Radius	2.5 mm
Material	Neodymium
Remanence	1.26-1.29 T
Type	axial magnetised

Table 4.1: Magnetic and dimensional characteristics of the used cylindrical magnets.

to be mounted onto the fingertips. With a 3D printer ring like supports are designed, to ease the donning and doffing of the magnets and to ensure a secure positioning on the fingers. The bottom of the ring is left open, to make the components flexible for various finger diameters. The socket on top of the ring is constructed to statically hold and align the magnet. The magnetic field is measured with four IMUs (see section 4.3), placed inside a self designed bracket. This bracket is constructed to be worn on the back of the hand. It ensures, that the alignment and positioning of the sensors relative to each other is held static, which is important for the pose estimation (see section 4.6). Pictures of the individual parts and the designed system are shown in Figure 4.2. Since four magnets are used, the sensor array consists also of four measurement units. For an easy and reproducible first evaluation of the system, a wooden hand is used (see 4.2c). This static setup ensures one to measure the positions and dimensions of the sensors, the joints and the bone lengths relatively accurate. To read out the sensor data, a RFduino microcontroller [RFd15] is used. This device is a clone of the Arduino environment [LLC], which simplifies the programming of the system. Since this part of the setup is only used to acquire the sensor data and perform basic signal processing tasks, the computational requirements are not very high. A plus of the RFduino device is, that a Bluetooth Low Energy (BLE) module is already built in. So the data can be send to a host PC, where the main processing and estimation steps are realized. A summary of the individual parts and their purpose is given in Table 4.2.

Component	Purpose
4 Magnets	causing the magnetic field
4 IMUs	measuring the magnetic field
RFduino	data acquisition and forwarding
PC	sensor data interpretation and state estimation

Table 4.2: Overview of the relevant system parts and their purpose

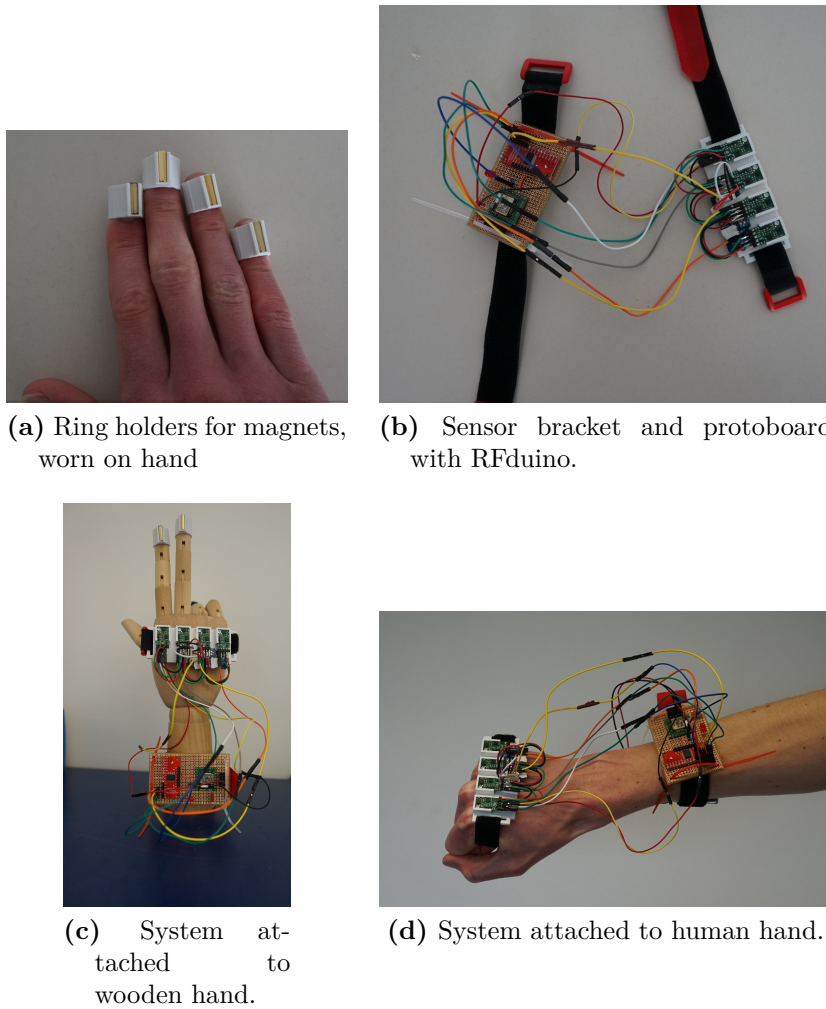


Figure 4.2: Self designed system parts

4.2 Human Hand Model

As already depicted in chapter 2 and section 3.1, the utilization of a proper kinematic model is a very important part, when it comes to the interpretation and estimation of finger poses. In this section the kinematic model, used to reconstruct the finger positions is described. It relies on the presented observations from section 3.1.

The underlying kinematic model tries to simplify the range of motion of the human hand, without loosing too much generality. Therefore the fingers are interpreted as ideal revolute joints. The complex movement of the thumb is totally neglected. The other four fingers naturally move mainly in one plane (by disregarding adduction-abduction), for the thumb however this does not hold. Trying to track the full five DOF for this finger would make the model much more complex. Another point is, that the thumb moves mainly “in front” of the other fingers. This would cause

remarkable influence on every sensor on the array, such that a distinction between the moving finger is more difficult. So for keeping the model and the pose estimation simple, the thumb will be neglected. As many other human hand models, the movement of the Metacarpal bones is neglected. Therefore the MCP joints are assumed to be always at a static position. Since the presented approach focuses on finger pose estimation and the sensors are mounted on the back of the hand, the movement of the whole palm does not need to be taken into account. As already stated, the index, middle, ring and pinky finger show four DOF each and can move in two planes by flexion-extension and adduction-abduction. For deriving a simpler hand model, the intra finger constraint for the joint angles of the DIP and PIP of one finger is used, being $\theta_{DIP} = \frac{2}{3}\theta_{PIP}$. So in the end one finger has 3 DOF. As a further step, this model can even be more simplified, by neglecting adduction-abduction and resulting in a system with 2 DOF per finger. The range of movement of the joints is assumed to be as described in [LWH00]. This means for the flexion-extension angle for the MCP being within $0^\circ \leq \theta_{MCP} \leq 90^\circ$ and the range of adduction/abduction $-15^\circ \leq \phi_{MCP} \leq 15^\circ$. The flexion-extension range for the PIP lies within $0^\circ \leq \theta_{PIP} \leq 110^\circ$.

In the end every finger is modelled equally as a kinematic chain with 3 joints, having 3 DOF in total. The position and orientation of the fingertip, and therefore of the magnet, is fully determined by the angles of the finger joints, using forward kinematics.

For a better visualization, the kinematic chain and the relevant parts are sketched in Figure 4.3 for a single finger. The Cartesian coordinate system, used in this drawing is adapted to the sensor alignment. This system convention is used throughout the whole thesis. For the calculation of the magnetic flux density according to the models, introduced in section 3.2, the distance vector from sensor to magnet and the orientation of the latter one is needed. Those two components can be derived using forward kinematics and the positions of the sensors and the joints.

The orientation vector \vec{h} is derived in the following way:

$$\begin{aligned} h_x &= \cos(-\theta_{MCP} - \theta_{PIP} - \theta_{DIP}) \\ h_y &= \cos(-\theta_{MCP} - \theta_{PIP} - \theta_{DIP}) \sin(\phi) \\ h_z &= \sin(-\theta_{MCP} - \theta_{PIP} - \theta_{DIP}) \cos(\phi) \end{aligned} \tag{4.1}$$

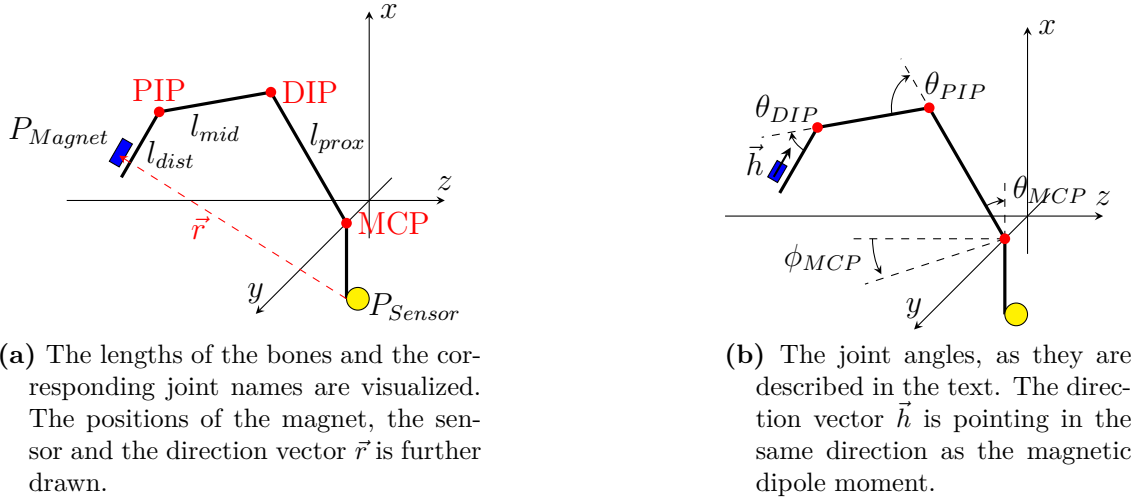


Figure 4.3: The introduced representation of the human hand as a kinematic chain.

For clarity, only a single finger is drawn. Figure (a) shows the location of the sensor, magnet and the joints. Also the direction vector \vec{r} is drawn. In figure (b), the joint angles are visualized and the direction \vec{h} of the magnet is drawn. The Cartesian coordinate system is aligned according to the sensor frame. This coordinate system defines the orientation, used throughout the whole thesis. The MCP joint lies on the y-Axis.

The position vector \vec{r} of the magnet is determined by

$$\begin{aligned}
 r_x &= l_{Prox} \sin\left(\frac{\pi}{2} - \theta_{MCP}\right) + \\
 &\quad l_{Mid} \sin\left(\frac{\pi}{2} - (\theta_{MCP} + \theta_{PIP})\right) + \\
 &\quad l_{Dist} \sin\left(\frac{\pi}{2} - (\theta_{MCP} + \theta_{PIP} + \theta_{DIP})\right) + (P_{MCP_x} - P_{Sensor_x}) \\
 r_y &= l_{Prox} \cos\left(\frac{\pi}{2} - \theta_{MCP}\right) + \\
 &\quad l_{Mid} \cos\left(\frac{\pi}{2} - (\theta_{MCP} + \theta_{PIP})\right) + \\
 &\quad l_{Dist} \cos\left(\frac{\pi}{2} - (\theta_{MCP} + \theta_{PIP} + \theta_{DIP})\right) \sin(\phi) + (P_{MCP_y} - P_{Sensor_y}) \\
 r_z &= -l_{Prox} \cos\left(\frac{\pi}{2} - \theta_{MCP}\right) + \\
 &\quad l_{Mid} \cos\left(\frac{\pi}{2} - (\theta_{MCP} + \theta_{PIP})\right) + \\
 &\quad l_{Dist} \cos\left(\frac{\pi}{2} - (\theta_{MCP} + \theta_{PIP} + \theta_{DIP})\right) \cos(\phi) + (P_{MCP_z} - P_{Sensor_z})
 \end{aligned} \tag{4.2}$$

with $l_{Prox}, l_{Inter}, l_{Dist}$ being the bone lengths of the proximal, intermediate and distal phalanges. P_{MCP} the position of the MCP joint and P_{Sensor} the position of the sensor. Those hand dimension parameters are very important, since they define

the expectable distance vector \vec{r} and have therefore an influence for calculating the magnetic flux density. Remember, that \vec{r} contributes nonlinearly to the magnetic models and therefore to the expected flux density. The hand dimension parameters should be determined very exact, to get a right representation of the proband, wearing the system. However, they can only be measured up to a certain grade of accuracy, since the bones and joints lie underneath the skin. An x-ray could provide exact anatomic values, but this would seem to break the range of effort. Therefore in the end a calliper is used for identifying the anatomic bone lengths and the sensor and joint positions of the hand. As mentioned, this has to be done very accurate to get a detailed representation of the fingers. If the model should be further simplified, the lateral movement of adduction-abduction could be neglected. One just has to set the ϕ value to 0. From that it directly follows, that the orientation and position vectors have only contributions on the x - and z -axis. The y -component stays 0.

Summarizing the derived hand model, one can define the state space of one finger pose to be completely described by 3 angular values (for the version neglecting adduction-abduction, the state space reduces to 2), being

$$x = \begin{bmatrix} \theta_{\text{MCP}} \\ \theta_{\text{PIP}} \\ \phi_{\text{MCP}} \end{bmatrix}$$

This state vector is further also refereed as the finger state vector. Thus all four fingers together have a state space of size 12. The presented model shows a basic approach to model the index, middle, ring and pinky finger of the human hand as ideal revolute joints. The constraints and simplifications introduced are comparable to other groups [LWH00]. The biggest simplification however is the disregard of the thumb movement.

4.3 Sensor Design and Data Acquisition

For measuring the magnetic field, four LSM303D sensors from ST are used [STM12]. This device comprises a 3 axis accelerometer and a 3 axis magnetometer in one module. It is chosen, because its magnetic full-scale range is selectable. It can be determined to ± 0.2 , ± 0.4 , ± 0.8 or ± 1.2 mT. The magnetic values are stored in 2 Bytes in 2's complement. The sensitivity per Least Significant Bit (LSB) is specified like shown in Table 4.3. The data rate can be set to a maximum of 100 Hz. The communication is established via a standard I2C bus, which means that a clock frequency of 100 kHz is used. In the end a breakout version of this device, available from Pololu [PE] is used. It is sold as a full 9 DOF IMU, carrying the LSM303D and L3GD20H gyroscope. However, since the gyroscope and the accelerometer are not further used, they won't be explained here in detail. A picture of the breakout board is shown in Figure 4.4. The communication is realised with an RFduino microcontroller. This device can be programmed via the Arduino environment,

Measurement Range [mT]	Sensitivity [$\mu\text{T}/\text{LSB}$]
± 0.2	0.080
± 0.4	0.160
± 0.8	0.320
± 1.2	0.479

Table 4.3: Magnetic sensitivity for the corresponding measurement range, according to the datasheet of the LSM303D sensor unit [STM12].



Figure 4.4: The utilized MinIMU-9 v3 breakout board from Pololu [PE]

which simplifies the process. It comes with a built in BLE module. This is used to send the data to a host PC, where the state estimation process is programmed. Since the same sensor is used four times on a single I2C bus, a small work around is established, to enable an individual communication to each one of the four sensors. The clock signal is splitted via a multiplexer and only redirected to the device, from which the data is desired. This ensures, that each sensor can be read out individually. Combining the data lines of the sensors and multiplexing the clock signal to each device individually leads to a single data information on the bus. As multiplexer, a breakout of the CD74HC4067 from Texas Instruments is used [Tex03].

4.4 Calibration and Preprocessing of Sensor Data

4.4.1 Calibration for Hard and Soft-Iron Coefficients

Magnetic sensors in general suffer from two main distortion effects, being the hard and soft-iron coefficients. Those parameters are caused by manufacturing processes, ferromagnetic materials on the Printed Circuit Board (PCB) and the immediate environment of the sensor [Ozy12]. If the device is moved in a field, free of artificial magnetic distortion, it should only measure the influence due to the earth's magnetic field. An ideal device would measure a constant value for the field strength, no matter in which way it is oriented. In other words, holding the device, such that the full earth field has only influence on the z-axis, should provide the same result on the other axes, when rotating it to the corresponding one. So in the end by measuring the earth magnetic field at various positions and plotting it, should result in a perfect sphere, centered at the origin. Due to the hard iron distortions the sphere is not

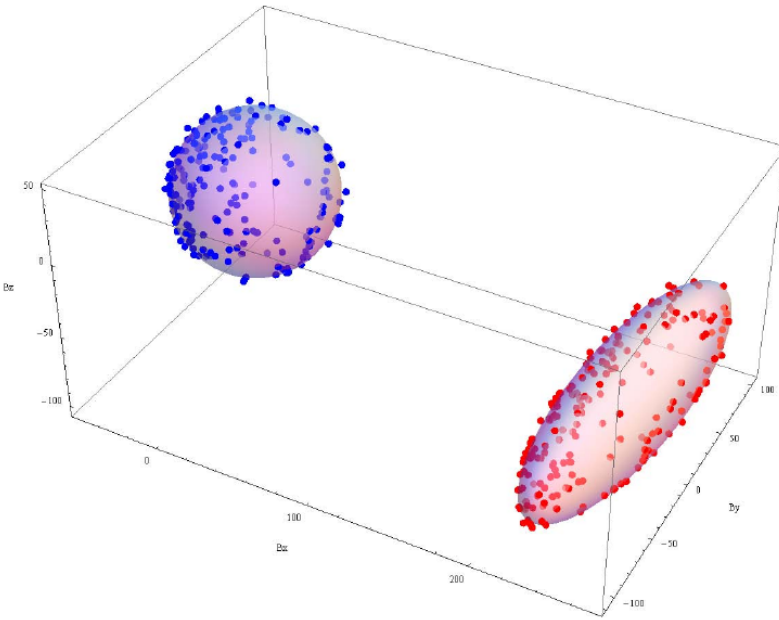


Figure 4.5: The plot shows the obtained sensor values for the earth magnetic field, by moving the sensor in space. The ellipsoid on the right side shows the influence of hard and soft-iron distortion coefficient. The red dots represent the uncalibrated measurements. The sphere around the blue dots on the left displays the calibrated, perfect sensor values [Ozy12].

perfectly located at the center. This effect is produced by materials, exhibiting a constant additive field, like wires or small ferromagnetic components, placed onto the PCB [Kon]. Soft iron effects however, cause that the shape of the sphere is deformed to an ellipsoid. They are induced by materials, influencing the pervasion of magnetic field lines and causing different gains on the axes. An example would be metallic materials such as iron or nickel. So in the end the shape of the expected sphere is more like an ellipsoid, shifted from the origin. A visualization can be seen in Figure 4.5.

The static hard-iron effects can be modelled as an offset H , shifting the magnetic values. The soft-iron effects are represented by a 3×3 matrix W , transforming the sphere into an ellipsoid. So in order to describe the measurement of a sensor in absence of artificial magnets, one could utilize the following model for the observable distorted magnetic flux density of the earth:

$$\mathbf{B}_{\text{earth}} = W^{-1}(\mathbf{B}_{\text{meas}} - H) \quad (4.3)$$

To determine and overcome these two distortion factors, several methods exist. For a naive approach, the offset parameters H can be determined like the following. One takes the average between the measured maximum and minimum along one axis. Equation 4.4 shows this exemplary for the x -axis.

$$\text{off}_x = \frac{x_{\max} + \text{abs}(x_{\min})}{2} \quad (4.4)$$

The six soft-iron parameters can be specified, by performing an ellipsoid fit. However, by using a more naive approach, one could perform a trivial compensation of those. The influence of the soft-iron distortion can be modelled as a one dimensional vector, increasing or decreasing the overall measured field along one axis. For this, the average amounts of the obtained magnetic field, representing the “radius” of each axis are determined. Those three values are averaged, to return the overall radius rad_{avg} . Equation 4.5 show how to derive this scaling factor for the x -axis.

$$\begin{aligned} rad_x &= \frac{x_{max} - x_{min}}{2} \\ rad_{avg} &= \frac{rad_x + rad_y + rad_z}{3} \\ scale_x &= \frac{rad_{avg}}{rad_x} \end{aligned} \tag{4.5}$$

Kok et al. [KHS⁺12] follow a more elaborated approach, by applying an elliptical fit in combination with measurements of inertial sensors. This approach also cares for the alignment of the magnetometer sensor axes with the ones of the gyroscope and accelerometer. Since only the magnetic sensor is used for the further experiments, this can be neglected. The Application Note 4246 by Freescale [Ozy12] presents a good and interesting calibration procedure. They reduce the determination of the three hard- and the nine soft-iron factors to four parameters. This is utilized, by assuming that the hard-iron offset dominates the soft-iron effects and one is trying to minimize the error between the measured field B_{meas} and the real, surrounding field B_{earth} . For this, they take a whole series of measurements into account, and not just the minimum and maximum, like for the naive approach in Equation 4.4. As a result, one gets a vector with the three offset values H and the flux density of B_{earth} .

In the end, independent on how the sensors get calibrated, this routine has to be performed for each sensor to get the individual parameters. Due to the performed calibration procedure, the measurement range of the sensor is slightly varied. As an additional step, the sensors have to be scaled to the same measurement range.

4.4.2 Cancellation of the Surrounding Earth Magnetic Field

The magnetic models, introduced in section 3.2 describe the influence of the magnets at a certain position and orientation, relative to the sensor. Another observation proven in that chapter is that multiple magnetic fields sum up. On earth we focus a static surrounding magnetic field, going from the south pole to the north pole. Depending on the position at the planet, this value ranges from 25 - 65 µT. This field cannot easily be shut down and automatically contributes to the sensor measurements. However, for a proper interpretation of the surrounding field, solely determined by the permanent magnets, the earth field has to be eliminated. For a

system with static geological sensor position and orientation, this would be trivial. One would just measure the field without any artificial magnets around and subtract this from every ongoing measurement. Obviously, the geological position and orientation of the human hand during normal tasks is naturally not static.

By knowing the orientation of the system and the corresponding earth magnetic field, it should be possible, to eliminate this offset. The following cancellation process is utilized, to get the earth magnetic field, relative to the sensor position:

1. Hold the hand with the sensors attached in a stable and calm position
2. The magnets for the fingertips are absent
3. Measure the orientation R_I of the sensors and the corresponding surrounding earth magnetic field B_{earth}
4. After this calibration phase, one tracks the orientation of the hand R_h
5. Calculate the relative orientation $R_d = R_I - R_h$
6. Convert R_d into a rotation matrix rot_d and apply this to B_{earth}
7. Subtract the rotated earth magnetic field from your actual measurement, s.t.

$$B = B_{meas} - rot_d \cdot B_{earth}$$

As stated in section 4.3 the used sensor breakout comes with a full 9 DOF IMU. With such a system the orientation can be estimated. The Madgwick filter [Mad10] is a widely used method for deriving the absolute orientation of a body in space, by using gyroscope, accelerometer and magnetometer data. However, this estimation uses the earth magnetic field, to compensate sensor drifts and to align its orientation, relative to it. So by introducing artificial magnets, which are stronger than the earth magnetic field, the Madgwick filter could break down and therefore the calculated orientation can drift. In subsection 5.2.2 the evaluation of this approach is shown.

4.5 Magnetic Field Interpretation Towards Finger Pose Reconstruction

For the following section it is important to note, that the Cartesian coordinate system, introduced in section 4.2 and visualized in Figure 4.3 is applied. It represents the orientation of the sensor frame. The following two sections show how to calculate the three dimensional magnetic field value $B(x)$ for the finger state vector x . As mentioned in section 4.2, the position of the sensors P_{sensor} , the lengths of the phalanges and the static positions of the MCP joints P_{MCP} have to measured very exactly, to get a proper value for the expectable magnetic flux density for a certain finger pose.

For describing a magnetic flux density with the dipole model (Equation 3.1), introduced in section 3.2, one has to define the vectors \vec{r} and \vec{h} accordingly. The

derivation of those two for a certain finger state x , according to the kinematic chain is described in section 4.2 (see Equation 4.1 and Equation 4.2). For describing the magnetic flux density of a certain finger state with the cylindrical bar magnet model, some further adjustments have to be done. Since the model uses cylindrical coordinates (z, ρ, φ) , the Cartesian (x, y, z) of the sensor and magnet positions have to be transformed. One also has to note, that the values, calculated by this model assume, that sensor and magnet are aligned equally and refer to the same coordinate frame. Since the magnet is rotating around the y - (by flexion-extension) and z -axis (by adduction-abduction) and the sensor keeps its static orientation on the back of the hand, the alignment of the two components relative to each other changes. To overcome this, the Cartesian values of the distance vector \vec{r} have to be rotated about the orientation of the magnet. The following formulas describe the required rotation and transformation adjustments:

$$\begin{aligned}\vec{r}_{rot} &= rot_y(\theta_{MCP} + \theta_{PIP} + \theta_{DIP}) \cdot rot_z(\phi) \cdot \vec{r} \\ &= rot_y(\theta_{MCP} + \frac{5}{3}\theta_{PIP}) \cdot rot_z(\phi) \cdot \vec{r} \\ z &= \vec{r}_{rot}[0] \\ \rho &= \sqrt{\vec{r}_{rot}[1]^2 + \vec{r}_{rot}[2]^2} \\ \varphi &= \arctan(\vec{r}_{rot}[1], \vec{r}_{rot}[2])\end{aligned}\tag{4.6}$$

Those values can now be applied to Equation 3.4 and Equation 3.5 to obtain the cylindrical magnetic flux density. In order to transform those components back to Cartesian again, the following calculations have to be done

$$\begin{aligned}B_{x_{rot}} &= B_z \\ B_{y_{rot}} &= B_\rho \sin(\varphi) \\ B_{z_{rot}} &= B_\rho \cos(\varphi) \\ B &= (rot_y(\theta_{MCP} + \frac{5}{3}\theta_{PIP}) \cdot rot_z(\phi))^{-1} \cdot B_{rot}\end{aligned}\tag{4.7}$$

As already depicted in section 3.2, the exact solution of a CEL is not trivial to calculate. Bulirsch et al. [Bul65] describe some approaches in their work to approximate the result. They extend ideas of Landen and Gauss for the solution. The used calculation algorithm can be found in [DO10]. Since it is a numerical approximation it uses a loop, to terminate at a certain accuracy level. This induces, that the function can not be further treated as a natural equation, when it comes to further differentiation.

4.6 Hand State Estimation

Assumed is a system with K magnets and N sensors. So the objective is to track K fingers, by taking the measurements from N sensor units into account. The

beforehand models for deriving the magnetic flux density are referred equally as $B_n(x_k)$ representing the field at sensor n , excited by the state vector x_k of finger k . Since magnetic fields sum up, for $K > 1$, this is a cumulative sum over all the presented magnets, being

$$B_n = \sum_{k=1}^K B_n(x_k) \quad (4.8)$$

for sensor n . Since the state x_k consists of 3 values, the complete system state vector has a shape of $(3 \cdot K) \times 1$ and is denoted by

$$\begin{aligned} X_K &= [x_1 \ x_2 \ \cdots \ x_K]^T \\ &= [\theta_{\text{MCP}_1} \ \theta_{\text{PIP}_1} \ \phi_{\text{MCP}_1} \ \theta_{\text{MCP}_2} \ \cdots]^T \end{aligned} \quad (4.9)$$

the overall calculated magnetic flux densities corresponding to the complete system state X_K by the N sensor units is

$$\begin{aligned} M &\equiv [B_1 \ B_2 \ \cdots \ B_N]^T \\ &= \left[\begin{array}{c} \sum_{k=1}^K B_1(x_k) \\ \sum_{k=1}^K B_2(x_k) \\ \vdots \\ \sum_{k=1}^K B_N(x_k) \end{array} \right] \\ &= M(X_K) \end{aligned} \quad (4.10)$$

The actual obtained measurement of sensor n is denoted by \tilde{B}_n , the measurement array of all sensors N has a shape of $(3 \cdot N) \times 1$ and is represented by

$$\begin{aligned} \tilde{M} &\equiv [\tilde{B}_1 \ \tilde{B}_2 \ \cdots \ \tilde{B}_N]^T \\ \text{with: } \tilde{B}_n &= [\tilde{B}_n(x) \ \tilde{B}_n(y) \ \tilde{B}_n(z)] \end{aligned} \quad (4.11)$$

In order to derive an estimate of the system state X_K , one can formulate an optimization problem. The objective function $f(X_K)$ for the minimization between the actual sensor measurements and the state representation of the model is described by:

$$f(X_K) = \frac{1}{2} \|\tilde{M} - M(X_K)\|_2^2 \quad (4.12)$$

It is formulated as a least squares problem and therefore tries to minimize a scalar, by taking the L2 norm. The corresponding optimization problem is defined by:

$$\begin{aligned}
 & \underset{\mathbf{X}_K}{\text{minimize}} && f(\mathbf{X}_K) \\
 & \text{subject to} && 0 \leq x_1(\theta_{MCP}) \leq 1/2 \cdot \pi, \\
 & && 0 \leq x_1(\theta_{PIP}) \leq 110/180 \cdot \pi, \\
 & && -30/180 \cdot \pi \leq x_1(\phi_{MCP}) \leq 30/180 \cdot \pi, \\
 & && 0 \leq x_2(\theta_{MCP}) \leq 1/2 \cdot \pi, \\
 & && \vdots \\
 & && -30/180 \cdot \pi \leq x_K(\phi_{MCP}) \leq 30/180 \cdot \pi
 \end{aligned} \tag{4.13}$$

The inequality constraints represent the natural range of motion for each finger. The determinedness of the system is dependent on the number of sensor measurements taken into account. The solvability and the uniqueness of the result for this minimization is dependent on the determinedness of the system. To gather unique solutions, the system has to be fully determined ($N = K$). Since one is trying to estimate the pose of four magnets, by also using four sensors, this condition is fulfilled. For minimizing such a function, one has to remember the mathematical form of the introduced magnetic models. The dipole model includes nonlinearities, the cylindrical model in contrary is solved by a numerical approximation, which in return means that differentiation or further mathematical operations can not be applied. Since the programming language *Python* [FP91a] is used to solve this problem, it is referred to methods provided by the *SciPy* [FP91b] package. The included *minimize* method comes with several user definable options, to provide the solver with additional information. In subsection 5.6.1 the used optimization methods are explained and the performance and quantity of the results are compared. Anyway, to speed up the computational time for solving the equations and the optimization problem, the functions are implemented in Cython [RB07]. This interface allows to write C-like Python code and to work with predefined variables.

4.7 Visualization

Another part of the system is the visualization of the estimated states. On the one hand, the values could be displayed with a graph. This way is very good, to get an accurate insight in the outcome of the estimation phase and for comparing it to ground truth data. However, this approach is not very intuitive and for untrained people, like patients of a clinical study not very helpful. For this, an application with the Blender Game Engine [Ble94] is implemented, which displays a 3D human hand. A 3D visual hand model is utilized. It already comes as a rigged component, which means that the bone structure is already given. This eases the further manipulation and setting of the corresponding finger angles. The bending of a joint can be modelled by rotating the corresponding points of the model. Blender provides a Python

programming interface, for modifying and animating 3D models. The underlying Python script, changes the orientation of bones and concentrates on the very basics for representing the estimated states, by setting the corresponding finger angles. For communicating with the state estimation module, a simple text file is used. The real time state estimation writes its values each time at the very beginning of the file. This ensures to keep additional disk space on the executing system small, since only $3 \times K$ float values are written each step. The Blender Game is executed in a loop, constantly reading the first line of this file. To ensure transmission security, one has to note that the estimation phase should only be allowed to write complete lines, describing the whole actual state. Some screenshots of the application are provided in Figure 4.6

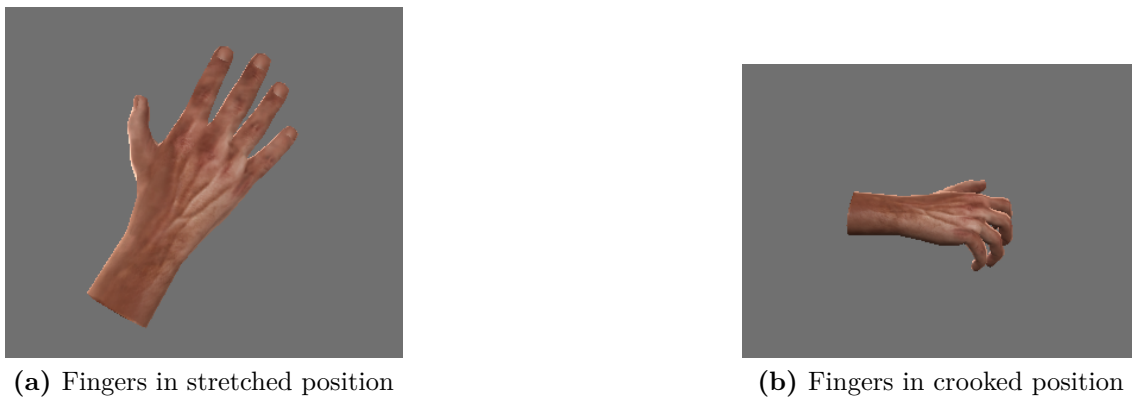


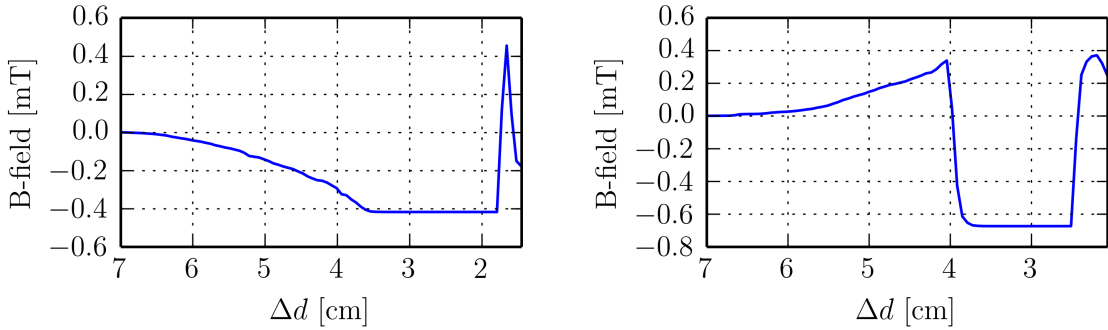
Figure 4.6: Screenshots of the visual representation with Blender

5 Results

5.1 Sensor Behaviour

The utilized LSM303D sensors show some general measurement characteristics. If they are exposed to a magnetic field, higher than the configured measurement range, a clipping of the returned value can be observed. In Figure 5.1 this effect can be seen for the values along the magnetic x -axis. The magnet is moved along this axis towards the sensor. One time with the magnetic north pole facing the sensor, the other time with the south pole. As expected, the measured field increases/decreases, by shrinking the distance Δd between sensor and magnet. Looking at 5.1a, approximately at a distance of 4.5 cm between sensor and magnet, the measured field reaches the current lower range. The sensor first stays a while on this value, before it clips to positive. By turning the magnet around 180° and therefore measuring an increasing magnetic field by the sensor, a similar behaviour can be observed. This time the clipping obviously occurs from positive to negative and happens at a gap of 4 cm (see 5.1b). Furthermore, this time the returned value clips directly and does not stay on a maximum value. To overcome this effect, one has to set the magnetic full scale range to an appropriate value. However, by setting for every user the maximum range of ± 1.2 mT, the precision of the measurements decreases. The approximately reachable maximum full scale range for one user can easily be determined. By simulating the range of possible flexion-extension, which would be performing a fist, and looking at the predicted outcome of the model, one gets an image for the expectable result of the magnetic field. From that the measurement range can be determined. However, due to the influence of surrounding magnetic fields, this value is only a guideline for the de facto measured field. Based on this context, the magnetic full scale range of the sensors for the ongoing measurements and experiments is set to ± 0.4 mT.

For evaluating the timing behaviour of the system, the code on the RFduino is debugged. As described in section 4.3, the sensor data rate could be set to a maximum value of 100 Hz, such that one could retrieve new magnetometer values each 10 ms. The switching and forwarding of the clock signal via the utilized multiplexer takes only 21 ns into account. This value composes a “break-before-make” pause of 6 ns, to prevent crosstalk between the channels and a propagation delay of 15 ns. In order to verify those values and to identify the overall time for acquiring, sending and receiving the measurement data, the respective code sections were timed. It is observed that the overall sampling frequency of the sensors can only be set to 50 Hz. The



(a) Moving the negative pole towards the sensor (b) Moving the positive pole towards the sensor

Figure 5.1: The magnet is moved towards the measurement unit, to record the clipping behaviour of the sensors. The distance from sensor to magnet is represented by Δd in cm. For the left figure, the overriding of the sensor begins at around 4.5 cm, for the right, this effect starts at 4 cm. The sensor range is adjusted to be ± 0.4 mT, which can be observed by the dataplots.

read out of the registers and the scaling for the hard- and soft-iron distortion values shows an insignificant influence on the timing. Furthermore it makes no difference whether only one sensor unit is read out, or all four, since they all show the same data rate and have measurements available after 20 ms.

The sending via BLE is implemented by the RFduino environment. The maximum transferable packet size is 20 bytes [RFd15]. The three float values of one sensor, plus an additional float for indicating the device number have a size of 16 bytes. The RFduino has implemented a queue of 20 bytes, to store the data till it is sent. The sending frequency depends on the distance between the host PC (which represents the client) and the RFduino module (which is the server). It is specified to range from 32 kbit/s to 24 kbit/s. In order to ensure that no data packet is overwritten, before it is sent, one has to check the size of the queue each time before writing to it. The client registers via the Generic Attribute Profile (GATT) protocol for listening to the notifications of the microcontroller. For the ongoing interpretation of the sensor values, only measurements from all four units are interesting, since in this way the most information about the actual system state can be represented. Therefore, for identifying the overall data rate, the time for receiving four individual data packets from the server is measured. It is observed that the receiving rate is not constant. For a sensor rate of 50 Hz approximately every 50 ms four new packets are received. This leads to a frequency of 20 Hz for the whole system. This high deviation from the actual possible sensor data rate is caused by the low sending frequency of the RFduino. Since the sensors are triggered with a frequency more than twice as high as the values can be received, their quality decreases. Therefore the data rate of the sensors is reduced to 25 Hz, in order to try to acquire more representative measurements. By doing this, the system frequency decreases to 12.5 Hz. However,

this leads only to slightly more representative measurements, since the frequency for receiving the obtained data packets is still twice as high as the sensor data rate. Those results were observed, by measuring the acquisition time of 200 packets (each representing the measurements of four sensor units). The stated system frequencies represent the mean over the 200 observed timestamps. Figure 5.2 represents the distribution of the measured duration for both sensor frequencies.

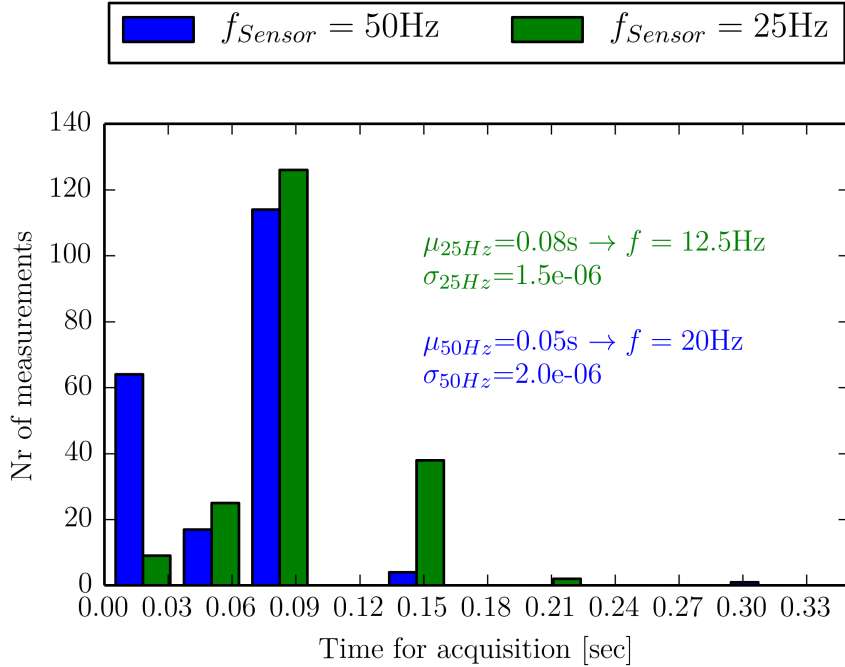


Figure 5.2: 200 sensor packets were timed. Each comprises the data from four individual sensor units. One time the data rate is set to 50 Hz, the other time to 25 Hz. The mean value for $f_{Sensor} = 25\text{Hz}$ is higher than, for $f_{Sensor} = 50\text{Hz}$. However, the variance of the acquisition time is smaller for this and therefore the outcome is more consistent. Moreover the sensor values from a data rate of 25 Hz represent the actual obtained measurements slightly better, than the higher data rate. In the ongoing evaluation, the results for both data rates are taken into account and compared against each other.

5.2 Quality of Calibration Procedures

5.2.1 Calibration for Hard and Soft-Iron Effects

Two methods are compared and classified for determining the hard- and soft-iron factors. One is the naive approach, declaring the distortion values by using the maximum and minimum of the obtained measurements for an axis. It is an often

cited and trivial method for compensating the distortion factors. On the other hand, the version from Freescale [Ozy12] which takes a whole series of measurements into account and only compensates for the hard-iron effects is implemented. 1000 measurements were collected, by rotating the sensor slowly around all possible axes. The environment is a normal lab, without any protections against additional, artificial magnetic fields. After all, the main observable influence on the measurements should still be caused by the earth magnetic field.

In Figure 5.3 the measurements of each axis combination are plotted in 2D for a clearer identification. The raw values are represented by the red dots, the calibrated by the green and cyan ones. The outline of the corresponding ideal sphere is visualized by the blue circle. It can easily be observed, that the hard iron effects dominate the soft iron factors. The scaling factors for the soft iron values, obtained by the naive approach also reflect this. They lie in the range of 1 ± 0.03 . Another fact is, that both calibration methods lead almost the same results. In order to compare the quality of the two calibration methods, the distance of each calibrated measurement value to the perfect sphere with radius B_{earth} is calculated. The deviation is plotted as a histogram in Figure 5.4. The obtained mean for the Freescale approach is calculated to be $\mu_{\text{Freescale}} = -0.02\text{mT}$, for the calibrated values, using the naive method to be $\mu_{\text{naive}} = -0.8\text{mT}$. So in the end the values adjusted by the Freescale approach represent slightly more the shape of a perfect centered sphere. One reason for this is, that for the used sensors the hard iron distortion effects dominate over the soft iron ones. Furthermore, since the whole measurement series is taken into account, the behaviour of the sensor is represented much better. The naive approach is very sensitive for noisy signals, since only the peak values characterize the calibration factors. One has to note, that those observations hold only for the used sensor units. For another PCB environment or device, the obtained values could be different and the soft iron factors could show a higher influence. For this, the naive approach would probably lead to better results than the Freescale. So in the end the calibration has to be verified and adjusted for the specific sensor and application.

The presented procedure was evaluated with several sensors, each showing similar and constant results. As already mentioned in subsection 4.4.1 this calibration procedure has to be performed for each sensor and the observed values should additionally be scaled to a common value for B_{earth} .

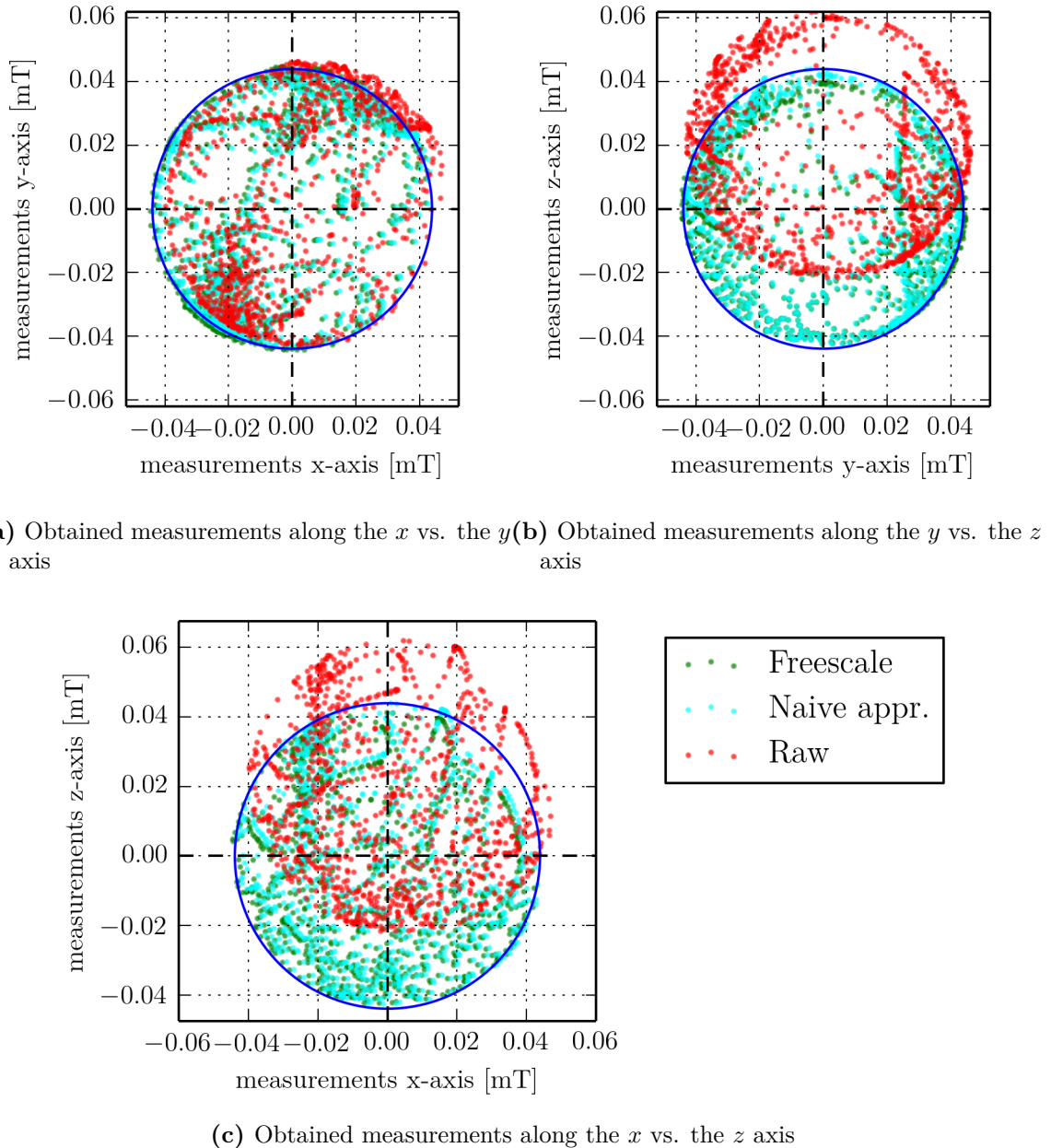


Figure 5.3: The measurements where recorded by rotating the sensor around each axis in an environment without artificial magnetic sources. 1000 measurements were collected. The obtained raw values are represented by the red dots. The results of the calibration procedures are plotted by the respective color. The perfect centered sphere is represented by the blue circle with $r = B_{\text{earth}}$. Already the unscaled values show only a very low influence of soft iron distortion. It is also observed, that the calibrated results do not differ much.

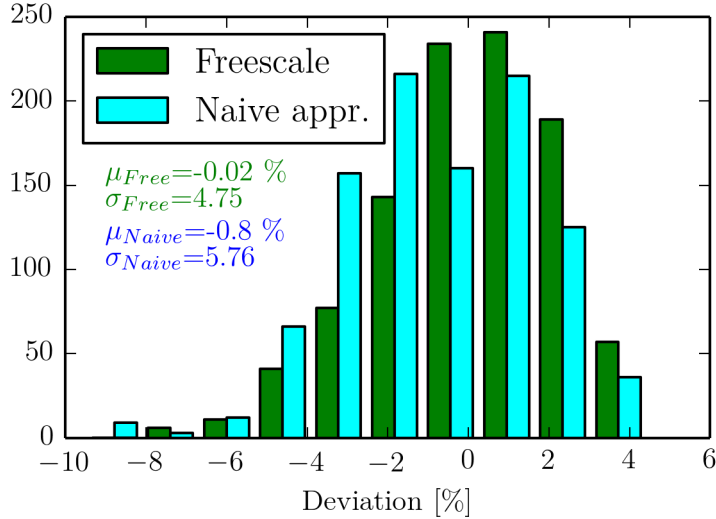


Figure 5.4: The procentual deviation of the two calibration methods to the corresponding perfect centered sphere is visualized. It can be obtained, that the Freescale approach leads to slightly more accurate results, since the mean and variance of the scaled measurements are smaller than for the naive approach.

5.2.2 Elimination of Earth Magnetic Field

Since a constant elimination of the earth magnetic field would be very important for a portable system, two methods of the approach, presented in subsection 4.4.2 are tested. The difference between those two lies in the determination of the sensor orientation. The one estimates it by using an implementation of a Madgwick Filter, provided by [mik]. This algorithm can directly be executed with the information of a single sensor device. The accelerometer and the gyroscope are already on the breakout board. So for this method, no additional sensors have to be mounted onto the sensor bracket. The other approach uses an additional IMU, which can output the orientation directly as quaternion. The MPU9250 from Invensense [Inv14] is used for this. This second method could lead to more exact orientation measurements, since the quaternion is calculated internally by the measurement unit itself. The orientation of the magnetometers relative to each other does not change, since they are placed inside the self designed bracket. Therefore it is sufficient, to determine the orientation of the sensor rack. For the implementation, follow the steps presented in subsection 4.4.2. As an intermediate step, the calculated relative orientation R_d of both methods was inspected and was proven to represent the truth.

As an early observation, the approach using the Madgwick filter is considered not to fulfil the needs. Since the readings of the magnetometer are used, for guaranteeing a stable and non-drifting estimation of the orientation, the artificial magnets interfere this algorithm. This was observed by a drift of the values over time, when

introducing the artificial magnets. So the further verification was only performed with the MPU9250 sensor, with whom this drift behaviour was not observed. Nevertheless it is mentionable that the upcoming results for cancelling solely the earth magnetic field (in absence of artificial magnets) were similar for both methods (beside the mentioned sensor drift). A proper working system should constantly return a magnetic field of almost 0 T, when it is rotated in an environment without artificial magnets. In order to verify this, the sensors are slowly moved around each axis. By comparing the results with and without the subtraction of the initially observed magnetic field, one should get an impression on the quality of the method. In Figure 5.5 the observed data of each axis is displayed.

The plot shows the measured magnetic field along all three axes for one sensor with

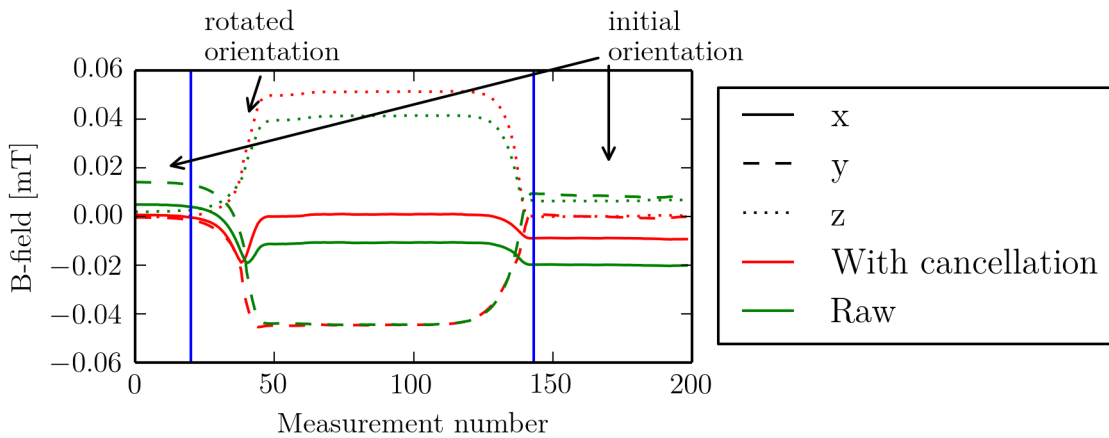


Figure 5.5: The result for the cancellation of the earth magnetic field, relative to the sensor rotation is displayed. One change in orientation is performed. The plot is divided into three orientation areas. The initial orientation at the beginning and end and a rotated orientation in between. That the surrounding magnetic field can be cancelled is shown if the sensor is orientated as introductory. However, the large deviations from 0 T during the movement in between the two orientation areas show, that the implemented approach does somehow not work for every rotation. As comparison, the raw values without subtracting the rotated surrounding magnetic field are also plotted.

and without subtracting the rotated initially observed field B_{earth} . It is visible, that unfortunately the elimination method does not work properly. At the beginning, the B-field with the cancellation is 0 T. However, by rotating the device, the observed field changes a lot. For the results along the x-axis, the offset can be compensated relatively good. But for the values observed along the y- and z-axis, this does not hold. By moving the sensor in its starting position again, it can be seen that the surrounding field is eliminated pretty well again. So the dynamic behaviour of the implemented approach is not good. This short example visualizes only a simple movement around one axis. Even for this, the surrounding magnetic field can not

be eliminated. Small changes could be claimed upon calibration errors or small static magnetic sources in the environment, such as cell phones or metallic objects. But the observed deviation from 0 T is much higher than this. So in the end, the surrounding magnetic field can not be cancelled with the presented method. Further investigation has to be done for this. However, since this work focuses on the evaluation for pose estimation with magnets, the cancellation of the earth magnetic field is left by that. For the ongoing evaluation, it has to be noted, that the sensors and therefore the hand is always held static. The influence of the surrounding magnetic field can then be seen as an offset which is statically subtracted.

5.3 Evaluation of the Magnetic Field Models

In order to verify the two introduced models for describing the magnetic field of a cylindrical bar magnet with real measurements, a trivial movement is inspected. The sensor is placed at the origin and the magnet is moved along its x -axis. The motion is performed from a distance of $x = 6\text{cm}$ to $x = 13\text{cm}$. The cylindrical model represents the ground truth for the utilized case of a bar magnet. This is valid, since in this simple case the influence along the axis of magnetization wants to be measured. Therefore the complex cylindrical formula is reduced to the common known Equation 3.2. The results are plotted in Figure 5.6. Note, that the offset due to the surrounding magnetic field of the measurement data is removed beforehand. The plot shows pretty well that the two magnetic field models have the same behaviour and can represent the measurements quite good. The dipole model serves as a reasonable approximation. As the influence of the magnet goes further away, also the deviation from the cylindrical model decreases. The maximum error is 0.008 mT. For the measurements, the highest deviation is observed to be -0.045 mT . Note that the sensor values suffer from a not perfectly consistent moving speed and accuracy restrictions. This can be seen, by regarding the positions to the corresponding observed magnetic field. The by hand moved magnet shows a bit of a “delay”, compared to the cylindrical model. Therefore the observed differences from the simulated values should not be overrated.

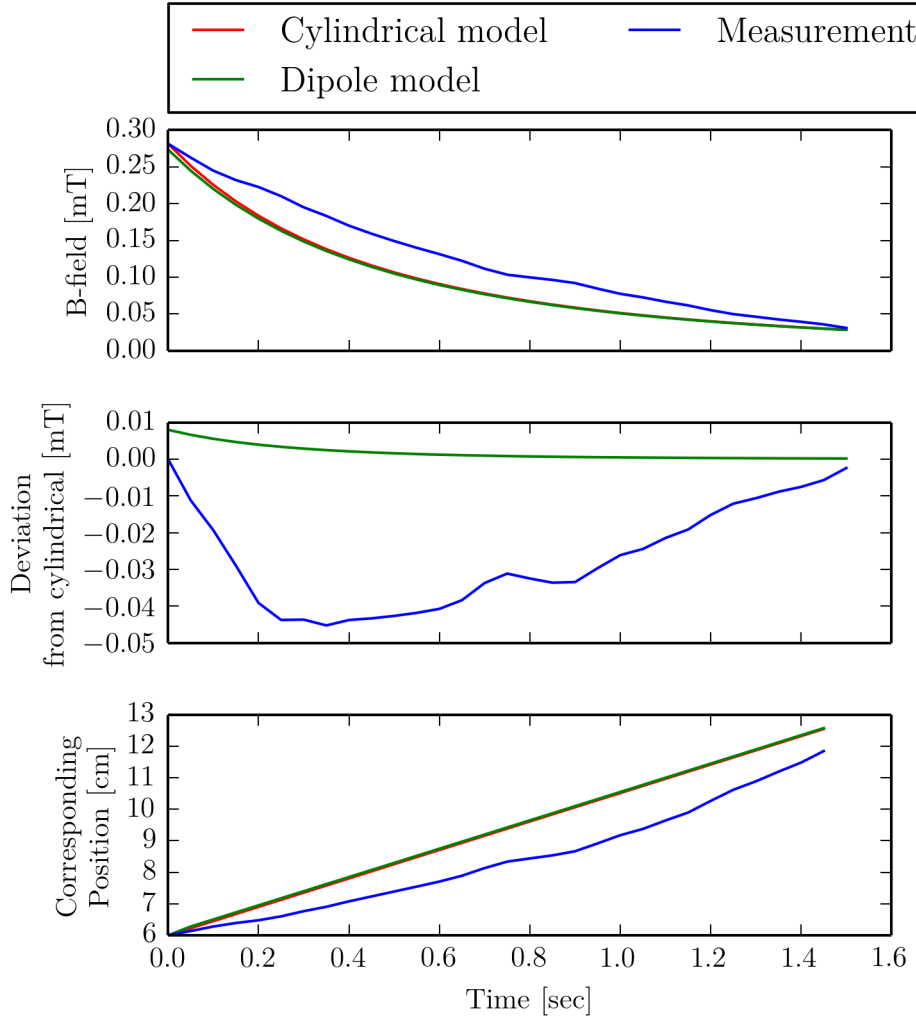


Figure 5.6: The magnetic field, for increasing the distance in x -direction from sensor to magnet. The values are calculated by the both magnetic model equations. The plot in the middle shows the difference of the measurements and the dipole model to the exact values of the cylindrical model. One can observe, that the error of the dipole model decreases over the distance. The error of the measurements should not be overrated, since the movement is performed by hand and a constant change in the distance x , as assumed by the models, is not perfectly performable. This can be seen by the lower plot, where the position to the corresponding observed magnetic field values is plotted. Furthermore the accuracy of the performed movement is also not perfect. The small deviations from to the predicted values show however, that both models represent the truth.

5.4 Evaluation of the Human Hand Model

A similar verification is done for classifying the measurements directly on the hand. Exemplary the bending of the index finger about 90° around the MCP joint is evaluated. For calculating the expected magnetic field at a single sensor unit for this movement, excited by wearing a single magnet on the fingertip, the hand parameters and positions have to be determined. Those are the bone lengths and the positions of the sensor and the joint. As already mentioned beforehand, those values are determined by hand with a calliper, what in turn introduces deviations from the actual real anatomic dimensions. So the predicted magnetic field calculated by the model equations is expected to show slightly different values as the actual sensor measurements. For the case of foreseeing the values, from a single sensor unit for one finger, the values to determine are the following: 3 bone lengths, one 3D position for the joint and one for the sensor, which makes in total 9 anatomic parameters. How good they can be measured and which influence they have on the predicted magnetic field is visualized in Figure 5.7a. It should be stated, that the actual behaviour over time should not be overestimated again, since the model assumes a constant motion velocity, which in turn cannot be achieved by a human. In the end, the difference between measured and predicted values should show a similar behaviour as for the trivial case presented in section 5.3. Beneath the predicted and de facto measured magnetic flux densities, the normed difference over the three dimensions is displayed. This should give an overall measure for the deviation of the measurements and the model results.

One can see, that the predicted and the measured values show a similar behaviour. But in the end, there is a high difference between them, especially for the values along the x axis. The highest observable divergence for the presented measurements and the applied anatomic dimensions lies at 0.019 mT. This shows that the hand determined parameters do not resemble the proband's hand anatomy good enough. Passing those sensor values to the minimization algorithm for the hand pose estimation and using the hand measured anatomic positions, no good results are expected to be observed. The obtained magnetic field is not representable with the model equations, using the underlying hand dimensions. However by remeasuring and adjusting the 9 dimensional parameters by trial and error, a set of satisfying values can be found. For the introduced easy case, a more reasonable magnetic field gets predicted for example by shrinking the length of the proximal bone by 3 cm. A measurement error of such a size is in turn not possible. Therefore to achieve a reasonable error compensation, all 9 dimensional parameters should be changed only up to a size of around 1 cm, which seems a more reasonable measurement error. However, performing this by trial and error did not lead to reasonable results. Especially regarding the overall goal to estimate multiple sensors with several magnets and introducing therefore even more anatomic parameters. Also attempts to estimate those parameters did not lead to reasonable results. For the presented case for one magnet and one sensor, nine anatomic parameters have to be estimated, with

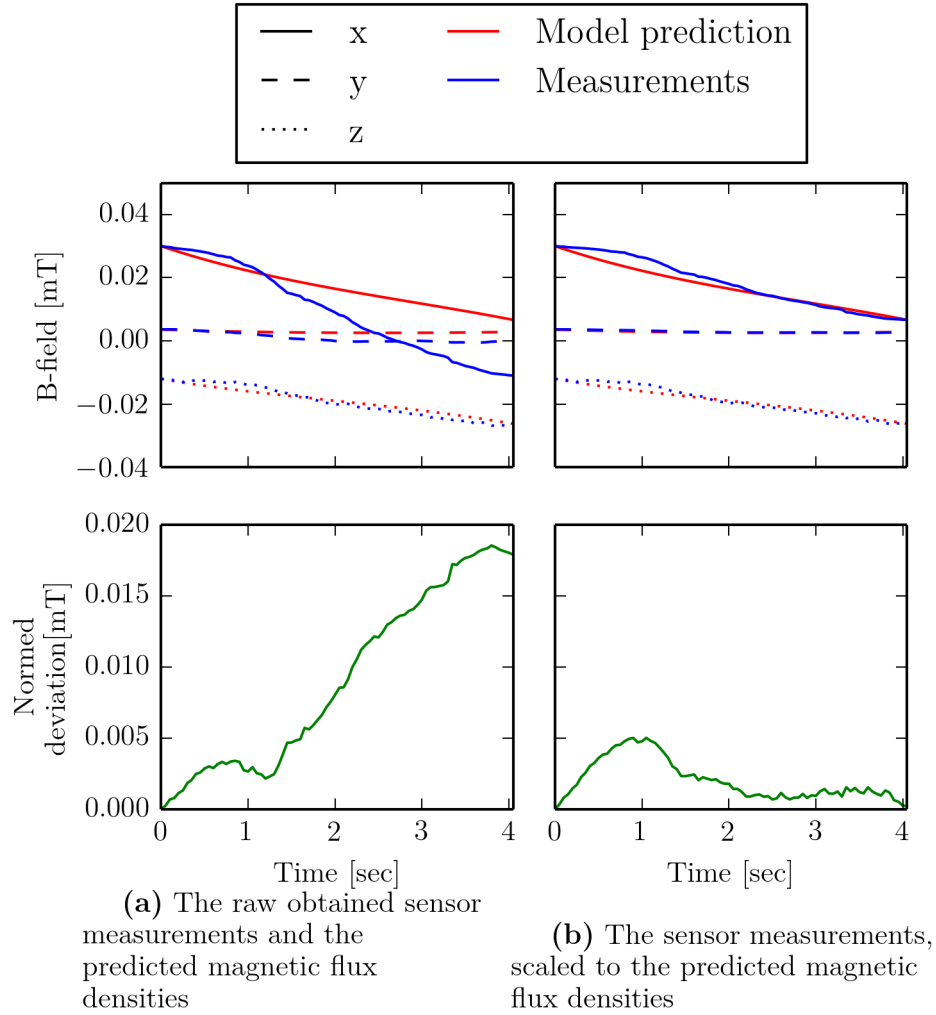


Figure 5.7: The difference between the model prediction of the magnetic flux densities and the actual measured sensor data can be seen in figure a. The values are calculated by using the hand measured anatomic parameters for the bone lengths, the joint and sensor positions. The high deviation from the measurements is not negligible. Passing the sensor values as is into the estimator for the finger state vectors would not lead to the representative angles. In figure b, the sensor values are naively scaled to the model prediction. With those measurements, adapted to the introduced fitting gesture, reasonable results for the state estimation are expected.

only a set of 3 measured magnetic flux densities. Additionally, one does not know the exact finger angles to the actual measurement and therefore also those states

have to be estimated. This brings in too much DOF and in the end the anatomic parameters can only be determined up to the non-satisfying accuracy.

A naive possibility to achieve at least a satisfying relationship between the measurements and the model predictions would be to scale the obtained sensor values along each axis to the respective predicted values. Of course, by this method the nonlinear influence of each of the dimensional parameter is dropped. However, Figure 5.7b shows that the difference can be reduced very efficiently for the introduced gesture of bending the MCP joint about 90° . The maximum error between the measured and the predicted values is now 0.005 mT. One could state, that this error is induced by the not constantly performed motion. Of course, the obtained scaling factors for each axis are only adapted to the performed gesture. However, it comprises the most expected movements, being the bending of flexion-extension. Another pose, to fit the measurements to, would be the bending of the fingers to a fist. By this calibration motion it is expected, to also compensate for the errors of the measured bone lengths. The suitability of the introduction of a fitting gesture, to naively scale the measured values to the error-prone anatomic parameters has to be evaluated with real measurement sets.

5.5 Expectable Magnetic Flux Densities

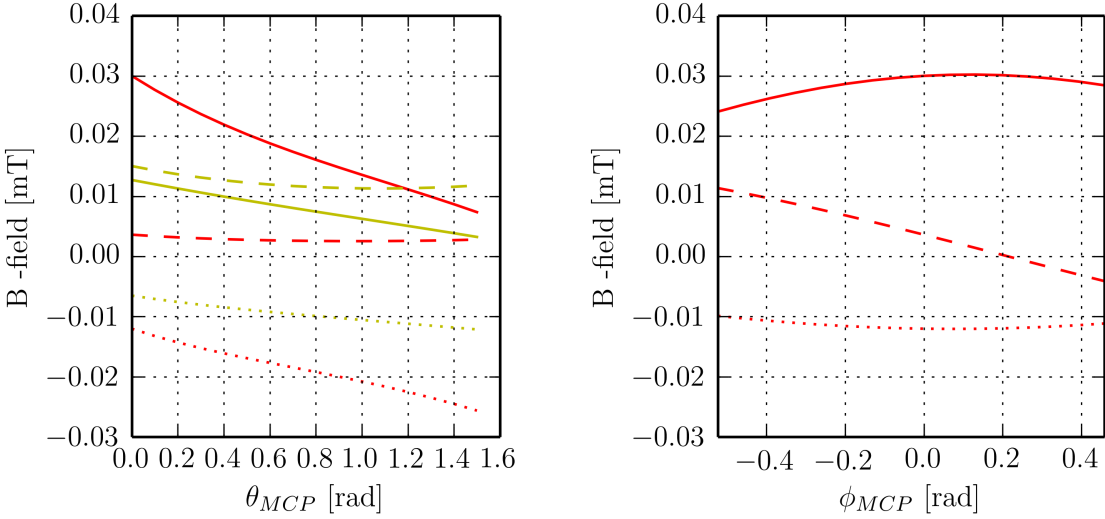
Nevertheless, by looking at the overall observed field for the individual measurement axes of the movement from beforehand, one could get an impression on the forthcoming observable magnetic flux densities. For a more natural picture of the observed magnetic field values along each axis, one could think of it as a vector in space, pointing from the magnetic south to the north pole.

The expected magnetic flux densities for the beforehand mentioned motion are plotted once more in Figure 5.8a. Since the gesture starts with a stretched finger, the biggest value for the magnetic flux density is measured on the x -axis. By bending the MCP joint around 90° , the influence on the x -axis decreases and on the z -axis increases. Remember, that the position of the magnet is moved towards the negative z direction, therefore also the observed values for this axis are negative. For the change of the magnetic flux density along the y -axis, only small changes are expected for the sensor beneath the index finger. This is only reasonable, since no lateral movement is performed and the sensor is almost directly beneath the magnet. By comparing those statements for the sensor under the index finger with the ones under the pinky, one could see the influence of different sensor positions. The values, expected for the unit beneath the index finger show higher changes along the x and z axes, than for the one under the pinky. The magnet is nearer to this unit and therefore this behaviour is only reasonable. For the expected measurements along the y -axis, the unit under the pinky finger shows higher changes, induced by the shift in this direction. Another observation, that can be made by this example is the range of the expected measurements. For these specific finger lengths and

sensor positions, the observable values lie in a range of $\pm 0.03\text{mT}$. This is a small range, especially compared to the range of the surrounding magnetic field, observed in subsection 5.2.1. The influence of this disturbing field along a single axis is measured to lie around 0.04 mT , which is as high, as the artificially induced field.

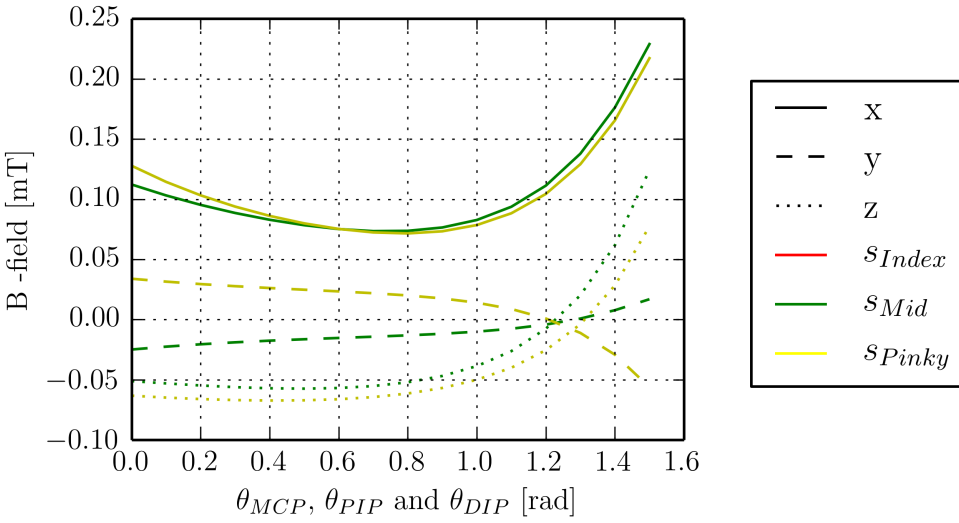
In 5.8b the influence of the maximum achievable adduction-abduction movement of the stretched index finger is visualized. Here, the main change of the magnetic flux density can be observed along the y -axis of s_{Index} . Since the movement happens only in the $x - y$ plane of the sensor, this is just reasonable.

As another example, the movement of the fist by all four fingers, each equipped with magnets on the fingertips is plotted in 5.8c. Note, that the values for the MCP, PIP and DIP are increasing simultaneously for each finger at the same time. The values, observed by s_{Middle} and s_{Pinky} are plotted exemplary. As mentioned beforehand, the values, especially observed along the x - and z -axis first go into the negative direction and then increase to the positive. This is because the magnet first is moved “away” and then gets nearer to the sensor units again. Along the y -axis, once more the influence of the sensor position is observable. The unit beneath the middle finger is influenced by magnets to the left (positive y -direction) and to the right (negative y -direction). The one beneath the pinky finger has only magnetic influences to the left of it. This is why the curve for the observable magnetic field along the y -axis is in the end slightly increasing for s_{Middle} and decreasing for s_{Pinky} . Another influence on this behaviour are the lengths of the bones, and therefore the overall distance, determined by the fingers. So for another constellation of hand parameters, the overall magnitude of the observed values could decrease or increase. Furthermore, one could note, that the overall observed magnetic flux density by four deployed magnets is around 10 times higher, than measuring only a single magnet. By the introduced sensor rack, a constant localization of the measurement units relative to each other is given. Therefore the observable behaviour and influence of the individual magnets compared to each other can be seen as kind of a characteristic for the performed finger motion. So by comparing the differences between each observed sensor measurements, one could make a first statement about the finger poses. By introducing more sensor units at various positions, one would expect to get better results for the estimated pose, since each pose causes an individual magnetic field at each sensor. Last but not least, this is why the group of Ma et al. is using six sensors in total, to estimate the position of a single magnet. Since the goal of the underlying thesis is to utilize a flexible and wearable system, only four sensor units are used. The presented claim is proven throughout simulation and real measurements. The results are given in the following chapters of this work.



(a) Bending only the MCP of the index finger. The values for the sensors beneath the index and the pinky finger are displayed. Only one magnet on the index fingertip is utilized.

(b) Simulating the maximum movement of adduction-abduction of the index finger. The measurements, observed by the sensor beneath the index finger are plotted. Only one magnet on the index fingertip is utilized.



(c) Bending the MCP, PIP and DIP of the four fingers simultaneously about 90°. The measurements, observed by the sensor beneath the middle and the pinky finger are plotted. All four fingers are equipped with magnets.

Figure 5.8: The anticipated values for various sensor positions, predicted by the cylindrical model for wearing one magnet on the index finger (a, b) and four magnets (c). It is observable, that the predicted fields are distinguishable among the different sensors. Even the slight movement of adduction-abduction causes a remarkable influence.

5.6 Pose Estimation

5.6.1 Identification of the Minimization Process

5.6.1.1 Utilized Minimization Methods

The size and complexity of the minimization problem, as described in section 4.6, is dependent on how many finger states K should be estimated with which number of sensors N . The beforehand introduced minimization problem Equation 4.13 is stated here once again for clarity:

$$\begin{aligned} \text{minimize}_{X_K} \quad & f(X_K) \\ \text{subject to} \quad & 0 \leq x_1(\theta_{\text{MCP}}) \leq 1/2 \cdot \pi, \\ & 0 \leq x_1(\theta_{\text{PIP}}) \leq 110/180 \cdot \pi, \\ & -30/180 \cdot \pi \leq x_1(\phi_{\text{MCP}}) \leq 30/180 \cdot \pi, \\ & 0 \leq x_2(\theta_{\text{MCP}}) \leq 1/2 \cdot \pi, \\ & \vdots \\ & -30/180 \cdot \pi \leq x_K(\phi_{\text{MCP}}) \leq 30/180 \cdot \pi \end{aligned}$$

Remind, that the overall size of the observable measurements \tilde{M} is $(3 \cdot N) \times 1$ (with N being the number of sensors, taken into account) and the size of the system state X is $(3 \cdot K) \times 1$ (with K being the number of finger poses to describe). In order to gather a fully determined system, the number of used sensors has to be at least as high as the number of magnets. This means, trying to estimate the state of four fingers with only one sensor would lead to ambiguous results. Furthermore, the objective function $f(X_K)$ can be described by the dipole or the cylindrical magnetic model. The problem can be solved by applying the anatomic constraints as bounds or not. It is implemented with methods, provided by the *SciPy* package. It provides the *minimize* function, which is especially for solving scalar minimization problems. It can be invoked with different algorithms and their corresponding additional options.

The following explanations should give a short overview on the principle of the utilized minimization methods and why they were chosen. For further reading on numerical optimization methods, please have a look at the work of Nocedal et al. [NW06] (on which the following paragraphs are based).

For solving the problem without taking the anatomic bounds into account, the Broyden-Fletcher-Goldfarb-Shanno (BFGS) algorithm is used. It is an approximation of Newton's method, for finding a solution. Newton's method describes derivative based approaches, to find local minima around a certain initial guess X_0 . To find values for the variable X_K , which minimizes the outcome of the objective function $f(X_K)$, different search methods exist. The BFGS algorithm uses a line search approach to find the local minimum along a line, which is determined by the Jacobian ∇f and Hessian $\nabla^2 f$. The BFGS approximates the Hessian $\nabla^2 f$ and is

therefore called a quasi-Newton method. The derivative ∇f is updated at every iteration. To calculate it, the objective function is evaluated with a state having slightly different values, than the provided initial guess X_0 . An iteration step consists of finding a value x_{k+1} , which minimizes f . This is done till the gradient norm $\|\nabla f\| < \epsilon$, with ϵ representing the convergence tolerance. In other words, a solution is found, if the change in the value of $\|\nabla f\|$ is smaller than ϵ . As a characteristic of the BFGS method, only the first derivative needs to be approximated. The rate of convergence for the method is stated to be linear. The overall termination tolerance, defining the magnitude of $f(X_K)$ is denoted to be $1.0e - 07$. Shrinking this value, would lead to more exact results, but would also induce more iteration steps and therefore a higher computation time.

For solving the problem by taking the anatomic conditions into account, *SciPy* provides a method called Sequential Least SQuares Programming (SLSQP). The constraints can be passed in as a pair of (min, max) for each variable, and reflect hard bounds. The underlying principle is based on least-squares methods. Therefore the system has to be overdetermined or at least fully determined. It tries to fit the observed data (i.e. the measurements) to a given model, by adjusting the model parameters. This is actually often used for data-fitting. While a system state is desired and the model comes with no additional parameters, the method is used in a slightly different way. In contrast to the classic approach, the model is fitted to the measurement data. The parameters in this case are the values of the system state X_K . In the least squares sense, the sum of the errors between the model at state X and the measurements is squared and minimized. Exactly this is expressed by the objective function $f(X_K)$. Again, a starting point X_0 has to be provided. For identifying the direction of x in each iteration step, Powells method [Pow64] is used. This derivative free approach identifies independent convergence vectors for each variable. It can be interpreted as the approximation of ∇f . At each iteration step, those search directions are redefined and therefore the new system state can be expressed by a combination of them in turn. In order to bring in the constraints, f is modified to represent those restrictions as a non-negative least squares problem. As the name suggests, the restriction to the system state is the following $X \geq 0$. Those reformulations are done by the *SciPy* method, therefore no further adjustments to the model or the bounds have to be made by the user. In the end the recursion gets performed, till the termination tolerance for $f(X_K)$ is fulfilled. This value is again chosen to be $1.0e - 07$.

It should be mentioned, that for the implemented estimation routine, the initial guess X_0 is always chosen to be the state, estimated one step ahead.

5.6.1.2 Classifying the Methods with Simulated Data

In order to get an impression on the expectable results of the minimization method, it is tested with a simulated dataset. A self chosen predefined set of states is determined, which should represent the motion of the fingers. This sequence of joint

angles is simulated using the cylindrical model, to obtain the value of the expectable magnetic flux density, measurable by a specific sensor for the corresponding system state. The cylindrical model is used, since it represents the de facto magnetic flux densities, excited by the bar magnet. Those values for the expectable magnetic flux density are then passed to the minimization routine, to estimate the system states. The result of the minimization should of course reflect the predefined motion sequence. Therefore it can directly be compared to the known state values, to identify the quality of the solver and its behaviour.

As stated previously, there are several parameters for formalizing the estimation problem and to tune the solver:

- Expressing the minimization as an unconstrained (by using the BFGS algorithm) or constrained (by using the SLSQP algorithm) problem
- Considering the influence of the movement of adduction-abduction or not.
- Formalizing the objective function using the cylindrical or the dipole model.
- The behaviour regarding different determinedness of the system, which means estimating the states of one or multiple fingers by taking one or multiple sensors into account.

The results will be compared by calculating the mean and standard deviation of the error-norm to the perfect system state for each finger. Moreover, the calculation times of the different methods allow a conclusion to the number of needed iterations to find a solution.

As a first step, the different optimization parameters are evaluated for the movement of a single finger. Therefore the size of the system state is $X_1 = 3$ for taking ϕ_{MCP} into account and $X'_1 = 2$ for neglecting this state variable. The size of the simulated measurement vector is dependent on the number of sensors, taken into account. The index finger is chosen for evaluating the different parameters, but the results are expected not to change, by choosing a different one. The used gesture sequence is displayed for the three states of the index finger in Figure 5.9.

The angular change, and therefore the stepwidth between two states is determined by combining the observations for the angular velocity from Ingram et al. [IKHW08] and the data rate of the sensor system. An acquisition frequency of 20 Hz in combination with a mean angular velocity of $10^\circ/\text{s}$ leads to an observable maximum change of $0.5^\circ/\text{s}$ ($= 0.0085 \text{ rad/s}$). Therefore, the whole set for the utilized motion is divided into 1419 datapoints. For obtaining this number of simulated measurements by the sensor units, would result in a total theoretical duration of 70.95 s. The state values are plotted against time. The motion is constructed to represent simple and complex movements of the finger, including flexion-extension, as well as adduction-abduction. The motion sequence includes joint movements, which happen as unique motions at a time. For example between 0 s and 20 s only the MCP joint moves. Some, which arise together, like between 40 s and 60 s, where all three joints are performing flexion-extension. Also only small movements are simulated. Between 38 s and 42 s, θ_{PIP} and θ_{DIP} change only about 0.26 rad. The movement of

adduction-abduction is applied during a short sequence, since the range of movement is small and also occurs more rarely, compared to flexion-extension.

The obtained error means and standard deviations for each parameter combination

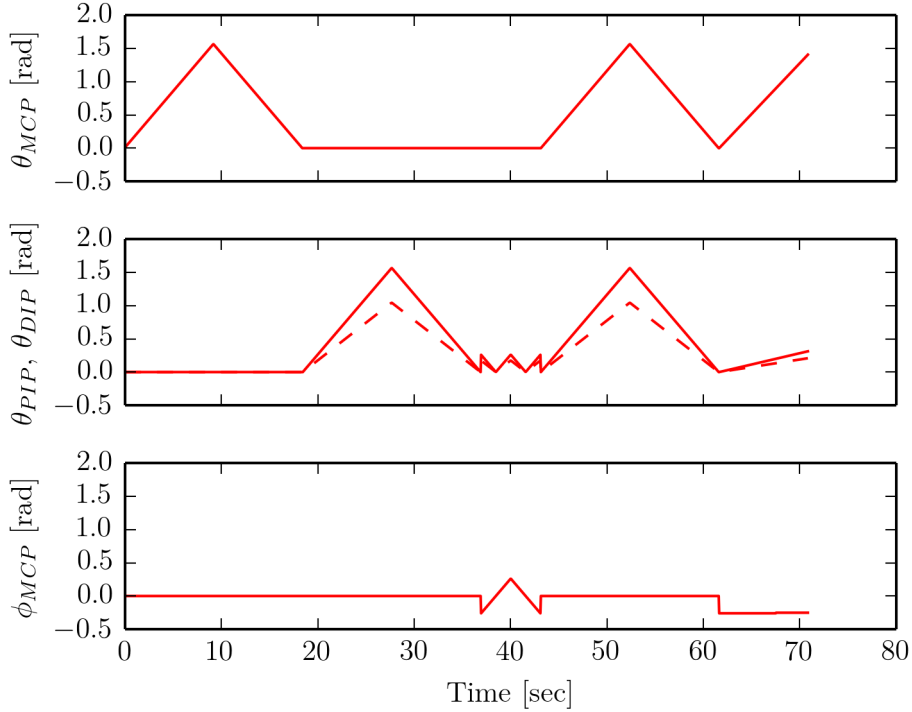


Figure 5.9: The introduced motion pattern for the estimation of the state vector for the index finger. For a better readability, the four states are divided into individual figures. The movements are chosen to test whether the estimation is capable of changes, happening to a single state or a combination of them.

are presented in Table 5.1 in radians. The numbers in the very first column indicate the combination of fingers and sensors. The first number represents the estimated finger state vectors K , which is for this comparison always one, since only the states of the magnet at the index finger are estimated. The second number represents the amount of simulated measurements N . By using only one simulated sensor reading, the unit beneath the index finger is meant. By taking two into account, the index and middle sensors are pointed. And four means that all four simulated units are regarded. The abbreviations in the second column reflect whether the movement of ϕ_{MCP} is regarded or not. “no ad-ab” stands for no adduction-abduction movement and “ad-ab” for the opposite.

One thing, that can be observed directly, is that for the case “11” which still represents a full determined system, the results show a very high deviation from the perfect values, regardless how the model is adjusted. The mean over all errors is 0.289 rad. The best observable values for taking only one sensor unit into account

		Unconstrained		Constrained	
		Dipole	Cylindrical	Dipole	Cylindrical
11	no ad-ab	0.194 ± 0.002	0.074 ± 0.001	0.367 ± 0.015	0.035 ± 0.000
	ad-ab	0.252 ± 0.003	0.257 ± 0.013	0.570 ± 0.020	0.570 ± 0.020
12	no ad-ab	0.124 ± 0.001	0.094 ± 0.001	0.052 ± 0.000	0.035 ± 0.000
	ad-ab	0.071 ± 0.000	0.000 ± 0.000	0.058 ± 0.000	0.000 ± 0.000
14	no ad-ab	0.112 ± 0.001	0.098 ± 0.001	0.040 ± 0.000	0.033 ± 0.000
	ad-ab	0.042 ± 0.000	0.000 ± 0.000	0.038 ± 0.000	0.000 ± 0.000

Table 5.1: The error mean and standard deviation for each tuning parameter of the minimization procedure are listed. The values are given in radians. “no ad-ab” means, that the used objective function did not comprise the state ϕ_{MCP} , vice versa for “ad-ab”. The system configuration is coded with the numbers. The first one stands for the size of the estimated finger state vectors K , the second for the number of simulated sensor units N taken into account. The best promising results are represented by the constrained methods, which take ϕ_{MCP} into account. It is also observable, that the system has to be overdetermined in order to lead to a good estimation of the system states. The minimization is performed on an introduced movement pattern for the index finger, whose values for the excited magnetic flux densities are simulated using the cylindrical bar magnet model. So only one finger state vector is estimated.

can be obtained by the method using the constrained cylindrical model and neglecting adduction-abduction. By regarding, that the inserted magnetic values were predicted by this model and that the overall system state is simplified, this seems reasonable. Furthermore, the constraints restrict the algorithm not to drift too far away. Figure 5.10 shows the results for this best guess and the deviation from the perfect values over time.

By deploying only one set of forecasted sensor values more ($N = 2$), the results get much better. The mean over all error means is 0.054 rad. Also the standard deviation is almost constant. One could even state, that by using all four simulated sensor units, the error does not decrease very much (the mean over all errors is 0.045 rad). Therefore it can be stated as a first observation, that the system has to be overdetermined. The objective function is described by more equations as there are variables to find. The solver is therefore directed into the right direction already by the additional system values.

By comparing the error from the objective function using the dipole model with the one formulated with the cylindrical, a decrease can be observed. As already stated for the “11” case, this just seems reasonable, since the magnetic flux densities were calculated by the same. However, for real observed measurements, this has to be further evaluated.

Also, while considering that the field values for the estimation still comprise the movement of adduction-abduction and since the ability to estimate the system state with a reasonable accuracy, the neglecting of those values just results in worse results. The biggest difference to the perfect values occur here at the time, the lateral movement is performed. The remaining parts, where ϕ_{MCP} is 0 are also almost perfect. By looking at the difference between the results of the constrained and unconstrained methods a slight decrease of the error if the constraints are obeyed can be observed. The algorithm shows better convergence by the deployed constraints. In the end almost fault free results can be observed by the cylindrical model, which takes the movement of adduction-abduction into account. Here it does not count too much, whether the minimizer is constrained or not.

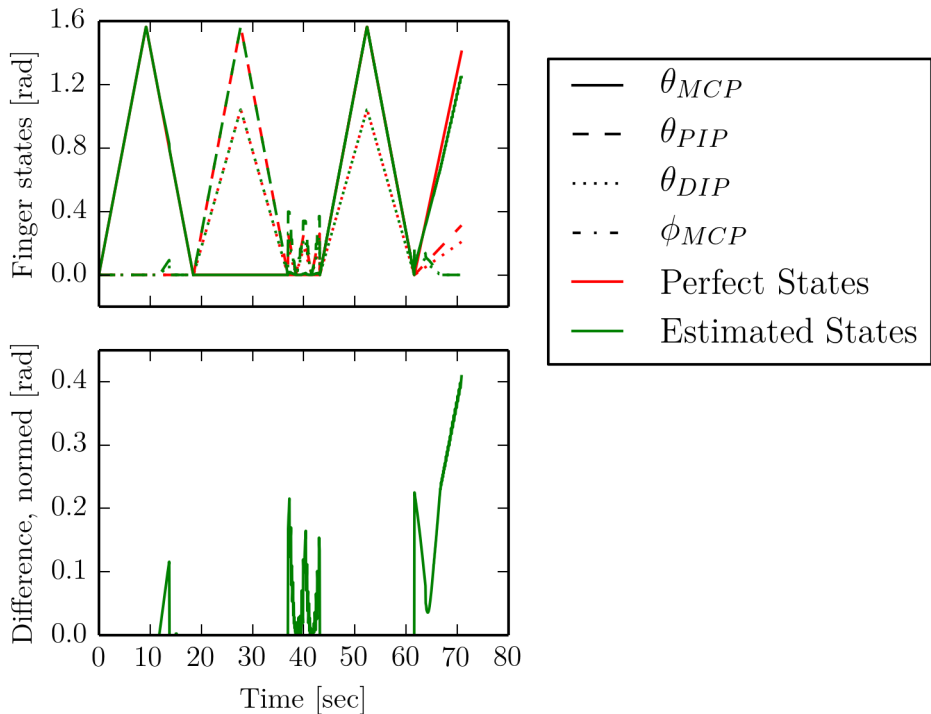


Figure 5.10: The estimated states and their deviation from the perfect values over time is displayed. The used objective function is described by the equation of the cylindrical model and does not comprise the state ϕ_{MCP} . Therefore the deviation around 40 s is acceptable. For the constrained minimization one sensor reading is used to estimate the pose of the index finger. This model represents the best expectable results for estimating one state vector with one magnet, with $\mu = 0.035 \pm 0.000$. At the end, the system tends to show bigger deviations from the perfect values.

In Table 5.2 the mean time, needed for one estimation cycle is listed in seconds. The computation time can be seen as a measure of how many iteration cycles are needed by the solver. It can be observed, that the time increases with the determinedness of

the system. This is only reasonable, since the algorithm has more equations to take into account and to evaluate. Also the constrained methods show a faster timing behaviour, than the unconstrained. As a reason the restricted search space of the solver could be mentioned. To reach a reasonable result, the solver needs less iterations. The reduced system state by neglecting the adduction-abduction movement is also faster than the model, comprising this state, what is because of the reduced system size. The objective function, formulated with the dipole model shows also a faster evaluation time, compared to the one using the cylindrical. Since the cylindrical model represents a numerical approximation, which has to be evaluated at each iteration, the time consumption for evaluation is higher.

By comparing the quality of the solver with its timing behaviour, it can be stated that an increase in precision comes with higher computation times. For this example, using the perfect simulated data for the magnetic field, the estimation is not always fast enough, to match the observed sensor system frequency of 20 Hz. However, it is evaluated, that the estimation results won't degrade drastically, if one or two measurements would be skipped, due to the computation time. The actually estimated system state is only used as initial starting guess for the next estimation. It is observed that the solver is capable to intercept changes of a minimum of $\pm 0.2\text{rad}$ between two measurements. So the initial starting point has a less important role for the solvability. For the assumed maximum angular velocity of 0.175 rad/s this change would reflect to a missing of one data set. What is more critical is the capability of estimating the state almost at real time. For the used simulated magnetic field values the best configuration for the minimizer to estimate the system state with an adequate frequency would be given by using the cylindrical magnetic model with adduction-abduction and taking the anatomic constraints into account. This would result in an estimation frequency of around 7 Hz, since the time needed to solve the problem is about 0.148 s. Compared to other hand tracking systems, this value is not good. However, for getting a rough feedback on the actual finger state, this value should be sufficient.

		Unconstrained		Constrained	
		Dipole	Cylindrical	Dipole	Cylindrical
	11	no ad-ab	0.037	0.077	0.008
		ad-ab	0.089	0.119	0.029
12	no ad-ab	0.063	0.139	0.014	0.031
	ad-ab	0.114	0.214	0.031	0.074
14	no ad-ab	0.110	0.251	0.025	0.059
	ad-ab	0.216	0.409	0.056	0.148

Table 5.2: The table allows a comparison of the mean evaluation time (in seconds), needed for the presented minimization methods for estimating one finger state vector. The time is displayed in seconds. Note the influence of using a constrained or unconstrained method. Also a reduction in evaluation time can be observed while shrinking the size of the measurement vector \tilde{M} . The fastest method shows an evaluation time of 0.029 s for estimating a single state vector. However, the quality of the results is not satisfying. For more exact estimated values, the time lies around 0.074 to 0.148 s. This results in low estimation frequencies, however an almost real-time-like representation should be possible.

For estimating the movement of multiple fingers, an adequate motion pattern is deployed. The simulated sequence consists only of 100 datapoints, reflecting a measurement time of only 10 s. This short time period is chosen, since first tests showed a high time consumption of the estimation stage. The utilized motion is visualized for each finger and each state in Figure 5.11. As visualized in the figure, the fingers are moving individually, to test whether the estimation is capable of that.

For getting an insight, how good the states for multiple magnets can be estimated, several sensor-magnet configurations are simulated. The evaluation is done for two fingers (the index and middle) and all four. As learned from the previous results, four sensors are used for the estimation of two fingers, to ensure overdeterminedness. However, for estimating all four finger state vectors, the introduced system can only satisfy determinedness. For reasons of completeness, four additional sensors were introduced to the simulation, placed behind the four existing ones, to achieve a value of $N = 8$. As for the estimation of one finger, the values are simulated using the cylindrical model. The results are listed in Table 5.3. The corresponding parameters are coded in the same manner as beforehand.

By looking at the results for the estimation of the state vectors for multiple fingers, a similar behaviour as mentioned for the fully determined case beforehand can be obtained. However, one interesting change can be observed. The unconstrained minimization method, described by the cylindrical model and taking ϕ_{MCP} into account shows here a better behaviour, than the constrained one. This is observable for each configuration of N and K . One reason could be, that the BFGS algorithm

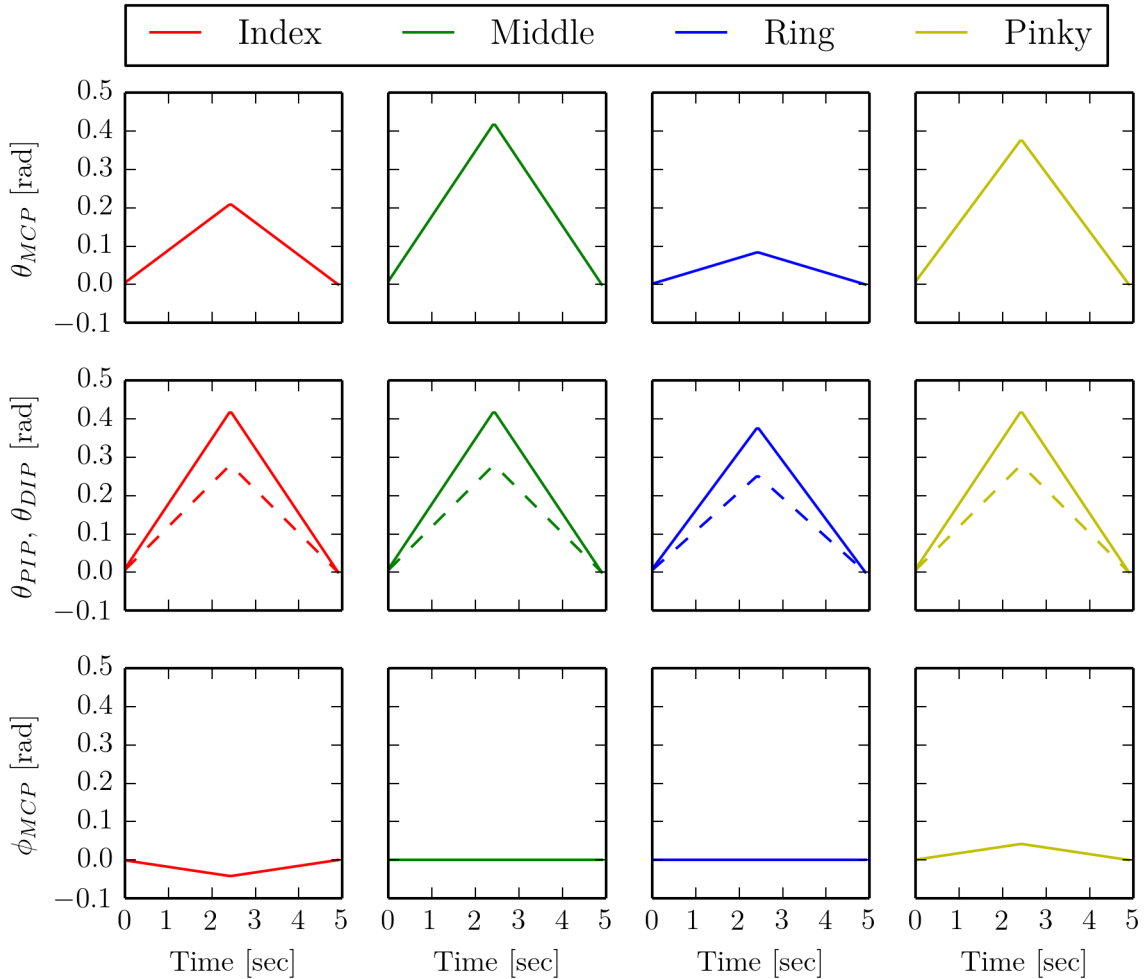


Figure 5.11: The introduced motion pattern for the estimation of the state vectors for multiple fingers. In each column the states for one finger are displayed. The motion is deployed to represent individual movements of the finger, to check whether they cause a reasonable influence on the magnetic field to be estimated. Therefore each finger state itself is slightly different to the other.

gives for those cases a better approximation for the search direction, than the constrained SLSQP method. With the increasing number of system states, also the complexity increases. The constrained solver reaches its bounds, by using not good enough search directions. The unconstrained method however has more freedom, to look in each direction. For the estimation of two finger states, the unconstrained method using the cylindrical model and taking ϕ_{MCP} into account leads to the best results. For the estimation of all four fingers however, the minimization is not capable to reflect the perfect system states anymore. The overall smallest error for the estimation of four fingers with four sensors is 0.024 rad. The information, provided by the simulated measurement units is not sufficient, to describe the variables. For the actually built system, comprising four sensors, an estimation of all four fingers

		Unconstrained		Constrained	
		Dipole	Cylindrical	Dipole	Cylindrical
24	no ad-ab	0.119 ± 0.000	0.081 ± 0.000	0.051 ± 0.000	0.039 ± 0.000
	ad-ab	0.114 ± 0.000	0.000 ± 0.000	0.085 ± 0.000	0.005 ± 0.000
44	no ad-ab	0.941 ± 0.006	0.484 ± 0.001	0.314 ± 0.000	0.216 ± 0.000
	ad-ab	1.361 ± 0.022	0.024 ± 0.000	0.223 ± 0.000	0.140 ± 0.000
48	no ad-ab	0.543 ± 0.001	0.509 ± 0.001	0.236 ± 0.000	0.183 ± 0.000
	ad-ab	0.494 ± 0.000	0.005 ± 0.000	0.385 ± 0.000	0.098 ± 0.000

Table 5.3: The error mean and standard deviation for the different system configurations and minimization methods in rad are listed. The values are given in radians. To achieve overall acceptable results, the overdeterminedness is again critical. The deployed system, consisting of four sensor units is therefore barely suited to estimate all four finger states which can be observed by a minimum error of 0.024 rad. As an extra, four additional sensor units were simulated. The results for this method show that it is in the end possible, to reconstruct four finger state vectors, as long as the system is overdetermined.

is expected not lead to reasonable results. For getting an impression on the estimated states, compared to the perfect ones, those obtained values are plotted in Figure 5.12.

However, by introducing four additional sensors (case “48”), the results are getting better. A mean error of 0.005 rad is observed by the unconstrained method, using the cylindrical model with adduction-abduction. However, as stated beforehand, the introduction of such a high number of magnets would break the goal of constructing a mobile and unobtrusive system.

By looking at the required estimation time of the several methods, a tremendous increase can be observed (see Table 5.4). This is not only due to more iterations, but mainly induced by the higher system states N and K . To still observe reasonable results of the estimated states, more than 1 s is needed. This can be observed by almost all minimization configurations. This means a proper real time evaluation of the finger pose estimation is not possible anymore. By increasing the number of sensors N to 8, about 17 s would be needed to achieve reasonable results, which is obviously far away from real time behaviour or acceptance for post processing.

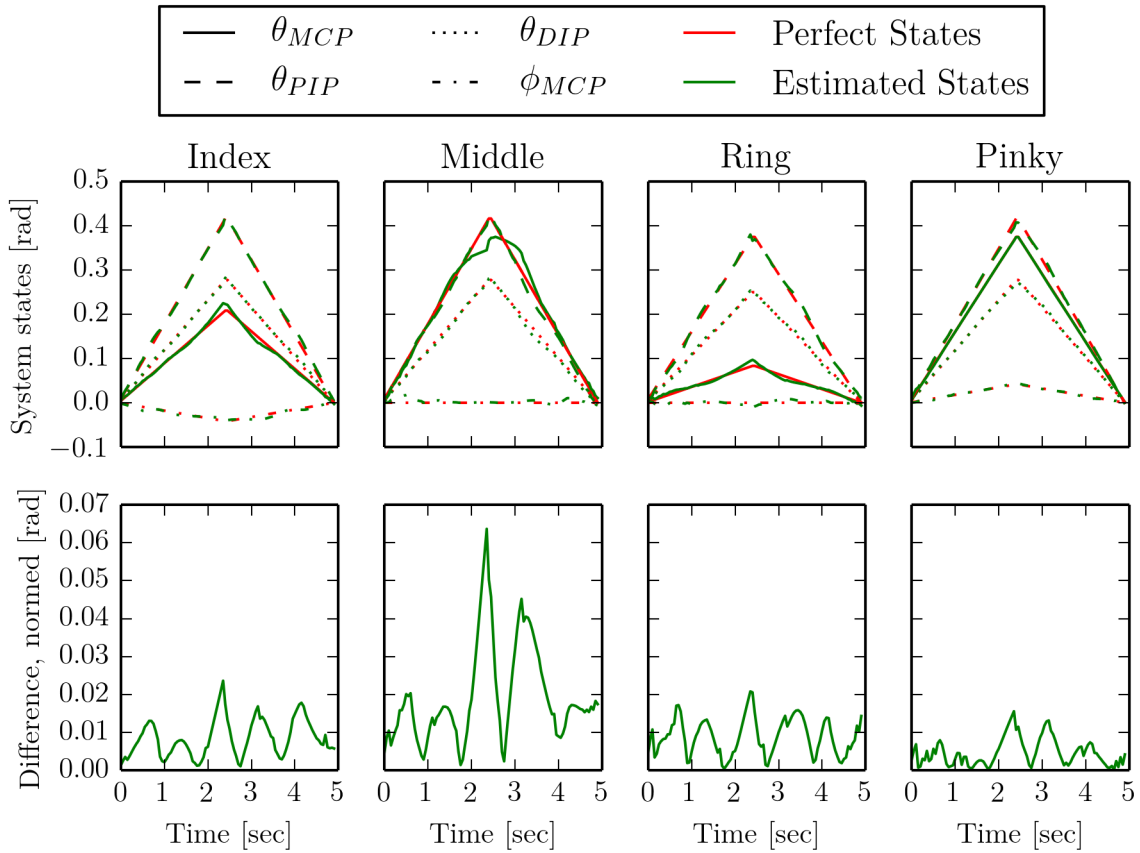


Figure 5.12: The displayed results are for the objective function which comprises ϕ_{MCP} and is formulated with the cylindrical model equation. The unconstrained minimization estimates on the base of four simulated sensor readings the state vectors of four fingers. The estimated and perfect states are plotted for each finger and their observed deviation over time. The mean difference over all for fingers is $\mu = 0.024 \pm 0.000$. The highest deviation can be recognized for θ_{MCP} of the middle finger. The states of the other fingers can be estimated pretty well.

		Unconstrained		Constrained	
		Dipole	Cylindrical	Dipole	Cylindrical
24	no ad-ab	0.920	1.632	0.291	0.382
	ad-ab	2.129	3.346	0.602	1.275
44	no ad-ab	3.365	5.012	0.629	0.947
	ad-ab	8.322	8.419	1.696	2.684
48	no ad-ab	7.130	9.670	1.137	1.988
	ad-ab	14.346	17.558	3.945	4.677

Table 5.4: The mean evaluation time in seconds for estimating multiple finger state vectors is listed above. It is observable, that the estimation of four fingers is far away from real time behaviour. This, in combination with the observations regarding the quality of the estimation, no good results are expected for real measurements. Only the estimation of the states for two fingers show adequate timing behaviour.

The presented results visualize the behaviour and influence of different system configurations N and K for different ways of describing the minimization problem. Note that the estimations are based on perfect, simulated magnetic field values. The following concluding statements can be derived:

- To get a reasonable accuracy for the estimated states, the system has to be overdetermined, i.e. $N > K$.
- The number of function iterations (and therefore the estimation time) increases significantly with the size K of the system state.
- An estimation of four fingers with the designed system, consisting of four sensors is expected to be barely possible in an adequate quality or real time behaviour.
- The state ϕ_{MCP} for adduction-abduction introduces higher estimation times, but can be estimated and should be used, to better reflect the human hand motion.

Since the results are based on perfect simulated magnetic flux densities from the cylindrical model, the estimation procedures comprising this model lead also to better results. It is evaluated, that the cylindrical method, including adduction-abduction and anatomic constraints leads to the overall best results for the estimation of one finger. However, when porting the observations to real measurements on a human hand, one has to note that several additional distortion factors are added to the system, like the inexact position information of the finger and sensor dimensions or the surrounding magnetic field. Therefore in the ongoing estimation of real datasets, the cylindrical and the dipole method (both including the state ϕ_{MCP} and constraints), are both used for the state estimation.

5.6.2 Results for Recorded Datasets

5.6.2.1 Recording Procedure

For the evaluation of the system at a real use case on the hand, the following setup is established. The proband wears the developed sensor unit and a number of magnets on the fingertips. The obtained magnetic field values are received and saved by a Laptop, to perform the state estimation phase afterwards. In this way specific parameters of the objective function or the system, like the number of sensor readings taken into account, can be adjusted later on and the results can be compared. The quality of the system is further compared to the Leap Motion [LM]. Therefore, the sensor data is recorded with the hand held above this device. For a rough qualitative judgement, a video of the performed movements is recorded. A poster with a circle and angular ticks is installed behind the motion area. A photo of the whole setup is shown in Figure 5.13. Each recorded dataset consists of the states, obtained by the vision based Leap Motion system and the sensor readings from the

measurement units. For the fitting of the sensor values to the hand measured joint and finger positions, each set comprises the introduced calibration gesture of bending the fingers around the MCP joints about 90°. Since the dynamic cancellation of the earth magnetic field is not possible with the method presented in subsection 4.4.2, the hand was tried to be held calm and at a constant position throughout the whole recording session. So in the end, by this setup a comparison between the presented magnetic approach and the existing vision based Leap Motion system is possible.

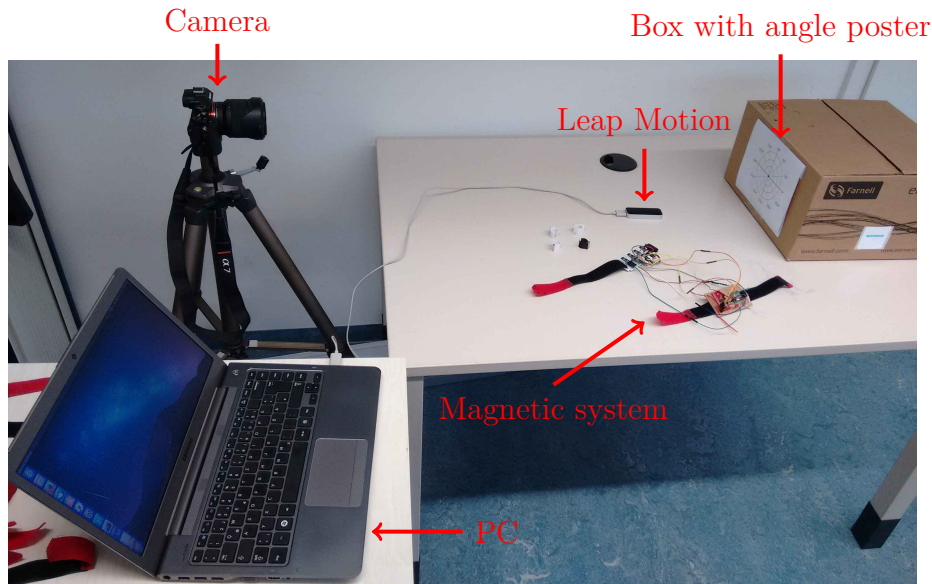


Figure 5.13: The measurement setup with all relevant parts.

5.6.2.2 Evaluation, Discussion and Comparison to Leap Motion and Video Data

The following paragraph presents and discusses the difference of the estimated states by the magnetic system with the data, returned by the Leap Motion. Both systems show different acquisition frequencies. While the magnetic system works at the evaluated 20 Hz, the Leap Motion shows a framerate of 110 Hz. For a direct comparison between the two systems, the data from the Leap is downsampled. For this, the magnetic and the Leap system save a timestamp, which represents the uptime of the system when the actual reading is observed. To adapt the Leap data to the magnetic system, only the data with the timestamp, the closest to the one of the magnetic system is chosen. This method was evaluated to do the resampling in a representative manner, without loosing too much information or degrading the data unintentional. The presentation and discussion is structured similar to subsubsection 5.6.1.2. So at first the state vector of only one finger (the index) is estimated. The observations, made in the previous chapters are deployed for the formulation of the ongoing estimation problem. Therefore the finger state vector includes ϕ_{MCP} and the results are

based on the minimization algorithm SLSQP, which takes the anatomic constraints into account. Therefore the results of six different combinations of formalizing the optimization problem can be compared and evaluated. Those are: Describing the objective function with the dipole or the cylindrical model and using the measurements of one, two or all four sensor units. The comparison to the Leap will show, which influence the determinedness of the system has on real measurements and whether the states could be better estimated by describing the objective function with the cylindrical bar magnet or the magnetic dipole model. Since the previous results on simulated data showed that only the estimation of a single finger state vector leads to reasonable outcomes, the emphasize of the evaluation is put onto the calculated finger states of the index finger.

15 datasets were recorded, each consisting of the state values, returned by the Leap system and the corresponding measurements of all four sensor units, excited by the magnet on the index finger tip. As already described, each set of obtained magnetic flux densities includes the initialization gesture, to compensate the hand measured system dimensions and to eliminate the surrounding magnetic field. Therefore, as an introductory step this movement has to be extracted to determine the scaling factors for each sensor unit, which have to be applied to the respective measurements. Based on those values, the states for the index finger were estimated. The difference vector to the states, returned by the Leap Motion system is calculated and normed for each estimated state, to get an overall measure for the deviation for each estimated set. Since the sets differ not only in the duration from each other but also by the speed and complexity of the performed movements, they have to be examined individually. Also if all sets would comprise the same length and the same predefined movements, a cumulative mean and standard deviation would not serve good and representative values for those. This is induced, since the system is conditioned by many external influences, like the often mentioned hand size parameters, the continuity of the hand's height and orientation and the speed and movement range of the motion. However, to proper evaluate the recorded sets and to compare them to each other, the method, showing the smallest error mean for one recorded set is determined. The results are listed in Table 5.5. For each set the best parameters of the optimization method are coded by *cyl/dip_ KN*, with

- *cyl* meaning that the cylindrical model and
- *dip* saying that the dipole model is used to formulate the objective function
- *K*, the number of finger state vectors to estimate and
- *N*, the number of sensors, taken into account for the estimation.

So for example “*cyl_12*” means, that the objective function is formulated with the cylindrical model for estimating one finger state vector ($K = 1$), by using the measurements from two sensor units ($N = 2$). In the case of $N = 1$, the sensor beneath the index finger is used, for $N = 2$, the one under the middle finger is added and $N = 4$ means that the measured values of all four sensors are taken into account. The time needed for the estimation of a measurement set is also reported.

	Method	$\mu[\text{rad}] \pm \sigma^2$
Set 1	cyl_12	0.581 ± 0.020
Set 2	cyl_12	0.587 ± 0.012
Set 3	dip_12	0.646 ± 0.010
Set 4	cyl_12	0.467 ± 0.017
Set 5	cyl_14	0.668 ± 0.027
Set 6	cyl_12	0.495 ± 0.011
Set 7	cyl_14	0.567 ± 0.026
Set 8	cyl_14	0.670 ± 0.052
Set 9	dip_14	0.606 ± 0.024
Set 10	cyl_14	0.581 ± 0.010
Set 11	cyl_14	0.603 ± 0.004
Set 12	dip_14	0.676 ± 0.022
Set 13	cyl_14	0.680 ± 0.018
Set 14	cyl_14	0.525 ± 0.010
Set 15	cyl_14	0.672 ± 0.012

Table 5.5: The table lists the methods, whose estimated states show the smallest difference to the one obtained by the Leap Motion system. The provided values represent the lowest mean and standard deviation in rad for each set individually. The states from the Leap system serve here as the truth values. The results for Set 3, estimated with the dipole model by using two sensor units shows the overall smallest difference to Leap system. It can be noted that the average error of those best estimated states is relative high. One has to note, that at each set different motion patterns were performed. Also the duration of each set varies. Therefore a direct comparison between them would not lead to a representative statement.

Here, almost no differences to the results, obtained in subsubsection 5.6.1.2 are observed. The timing behaviour of the slowest set was evaluated to be 0.092 s and is observed by a method using four sensor readings. This value is in fact higher, than the system frequency, but the results are expected not to degrade with a loss of measurement sets. Since by the recognized maximum evaluation time at most one data set gets neglected. Regarding the realtime capability, the respective worst estimation frequency would be 10 Hz. Since those results are not very surprising and were already discussed in subsubsection 5.6.1.2, the time values are not further explained here.

From Table 5.5, the observations regarding the formulation of the optimization method from subsubsection 5.6.1.2 are confirmed. The system has to be at least overdetermined, since no good results are reached by the method using only one sensor unit for the estimation. Also taking as much measurements into account as available leads more often to better results, than taking only two sensors into account. As an explanation one can name the same reason as before, the minimizer

has more information about the actual system state and can therefore find a more exact solution for the problem. However, 5 out of 15 sets show better results with $N = 2$, than with $N = 4$. Also the two sets with the lowest difference to the Leap states use only two sensor values. This can be put down to faulty measurements, induced by unstable positions and alignments of the hand during the data acquisition. By using faulty measurements it is harder to find a solution. Introducing a higher number of those leads to a worsening of the results. Therefore sometimes it is better to take less measurements into account, if one knows that they are bad. By taking more sensor units into account, one puts a higher trust into them. Regarding less, one relies more on the capabilities of the minimization method. In the end it's a trade off between both.

Moreover it can be stated, that the objective function, described by the cylindrical bar magnet model leads to better results as the dipole model. So it is verified, that this model describes the magnetic field, induced by a cylindrical bar magnet, better, than the approximation with the dipole model. However, 3 out of 15 datasets return better results for the dipole model. But by looking a bit closer to the errors, returned by the other minimization methods for these data sets, one recognizes, that the difference to the error, observed by a cylindrical method is only slightly smaller. For example for Set 3, the results for the *cyl_12* method are only worse by 0.008 rad.

So in the end, the smallest deviation to the observed states from the Leap motion can be provided most often from the highest overdetermined minimization method, formulated with the cylindrical model equation, *cyl_14*. In numbers: 8 out of 15 sets. However, set 4 is showing the smallest deviation over all recorded datasets and uses only two sensor units for the estimation (*cyl_12*). Set 4 shows a mean and standard deviation of $0.467\text{rad} \pm 0.027$. By regarding at the general quality of the states, obtained of the magnetic estimation versus the data from the Leap system, one can note that the errors are pretty high. The mean over all sets is 0.602rad , which corresponds to a difference of 34.5° . As mentioned beforehand this value has to be handled with care, since each dataset shows a different size and motions. That the presented magnetic system is despite that big difference capable to track the finger motions under certain conditions is further evaluated. It will be determined which motions and effects cause this high error value. For the visualization of the returned states of both systems, set 4 is plotted in Figure 5.15. An explanation to the magnitude and the characteristics of the differences is provided a bit later in this section.

As next step, the results for estimating four finger state vectors are presented. The recording procedure is done in the same way as for one state vector, beside that now each finger is equipped with a magnet on its tip. The estimated finger state vectors are each compared individually to the corresponding data of the Leap system. In this way, the means and standard deviations of the differences between the two systems are determined for each finger individually. Mind, that the state estimation problem has now the following size: $N = 4$, $K = 4$. As additional parameter for

the estimation phase, the problem is concerned to be constraint and to include the state ϕ_{MCP} . Only the type of the objective function is varied. It was evaluated, that the one, described by the cylindrical model leads better results, compared to the states observed by the Leap Motion. The mean values for the difference of each finger state vector to the Leap data and the corresponding standard deviation over the sets are presented in Table 5.6.

$\mu\text{rad} \pm \sigma^2$					
	Index	Middle	Ring	Pinky	Cumulative
Set 1	0.918 ± 0.053	0.975 ± 0.044	0.746 ± 0.029	0.709 ± 0.008	0.837 ± 0.000
Set 2	1.077 ± 0.039	1.066 ± 0.107	0.912 ± 0.043	0.618 ± 0.015	0.918 ± 0.001

Table 5.6: The mean and standard deviation from the obtained estimation results to the Leap Motion data. Four finger state vectors are estimated. Since the obtained results show such a big difference to the Leap data and the actual performed movement, only two datasets were recorded. The high values for the mean difference and standard deviation for each finger, show that an estimation of four fingers with the deployed system is not possible.

For the case of $N = 4$, only two datasets were recorded, since the results show similarities and the calculation time is quite long. For set 1 the average time per estimation step is measured to be 0.837 s, for Set 2 even 0.918 s were observed. Therefore an estimation with real time behaviour would not be possible anymore. While for the estimated results of one finger state, the difference to the Leap system is already pretty high, here a further increase is observable. The two sets comprise finger movements, which are performed simultaneously by all four fingers and alone, by only a single finger. In this way it can be checked whether the systems can distinguish between separate finger motions or not. The direct comparison of the two system states against each other shows that the magnetic estimation approach is not capable to identify individual finger movement reliably. Figure 5.14 tries to proof this visually. The norm of the states for the index and the middle finger, obtained by the Leap system and the magnetic estimation are plotted over time. The norm over all states for one finger is chosen, since it represents a measure for the actual predicted bending of the joints. In combination with the provided pictures, extracted every 5 s from the recorded videotream, Figure 5.14 serves as an example to proof, that individual finger movements can not be estimated reliably by the magnetic system. At the beginning of the short sequence, two movements which are performed by all four fingers were executed. Here the Leap and the magnetic system show both a change for the angles of the index and middle finger. Therefore both systems return in some sense the truth. The measurements of the magnetic system are fitted to the initialization gesture, which is performed around 5 s. However, when it comes to individual finger movements, the states for the presented fingers are estimated wrong. Around 20 s only the index finger is bent. This is captured

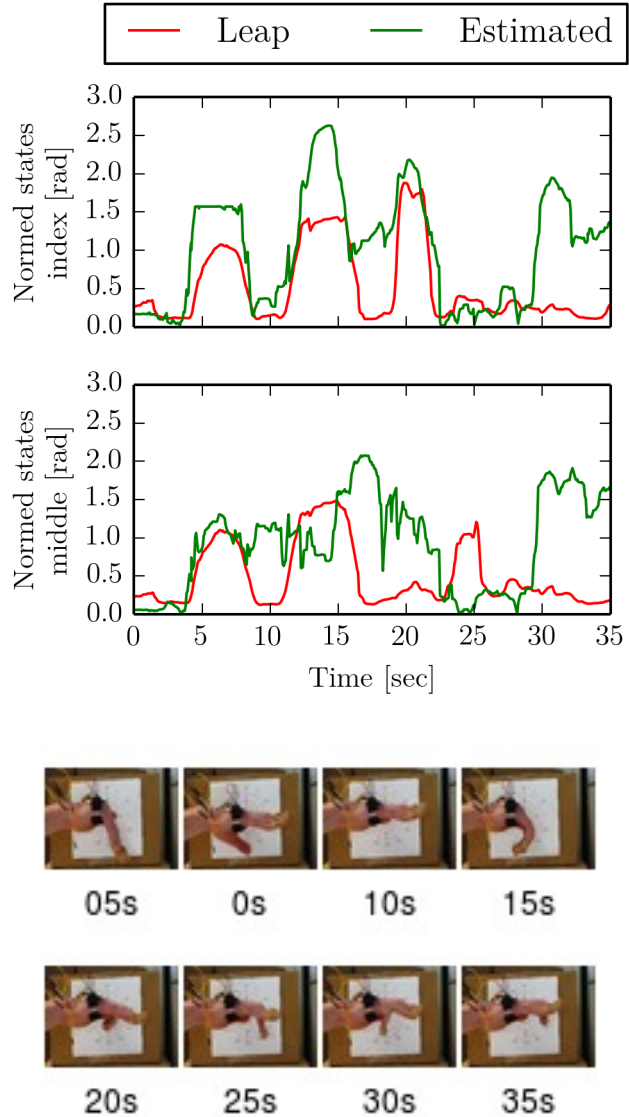


Figure 5.14: The norm over the states for the index and the middle finger are plotted. This should resemble a measure of the actual amount of bended angles of the finger, but does not reflect actual individual joint states. During the first 17 s parallel movements of all fingers are performed. Both systems show an increase for this. However, when it comes to individual movement of the fingers, the states of the magnetic system don't represent the truth anymore. At 20 s, the single flexion-extension of the index finger is also estimated for the middle. Furthermore between 30 s and 35 s, a movement of the pinky finger is performed, but the states are changing for the middle and index finger, which are held still. The states of the Leap motion system represent the truth much better. The pictures beneath the state figures serve as a rough visual reference.

by the Leap Motion correctly, since the state of the middle finger stays almost at 0 rad. Also the other finger states, which are unseen here for visualization reasons, are almost at 0 rad. The magnetic system however estimates an additional excessive change for the middle finger, which does not happen. During 30 s and 35 s a flexion-extension is performed by the pinky finger. However, the estimated states of the magnetic system during this time interval interpret a movement of the index and middle finger. The Leap system again reflects the right angles and shows only small changes for the two presented finger state vectors. This behaviour of the magnetic system can be obtained almost every time when individual finger movements occur. As a reason for the bad estimation results, one could head the following: On the one hand, the system is only fully determined, which degrades the results for the estimation, as observed in subsubsection 5.6.1.2. On the other hand, the obtained changes of the magnetic field, induced by the movement of a single finger are only small. The parameters for the hand dimensions can only be determined up to a certain accuracy, additional erroneous contributions are introduced. The optimizer tries to fit the values to a slightly different hand model and can not reach reasonable results. The estimated angles could be improved, by acquiring more exact values for the hand dimensions and by taking the readings of more sensor units into account. However, since the deployed system consists only of four sensors, this is not further evaluated. In the end the presentation of this short example for the results of estimating the states of four magnets by using four sensor units shows, that no truthfully values can be estimated for this system configuration.

The estimated values, obtained for the at first presented predictions of a single finger state vector showed a smaller difference to the states from the Leap Motion. On the basis of those recorded datasets and their results, a more detailed comparison to the Leap system is further presented, to identify the capabilities and drawbacks of the magnetic system. The reduced state size ($K = 1 \rightarrow \text{size}(X_1) = 3 \times 1$) allows an easier examination of the results and possible sources of error. The estimated finger states of dataset 4 showed the smallest difference to the angles obtained by the Leap system. The values for the finger state vector of both systems are plotted in Figure 5.15 over time. As a first impression and especially focusing on the values of θ_{MCP} , the two systems show a quite common angle prediction. The initialization gesture, which happens at the beginning at around 5 s, is responded by both systems as nearly a bare movement of the MCP joint. Only the Leap shows here contributions of adduction-abduction, which actually did not happen. This behaviour can be recognized right at the following gesture till 15 s, again. During this time, the beforehand mentioned movement is performed once again, just a bit slower. By regarding the magnetic estimation, some none smooth peaks for θ_{MCP} are observable over the whole set. They mainly occur, at the time, when a change of θ_{PIP} is estimated and the finger is bent to a fist. It is assumed, that at those points the solver can't find an optimal solution. It is also to note here, that for the estimated angles of the PIP and DIP the biggest differences between the two systems are observable. Note, that those two states are estimated as a combined one by the magnetic approach, since the

Anatomic condition $\theta_{DIP} = \frac{2}{3}\theta_{PIP}$ is used. The direction returned by both systems is the same, which means that both show a parallel increase or decrease of the angles. However, the states from the magnetic system are much higher than the ones from the Leap Motion. Furthermore, the movement of adduction-abduction shows remarkable differences. The estimated values of ϕ_{MCP} by the magnetic system show a more stable behaviour than the ones returned by the Leap. It should be noted, that during the movement of flexion-extension the motion was tried to be performed with very small lateral movement. Nevertheless for this state both systems show also similarities. For example between 40 s and 50 s, the motion in negative direction and back is captured by both systems. Also the other three finger states have almost no contributions during this time interval. The pictures which are extracted each 5 s from the video allow a qualitative comparison of the both systems.

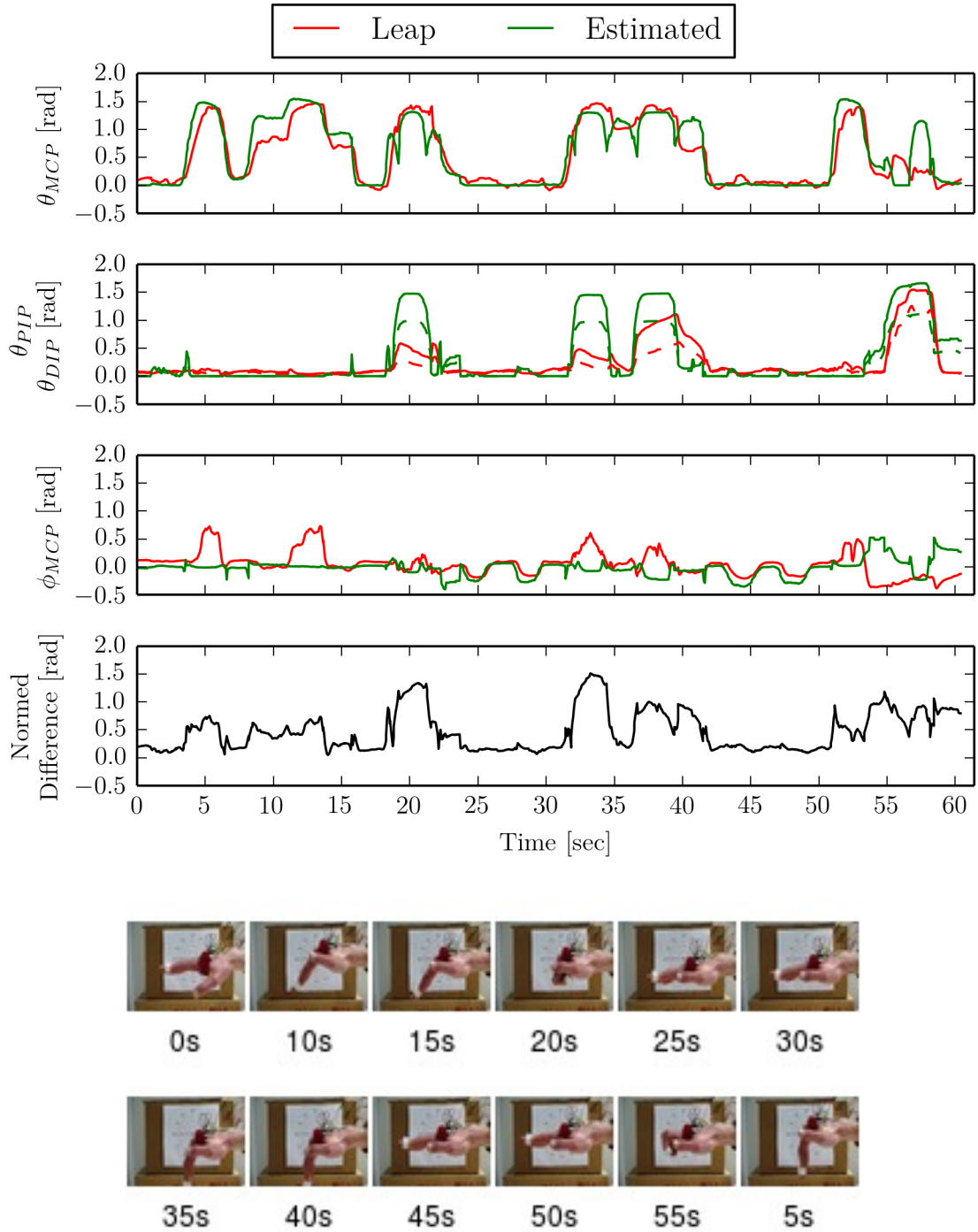


Figure 5.15: Each state value of the index finger, obtained by the Leap Motion and the magnetic estimation are plotted over time. The results are for set 4, which shows the smallest deviation between both systems. The values for θ_{MCP} show the most similarities. θ_{PIP} and θ_{DIP} show common directions, however the estimated states are much higher. For the movement of adduction-abduction the Leap Motion recognizes a more restless behaviour but they also have common phases. The difference, normed over all four states is plotted at the bottom. Here the differences for θ_{PIP} and ϕ_{MCP} show the highest impact.

For the presented dataset the estimation results were only compared to the Leap Motion, which is assumed to return the ground truth for the actual state. As already observed for set 4, those values are also not totally perfect and constant over time, which is shown for example by the very high lateral changes for ϕ_{MCP} in positive direction (at around 5 s and 12 s). The recorded angles indicate, that the bones move about 0.8 rad ($=45^\circ$) towards the middle finger, which was definitely not performed. Most of the datasets from the Leap show a high deviation for the state of adduction-abduction from the de facto values for this. For example in Figure 5.16 a similar behaviour during the movement to a fist is visualized. This time however the recorded contribution of ϕ_{MCP} at 14 s is negative. The observed values at around 20 s, where again the finger is bent to a fist, show a more or less small fluctuation and can therefore be stated as an evidence, that the false motion is not always detected. Over all the de facto performed movement did not comprise such high lateral motions. By the induced constraint and intuition from natural hand movement, it is accepted, that a maximum range of motion from -15° to 15° (-0.262 rad to 0.262 rad) is possible. During most of the time the recorded motions were performed to mainly show contributions of flexion-extension, therefore the view of the camera is also aligned to capture those movements best. Unfortunately, an exact value about the de facto size of the deviation from the real state of ϕ_{MCP} to the predicted cannot be stated. However, it can be stated, that the Leap shows here quite often values, which do not represent the truth. One reason for this could be the underlying method for the detection of the bone and hand directions. The Leap Motion provides normalized direction vectors for each finger and the palm. For calculating the angle of adduction-abduction from this, the angle between the direction vector of the proximal index bone and the palm, relative to the palm normal is determined.

Further, concerning the behaviour of the Leap system, one can head that a kind of relationship between θ_{DIP} and θ_{PIP} exists. In almost every set, a motion of the PIP joint introduces also a change of θ_{DIP} . In Figure 5.16 this behaviour is presented. The observed states for θ_{PIP} and θ_{DIP} are plotted over time with the corresponding parts from the video, placed beneath. As an additional verification to the before-hand mentioned false interpretation of the adduction-abduction angle, those states are also plotted. This observation should not be stated to be false or introduce erroneous system states. The developed magnetic estimation assumes even a static relationship between those two state values. The Leap system verifies this assumption in some way. As stated in section 3.1 it is quite usual to assume the observed relationship. However, from the information available for the Leap, a hard programmed explanation of this behaviour is not provided.

Another observation, by regarding the state vector for performing a fist from the Leap, is that the values for θ_{DIP} and θ_{PIP} are relative low and $\theta_{MCP} \simeq \pi/2$. For example at set 4 Figure 5.15 between 18 s and 22 s. When examining the video data qualitatively, one can recognize that the angle of θ_{DIP} and θ_{PIP} are actually higher than 0.5 rad. This can be explained by the fact of occlusion. While crooking the

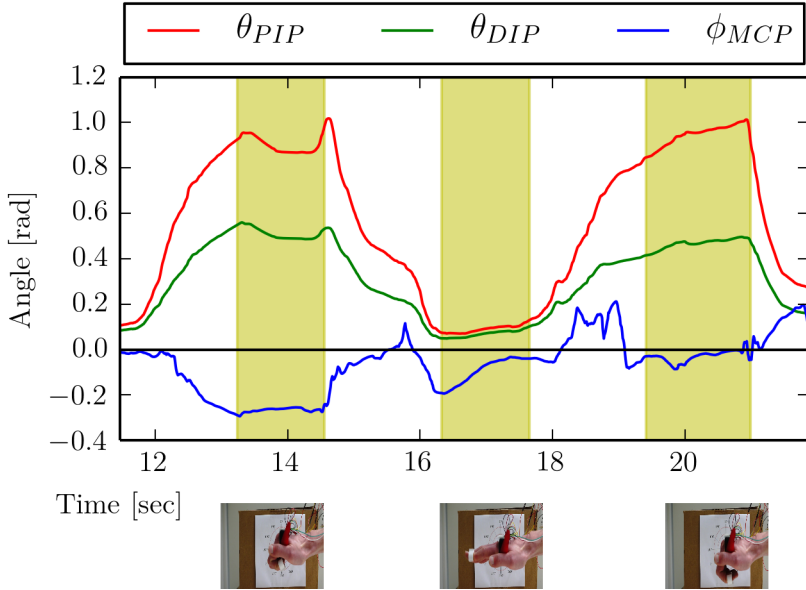


Figure 5.16: The states, provided by the Leap Motion for performing two times a fist. By regarding the flexion-extension angles for PIP and DIP, the introduced intra finger relation between those values is verified. However, the Leap system does not show a static relation between those two angles, as it is assumed by the magnetic estimation. The states of ϕ_{MCP} are provided additionally, to visualize once more, that this value often returns erroneous state configurations. During the plotted motion sequence a change of this angle about the observed amount was definitely not performed. While performing the second fist, only small false motions are observed and therefore show that the returned values are not always erroneous.

finger to a fist, especially the distal bone and the tip are hidden by the other bones. By comparing the estimated angle of the PIP joint from the magnetic estimation, one can judge qualitatively, that those reflect the real behaviour a bit better than the Leap. The presented observations for the predicted angles from the visual system prove, that it is also not totally free of errors. So one has to keep those presented drawbacks in mind, while examining the data from the Leap Motion system.

By checking the estimation results of the magnetic approach for all sets qualitatively with the Leap Motion and the recorded video data, one could determine some sort of gestures, which can be reconstructed relative reliable and correct. On the one hand the gesture, where the values were fitted to can be observed very stable along one dataset. This sounds only reasonable, since the obtained magnetic flux densities are adjusted right for this movement. Therefore all motions, which induce the most changes of flexion-extension on the MCP joint fall into this category, too. Those motions can be classified as “pre-states” of the initialization gesture and are therefore a subset of it. This is also observable by set 4, since at 10s and 5s the angle of MCP is estimated to be smaller 90°, which is also observed by the Leap and can

be verified qualitatively with the pictures. Furthermore, as already observed by set 4, a slow change of ϕ_{MCP} can also be tracked quite well. However, by assessing the results of other datasets, the reliability of the estimation for the lateral motion can not be generalized. Especially where the state of ϕ_{MCP} changes, while the MCP joint is additionally in flexion.

By adding the angular velocity and therefore the change over time as a parameter, some additional weaknesses of the developed system can be judged. With faster motions, the estimation results are getting worse. As already stated in section 5.1, the overall system frequency for acquiring data of all four sensor units is 20 Hz. As further introduced in subsection 5.6.1, the maximum detectable angular velocity was determined to be 0.5 °/s. Some recorded datasets include very fast finger motions, by which the maximum detectable angular change is exceeded. Especially for the estimation of small motions, like the reconstruction of lateral changes, an adequate number of measurements is important. A detailed statement for the maximum detectable angular velocity is not evaluated. However, with the provided video material, this could be a future task to be determined. In the end it can be stated, that rapid or staccato like movements can not be tracked reliably and the angular velocity has an impact, due to the overall system frequency. If the states would now also be estimate in real time, the overall results are expected to worsen only marginally, because the most time consuming part would still be the sensor system. Another, quite common observed behaviour of the system are the implausible values for θ_{MCP} . Some of those peaks are exemplary discussed for set 4 (Figure 5.15). However, by examining other datasets, this behaviour can often be recognized in an extreme variant, where the flexion-extension angle for the MCP joint even becomes 0 rad and stays at this value for some time. In set 5, such cases are detected. A sequence of the estimation results for the angles of flexion-extension is plotted in Figure 5.17. In the presented figure, the errors during the performance of a fist are not only just small fluctuations anymore. Here the estimated angle of θ_{MCP} goes to 0 rad and also stays there, while the fingers are bent. The plot represents two sequences for the flexion and extension for a fist and back. Each sequence is performed a bit differently, concerning speed and process. But as it can be observed, at a certain angle for θ_{PIP} and θ_{DIP} , the values for MCP become 0. This behaviour comes up, because the solver cannot find a solution within the provided bounds, for the actual system configuration. This can be traced back, to the erroneous dimensions for the provided hand model. As stated beforehand, the positions and lengths of the sensors, joints and bones can only be determined by hand and therefore errors are introduced to the hand model. The minimizer tries to find a solution for a hand with exactly those erroneous provided hand dimensional values. Since they represent not exactly the real hand, the solver cannot for every sensor value a suitable system state, for solving the problem. The initialization gesture, which basically should remove the surrounding earth magnetic field and scale the values exactly for those measurement errors, is performed by only bending the MCP joint and not the other two. For the case of bending the fingers to a fist, the false determined lengths of the bones are assumed to cause the most errors here. By regarding the results for

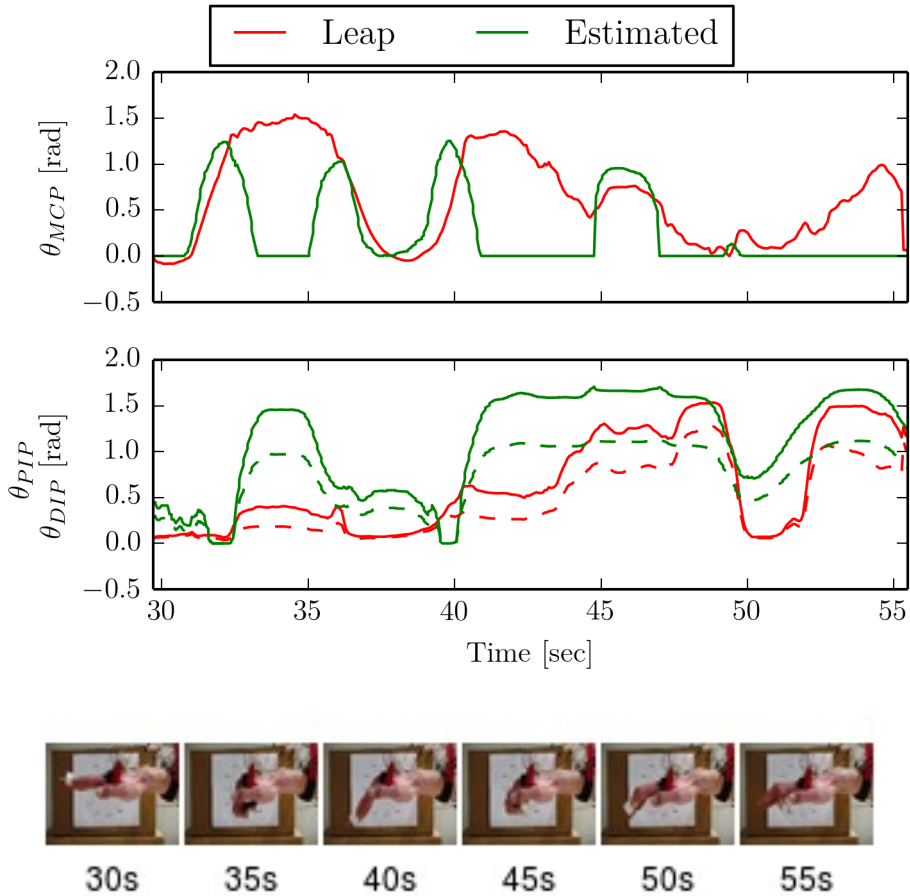


Figure 5.17: The estimated results for θ_{MCP} are often wrong, if a fist is performed. The results for θ_{PIP} and θ_{DIP} show more realistic values. As soon as the intermediate and distal phalanges get to close to the palmar side, the angle of MCP is estimated as 0 rad. The visualized sequence of set 5 includes two fist motions, each performed a bit different concerning speed and process. It can be stated, that a fist cannot be detected reliably, due to unsatisfied evaluations of the minimization procedure.

the Leap system, also a slight inaccuracy in the state representation can be observed. The angles for the PIP and DIP joints are represented for each fist quite differently. At the first time, very small values are returned. The second fist movement however shows much higher values. As said, the movements were performed a bit different each time, but the differences were definitely not as high as returned by the Leap Motion. As beforehand mentioned, the occlusion of the distal bones is responsible for that. At the first bending to a fist, the bones were probably detected not as good as for the second performed motion.

The errors, induced by this characteristic behaviour of the magnetic system cause the main differences, compared to the almost perfect states of the Leap System. So the determination and the positioning of the sensor and hand dimensions is

one of the most important parts for describing the system. The good results for set 4 can somehow be seen as a lucky coincidence, where the parameters suited best. As described section 5.4, the estimation of the hand dimension did not lead to reasonable results. For the presented datasets for estimating one finger state vector by up to four sensor units, the hand dimensions are defined by the three bone lengths, the 3D joint position and the four three dimensional sensor positions. Therefore 18 values have to be measured by hand and can introduce nonlinear errors to the underlying hand dimensions. The obtained estimation results show, that the compensation of those erroneous hand model parameters by a fitting gesture can lead to reasonable results under certain conditions.

5.6.2.3 Influence of Different System Parameters

In order to tune and improve the magnetic system for the estimation of finger poses, several methods were evaluated, based on the beforehand mentioned estimation results. As a very critical factor one can state the exact determination of the individual bone lengths, joint and sensor positions. Since those parameters are given into the equations, to represent the actual human hand, they are used by the solver, to estimate and reconstruct the measured magnetic flux densities. They are plugged in as static values and therefore have a constant nonlinear contribution to the estimated observable magnetic values.

The hand dimensions are measured with a calliper. As introduced in section 4.2, the finger joints are assumed to have a static rotation point and the relative distance to each other is also static. Every time before measurements were recorded, the distances from the sensors to the joints are measured. Here the sensor rack is a big plus in position determination, since the locations of the sensors relative to each other are predetermined and exactly known. Furthermore, the bone lengths are measured by hand. In the end 12 bone sizes (3 for each finger), four 3D joint (one for each finger) and four 3D sensor positions (one for each sensor) have to be measured. This whole determination process is very error prone. For trying to compensate those false measured values, the initialization gesture to determine the scaling factors is introduced. By applying them to each sensor measurement one can only push the observed values into the direction of the expected results by the model. The single flexion of the MCP joint was evaluated to serve as a repeatable motion. Also the pose of a fist was evaluated, whether it would suit the need better, since it also includes movements of the PIP and DIP. Figure 5.18 shows, that this is not the case. The observed magnetic fields by the sensor beneath the index finger, for a magnet located at the tip of it are displayed. The single flexion-extension of the MCP is performed two times during 3 s and 11 s. Afterwards the finger is bended to a fist two times. From the first closed state, the motion to the straight position is performed slowly.

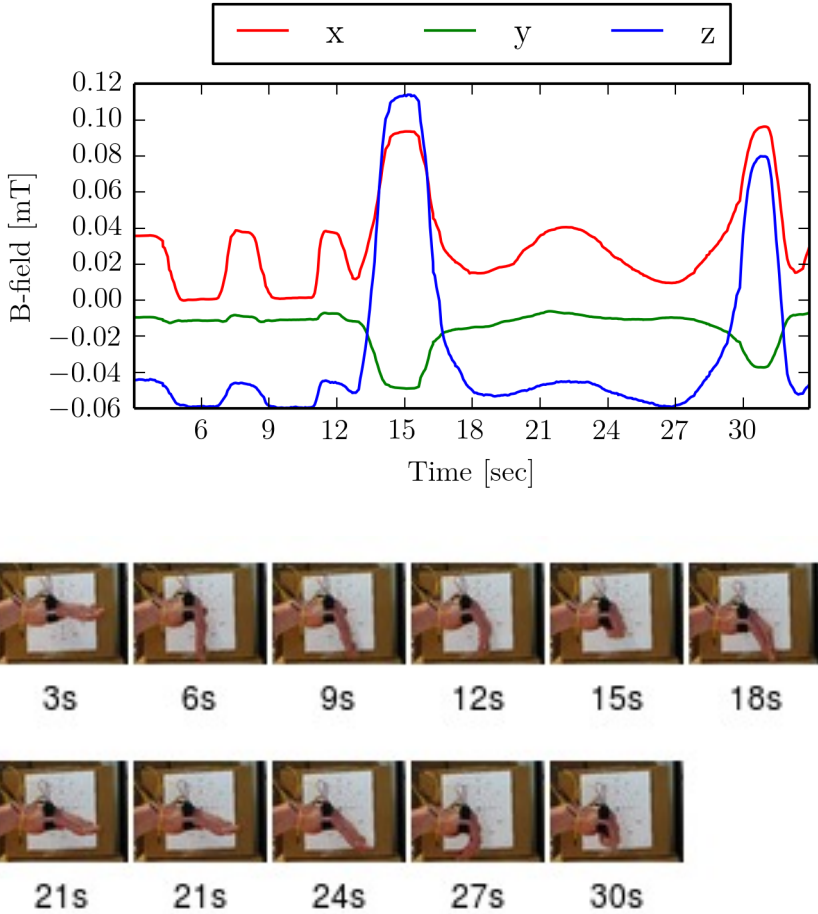


Figure 5.18: Sequence, showing the measured magnetic flux densities while performing two different initialization gestures. The named sensor is located beneath the index finger and the magnet is on that tip. During 3 s and 11 s only θ_{MCP} is moved. The remaining sequence shows the performance of closing and opening the fingers to a fist. While the first gesture leads to repeatable results, the second don't.

By the development of the measured magnetic flux densities, it can be seen, that the single motion of the MCP leads to more repeatable values, than the performance of a fist. The measurements obtained for the latter motion are highly dependent on the strength and manner of the end position. The first fist gesture shows much higher changes for the values, than the second one. Therefore the intensity of the closed hand is stronger. By looking at the simpler gesture, the two performed motion sequences look pretty much the same. Therefore the fist as initialization gesture is discarded. Like introduced in section 5.4 it was evaluated whether the performance along a rectangular, non-magnetic object, like a cardboard, would improve this initialization process. Therefore this gesture was performed along a cardboard before some datasets. It turned out, that the quality of the results did not increase or got

even worse, by this more standardised fitting. The movement along the box and the subsequently aside putting introduces additional movements to the system. Therefore the pose of the hand changed during the calibration and the actual recording. This is critical, since the influence of the surrounding magnetic field changes due to that. Moreover, the process is performed directly over the Leap Motion controller. Since it is a vision based system, it adjusts its cameras to the surrounding light conditions. The cardboard covers the surface totally and by putting it away, the cameras have to refocus. It turned out, that if the Leap should detect a hand directly at this rescaling phase, the results are very bad or the hand even does not get detected at all. So in the end the best way for compensating the errors, induced by the hand dimensions, a gesture of single flexion-extension of MCP has to be performed during the measurements.

Some of the recorded sets were also evaluated with slightly different dimensional parameters. However, no mentionable change in the results for the estimation could be observed. For estimating only a single finger by using four sensor units, the hand dimension comprises already 18 values. As presented in section 5.4, tuning the measured dimensional parameters by trial and error is no option. Also the estimation of those parameters was evaluated and lead to implausible results, due to the high number of variables.

As another approach, the influence of the distance from the sensors to the magnets was evaluated. For the presented datasets, the sensors were located at the back of the hand at around 2 cm beneath the joints. From there the corresponding bone lengths contributed, such that in full flexion, a maximum distance of around 12 cm was established between sensors and magnets. A few recordings were done, by placing the sensor rack at the wrist. This leads to a maximal sensor to magnet distance of around 17 cm. The measurable magnetic flux densities at this position, excited by the magnets at the fingertips were very low. Since the earth magnetic field cannot be eliminated reliably enough, even small motions of the hand induce errors here. The estimation results were reasonably bad.

As one critical influence factor, the earth magnetic field is determined. However, the approach presented in subsection 4.4.2 to overcome this showed non-satisfiable results (see subsection 5.2.2). To also verify this with the whole system, some experiments where executed, with different hand positions. The motions were recorded, with the hand facing different axes. This means, that the hand is also facing different orientations, compared to the Leap Controller, such as upward or downward, sideways or with the back to the camera. The results from the Leap suffered from inconsistencies, caused by occlusion of fingers or the wrist. The magnetic system, only showed reasonable results if the hand was oriented in the initial position.

A further analysis of the sensor data acquisition rate was also evaluated. Since the system frequency for acquiring magnetic readings from all four sensors is evaluated to be 20 Hz, the sensor readings, which are actually sampled with 50 Hz are not very representable. Therefore the sampling frequency of the sensors was set at 25 Hz, to try to align the sensor and system frequency. However, after evaluation, the

estimation results, based on the sensor data, acquired with the lower sampling rate showed the same quality as set with the higher sensor rate. Therefore, to gain the maximum possible system frequency, the sensor data rate should be put to 50 Hz

5.6.2.4 Concluding Observations

Based on the presented results from the experiments, one could state that the system is dependent on a lot of variables. It can be stated, that the presented approach in combination with the utilized system cannot lead to constant and reliable results for hand pose reconstruction. In comparison to an existing camera based system, which in turn is not free of errors, the states of one finger could only be estimated with an accuracy of up to $0.467 \text{ rad} (=26.757^\circ)$. This high difference is induced among others by not accurate determinable anatomic dimensions. The utilized hand model simplifies the natural human behaviour and constraints the range of motion in a reasonable way. However, on the real human hand, the position parameters, which are critical for the utilized model, can only be determined by hand with a caliper. Trying to reproduce the actual measurements by the hand model with error-prone position information leads to a bad model description and therefore to unsatisfying estimation results. Furthermore, the utilized models for describing the magnetic field of an artificial magnet with a certain position and orientation does not comprise the surrounding magnetic field. However, the earth field has a permanent influence on the measurements, dependent on the actual orientation, and cannot be eliminated through the presented approach. Therefore the mobility of the finger pose estimation system is highly restricted. It has to be noted, that the measurable magnetic flux density, induced by a single magnet on the fingertip, excites a field, only slightly higher, than the disturbing environment. It is evaluated, that the cylindrical bar model leads better results, than the description of the objective function with the dipole model. A fitting gesture is proposed to reduce the influence of the error-prone position and surrounding distortion factors from the measurement system. A flexion-extension about 90° of the MCP joint is evaluated to be a reconstructible gesture for this. In the end reasonable results for the prediction where only achieved by movements, which are similar to this introduced gesture. Concerning the general solvability of the optimization problem, one can state that the system has to be overdetermined. This means that the number N of sensors, taken into account for the estimation has to be higher than the desired finger state vectors K .

6 Conclusion and Future Work

A magnetic sensor system for hand pose reconstruction is designed and evaluated. Since the objective was to develop a mobile and unobtrusive system, four sensors are used. They are mounted into a rack which can be worn at the back of the hand. The overall frequency for acquiring the most recent measurements of all four sensor units is evaluated to be 20 Hz. The calibration for hard and soft iron distortion factors of the sensors is implemented via a fit over a dataset of 1000 measurements. To estimate the finger states, static magnets are mounted onto the fingertips with a ring aperture. The induced magnetic fields are used, to estimate the angles of flexion-extension and adduction-abduction for each finger joint. For describing the magnetic flux density, induced by the utilized bar magnets, two different models for the description of the magnetic field lines were established. The cylindrical bar magnet model lead to better results, since it is the more accurate description for utilized permanent magnets.

To represent the human hand, a kinematic chain with 12 DOF is chosen, in order to represent the pose of the index, middle, ring and pinky finger. The movement of the thumb is left out. The introduced kinematic model is constraint to natural ranges of movement and can in the end describe the pose of one finger by three angular values. Those are the angles of flexion-extension and adduction-abduction of the MCP and the flexion-extension angle for the PIP joint. Via an introduced intra finger constraint, the angle of the DIP joint is derived via the PIP angle. In the end, by knowing the dimensions of the bone lengths and the positions of the joints and sensors, the distance and orientation of the fingertip (and therefore of the magnet) can be calculated relative to the sensor unit. Those distance and orientation vectors \vec{r} and \vec{h} can be plugged into the magnetic models, to estimate the cumulative measurement at the sensor units.

An optimization problem is formulated, which reduces the error between model and sensor measurement, by minimizing for the finger state angles. In this way the actual states for each finger can be estimated. By using a certain number of sensors to predict the position of the four fingers, it is evaluated, that the system has to be overdetermined. Therefore, the results for estimating all four magnets with the deployed four sensor units does not lead to reasonable results. Furthermore, it can be stated, that the problem has to be constrained and that the slight lateral movements of the MCP joint can be reconstructed.

For an evaluation of the system performance, the estimated finger states were compared to the vision based Leap Motion system. Reasonable results could only be reached for the prediction of a single finger state vector. The estimated states show

a non static difference to the Leap system for most of the measurement sets. For the evaluated recorded sets, the overall smallest difference to the Leap Motion was observed to be $0.467\text{rad} \pm 0.027$ ($=26.757^\circ \pm 1.547$), for predicting the states of the index finger with the measurements of two magnetic sensor units. This high deviation is due to the following drawbacks, the magnetic system suffers from:

- The parameters of the underlying hand model can not be measured accurate enough. This causes nonlinear errors for the predictable magnetic flux densities. This is tried to be compensated by introducing a fitting gesture.
- The surrounding magnetic field can not be eliminated dynamically. This is critical, since the observable magnetic field, induced by the static magnets is in the range of the earth magnetic field.
- The hand, trying to be tracked has to be held calm during the measurements.
- The achievable acquisition frequency for four sensor units is only capable of slow finger motions

In the end it can be stated, that the presented approach can be used to track finger poses reliably and dynamically under the named conditions. The detection of several movements and finger gestures can be distinguished and identified. The exact determination of the actual human hand parameters is critical for achieving good estimation results. Therefore, for future work on this concept, the exact determination of the anatomic hand dimensions could be further investigated. Additionally, the dynamic and reliable cancellation of the surrounding magnetic field would be important to remove the influence of the external magnets from the measurements. It is shown, that the determinateness of the system plays an important role for the estimation accuracy. Hence, designing a still wearable system by deploying more sensors could also be evaluated in the future. As another point, the overall acquisition frequency could be improved, to also being capable of faster finger movements. Moreover, it can be evaluated whether an approach, based on a learned set of motions would lead to better results for reconstructing finger postures.

Bibliography

- [201a] 2010, Northern Digital I.: *Optrak Certus Brochure*. http://www.ndigital.com/msci/wp-content/uploads/sites/11/2014/02/8300324_rev001_optotрак_Certus.pdf, . – Accessed: 2016-01-04
- [201b] 2010, Northern Digital I.: *The wave tracking system Company Brochure*. http://www.ndigital.com/msci/wp-content/uploads/sites/11/2014/02/Wave_4page_Brochure_Nov2010_email.pdf, . – Accessed: 2016-01-04
- [Ant] ANTHROTRONIX, Inc.: *Anthrotronix, Human Machine Interfaces*. <http://www.anthrotronix.com/our-work/human-machine-interfaces>, . – Accessed: 2016-01-06
- [BBD12] BULLOCK, Ian M. ; BORRÀS, Júlia ; DOLLAR, Aaron M.: Assessing assumptions in kinematic hand models: a review. In: *Biomedical Robotics and Biomechatronics (BioRob), 2012 4th IEEE RAS & EMBS International Conference on* IEEE, 2012, S. 139–146
- [BBPB02] BOUZIT, Mourad ; BURDEA, Grigore ; POPESCU, George ; BOIAN, Rares: The Rutgers Master II-new design force-feedback glove. In: *Mechatronics, IEEE/ASME Transactions on* 7 (2002), Nr. 2, S. 256–263
- [BGT12] BOYD, Jeffrey E. ; GODBOUT, Andrew ; THORNTON, Chris: In Situ Motion Capture of Speed Skating: Escaping the Treadmill. In: *Computer and Robot Vision (CRV), 2012 Ninth Conference on* IEEE, 2012, S. 460–467
- [Ble94] BLENDER, Foundation: *Blender*. <https://www.blender.org/>, 1994
- [Bul65] BULIRSCH, Roland: Numerical calculation of elliptic integrals and elliptic functions. In: *Numerische Mathematik* 7 (1965), Nr. 1, S. 78–90
- [BWCL01] BOWMAN, Doug ; WINGRAVE, Chadwick ; CAMPBELL, Joshua ; LY, Vinh: Using pinch gloves (tm) for both natural and abstract interaction techniques in virtual environments. (2001)
- [Cha] CHANG, Hilliges Kim: *Intuitive UIs Featured During UIST 2012*. <http://research.microsoft.com/en-us/news/features/uist2012-100812.aspx>, . – Accessed: 2016-01-02

- [CS13] CAMACHO, JM ; SOSA, V: Alternative method to calculate the magnetic field of permanent magnets with azimuthal symmetry. In: *EDUCATION* 59 (2013), Nr. 2013, S. 8–17
- [DO10] DERBY, Norman ; OLBERT, Stanislaw: Cylindrical magnets and ideal solenoids. In: *American Journal of Physics* 78 (2010), Nr. 3, S. 229–235
- [DSD08] DIPIETRO, Laura ; SABATINI, Angelo M. ; DARIO, Paolo: A survey of glove-based systems and their applications. In: *Systems, Man, and Cybernetics, Part C: Applications and Reviews, IEEE Transactions on* 38 (2008), Nr. 4, S. 461–482
- [DSW07] DURFEE, William K. ; SAVARD, Lynda ; WEINSTEIN, Samantha: Technical feasibility of teleassessments for rehabilitation. In: *Neural Systems and Rehabilitation Engineering, IEEE Transactions on* 15 (2007), Nr. 1, S. 23–29
- [EK05] EKVALL, Staffan ; KRAGIĆ, Danica: Grasp recognition for programming by demonstration. In: *Robotics and Automation, 2005. ICRA 2005. Proceedings of the 2005 IEEE International Conference on* IEEE, 2005, S. 748–753
- [FH93] FELS, S S. ; HINTON, Geoffrey E.: Glove-talk: A neural network interface between a data-glove and a speech synthesizer. In: *Neural Networks, IEEE Transactions on* 4 (1993), Nr. 1, S. 2–8
- [Fif] *Fifth Dimension Technologies - 5DT.* <http://www.5dt.com/products/pdataglove14.html>, . – Accessed: 2016-01-03
- [FP91a] FOUNDATION PYTHON software: *Python programming language.* <https://www.python.org/>, 1991
- [FP91b] FOUNDATION PYTHON software: *SciPy programming language.* <https://www.scipy.org/>, 1991
- [Glo16] *Gloreha, Italy.* <http://www.gloreha.com>, 2016. – Accessed: 2016-01-03
- [Gre96] GREENLEAF, Walter J.: Developing the tools for practical VR applications [Medicine]. In: *Engineering in Medicine and Biology Magazine, IEEE* 15 (1996), Nr. 2, S. 23–30
- [HKW⁺07] HEUSER, Andrew ; KOURTEV, Hristian ; WINTER, Scott ; FENSTERHEIM, Devin ; BURDEA, Grigore ; HENTZ, Vincent ; FORDUCEY, Pamela: Telerehabilitation using the Rutgers Master II glove following carpal tunnel release surgery: proof-of-concept. In: *Neural Systems and Rehabilitation Engineering, IEEE Transactions on* 15 (2007), Nr. 1, S. 43–49
- [HTHK14] HUANG, Jiawei ; TAKASHIMA, Kazuki ; HASHI, Shuichiro ; KITAMURA, Yoshifumi: IM3D: magnetic motion tracking system for dexterous 3D interactions. In: *ACM SIGGRAPH 2014 Emerging Technologies* ACM, 2014, S. 12

- [HTY⁺06] HASHI, Shuichiro ; TOYODA, Masaharu ; YABUKAMI, Shin ; ISHIYAMA, Kazushi ; OKAZAKI, Yasuo ; ARAI, Ken I.: Wireless magnetic motion capture system for multi-marker detection. In: *Magnetics, IEEE Transactions on* 42 (2006), Nr. 10, S. 3279–3281
- [ICLB05] IONESCU, Bogdan ; COQUIN, Didier ; LAMBERT, Patrick ; BUZULOIU, Vasile: Dynamic hand gesture recognition using the skeleton of the hand. In: *EURASIP Journal on Applied Signal Processing* 2005 (2005), S. 2101–2109
- [IKHW08] INGRAM, James N. ; KÖRDING, Konrad P. ; HOWARD, Ian S. ; WOLPERT, Daniel M.: The statistics of natural hand movements. In: *Experimental brain research* 188 (2008), Nr. 2, S. 223–236
- [Inv14] INVENSENSE INC. (Hrsg.): *MPU-9250 Product Specification*. 1. San Jose, California: InvenSense Inc., 1 2014. (Rev 1)
- [KHS⁺12] KOK, Manon ; HOL, Jeroen ; SCHÖN, Thomas B. ; GUSTAFSSON, Fredrik ; LUINGE, Henk: Calibration of a magnetometer in combination with inertial sensors. In: *Information Fusion (FUSION), 2012 15th International Conference on IEEE*, 2012, S. 787–793
- [KMA08] KIM, Jonghwa ; MASTNIK, Stephan ; ANDRÉ, Elisabeth: EMG-based hand gesture recognition for realtime biosignal interfacing. In: *Proceedings of the 13th international conference on Intelligent user interfaces* ACM, 2008, S. 30–39
- [Kon] KONVALIN, Christopher: *Motion/Velocity/Displacement Compensating for Tilt, Hard-Iron, and Soft-Iron Effects*. Sensors Online,
- [KSRV14] KORTIER, Henk G. ; SLUITER, Victor I. ; ROETENBERG, Daniel ; VELTINK, Peter H.: Assessment of hand kinematics using inertial and magnetic sensors. In: *Journal of neuroengineering and rehabilitation* 11 (2014), Nr. 1, S. 70
- [LLC] LLC, Arduino: *Arduino*. <https://www.arduino.cc/>, . – Accessed: 2016-02-07
- [LM] LEAP MOTION, Inc: *Leap Motion web presence*. <https://www.leapmotion.com/>, . – Accessed: 2016-01-04
- [LWH00] LIN, John ; WU, Ying ; HUANG, Thomas S.: Modeling the constraints of human hand motion. In: *Human Motion, 2000. Proceedings. Workshop on IEEE*, 2000, S. 121–126
- [MA⁺01] MASCARO, Stephen ; ASADA, H H. u. a.: Photoplethysmograph finger-nail sensors for measuring finger forces without haptic obstruction. In: *Robotics and Automation, IEEE Transactions on* 17 (2001), Nr. 5, S. 698–708

- [MA09] MLAĐENOVIC, Ana N. ; ALEKSIC, Slavoljub R.: Magnetic field calculation of permanent magnet. In: *International Scientific Colloquium*, 2009
- [Mad10] MADGWICK, Sebastian O.: An efficient orientation filter for inertial and inertial/magnetic sensor arrays. In: *Report x-io and University of Bristol (UK)* (2010)
- [mik] MIKESHUB, Github user: *Implementation of Madgwick filter for Pololu MinIMU-9 v3.* https://github.com/mikeshub/Pololu_Open_IMU/blob/master/Pololu_Open_IMU/Pololu_Open_IMU.ino, . – Accessed: 2016-02-12
- [MJL⁺10] MA, Yanru ; JIA, Weihua ; LI, Cong ; YANG, Jian ; MAO, Zhi-Hong ; SUN, M: Magnetic hand motion tracking system for human-machine interaction. In: *Electronics letters* 46 (2010), Nr. 9, S. 621–623
- [MK02] MEHDI, Syed A. ; KHAN, Yasir N.: Sign language recognition using sensor gloves. In: *Neural Information Processing, 2002. ICONIP'02. Proceedings of the 9th International Conference on* Bd. 5 IEEE, 2002, S. 2204–2206
- [MMJ⁺11] MA, Yinghong ; MAO, Zhi-Hong ; JIA, Wenyan ; LI, Chengliu ; YANG, Jiawei ; SUN, Mingui: Magnetic hand tracking for human-computer interface. In: *Magnetics, IEEE Transactions on* 47 (2011), Nr. 5, S. 970–973
- [MNC⁺08] METCALF, Cheryl D. ; NOTLEY, Scott V. ; CHAPPELL, Paul H. ; BURRIDGE, Jane H. ; YULE, Victoria T.: Validation and application of a computational model for wrist and hand movements using surface markers. In: *Biomedical Engineering, IEEE Transactions on* 55 (2008), Nr. 3, S. 1199–1210
- [MRM⁺13] METCALF, Cheryl D. ; ROBINSON, Ricky ; MALPASS, Adam J. ; BOGLE, Tristan P. ; DELL, Thomas ; HARRIS, Colin ; DEMAIN, Sara H. u.a.: Markerless motion capture and measurement of hand kinematics: validation and application to home-based upper limb rehabilitation. In: *Biomedical Engineering, IEEE Transactions on* 60 (2013), Nr. 8, S. 2184–2192
- [NW06] NOCEDAL, Jorge ; WRIGHT, Stephen: *Numerical optimization*. Springer Science & Business Media, 2006
- [OSA⁺13] O'FLYNN, Brendan ; SANCHEZ, Javier T. ; ANGOVE, Philip ; CONNOLLY, James ; CONDELL, Joan ; CURRAN, Kevin ; GARDINER, Philip: Novel smart sensor glove for arthritis rehabilitation. In: *Body Sensor Networks (BSN), 2013 IEEE International Conference on* IEEE, 2013, S. 1–6
- [Ozy12] OZYAGCILAR, Talat: Calibrating an ecompass in the presence of hard and soft-iron interference. In: *Freescale Semiconductor Ltd* (2012)

- [PBBH00] POPESCU, Viorel G. ; BURDEA, Grigore C. ; BOUZIT, Mourad ; HENTZ, Vincent R.: A virtual-reality-based telerehabilitation system with force feedback. In: *Information Technology in Biomedicine, IEEE Transactions on* 4 (2000), Nr. 1, S. 45–51
- [PE] POLOLU, Robotics ; ELECTRONICS, Las Vegas U.: *MinIMU-9 v3 Gyro, Accelerometer, and Compass (L3GD20H and LSM303D Carrier)*, Product 2468. <https://www.pololu.com/product/2468>,
- [Pow64] POWELL, Michael J.: An efficient method for finding the minimum of a function of several variables without calculating derivatives. In: *The computer journal* 7 (1964), Nr. 2, S. 155–162
- [RB07] ROBERT BRADSHAW, et a. Stefan Behnel B. Stefan Behnel: *Cython: C-extensions for Python*. <https://www.scipy.org/>, 2007
- [RFd15] RFDIGITAL CORPORATION (Hrsg.): *BLE RF module RFD22301*. Hermosa Beach, California: RFdigital Corporation, 8 2015. (R25)
- [SAG⁺03] SU, Yu ; ALLEN, Charles R. ; GENG, David ; BURN, David ; BRECHANY, Una ; BELL, G D. ; ROWLAND, Roger: 3-D motion system ("data-gloves"): Application for Parkinson's disease. In: *Instrumentation and Measurement, IEEE Transactions on* 52 (2003), Nr. 3, S. 662–674
- [SBZ08] SUPUK, Tamara ; BAJD, Tadej ; ZANCHI, Vlasta: Evaluation of hand grasping by instrumented glove. In: *WSEAS Trans Syst Control* 3 (2008), Nr. January (1)
- [SKR⁺15] SHARP, Toby ; KESKIN, Cem ; ROBERTSON, Duncan ; TAYLOR, Jonathan ; SHOTTON, Jamie ; LEICHTER, David Kim Christoph Rheemann I. ; WEI, Alon Vinnikov Y. ; KRUPKA, Daniel Freedman Pushmeet Kohli E. ; FITZGIBBON, Andrew ; IZADI, Shahram: Accurate, Robust, and Flexible Real-time Hand Tracking. In: *Proc. CHI* Bd. 8, 2015
- [SLU] SYNERTIAL LABS UK, US: *Synertial, Glove Systems overview*. <http://synertial.com/brochure-gloves>, . – Accessed: 2016-01-06
- [STM12] STMICROELECTRONICS N.V. (Hrsg.): *LSM303D - Ultra compact high performance e-Compass 3D accelerometer and 3D magnetometer module*. STMicroelectronics N.V., 4 2012. (Rev 1) . – ID 023312
- [Sys] SYSTEMS, Cyberglove: *Cybergrasp Brochure*. http://static1.squarespace.com/static/559c381ee4b0ff7423b6b6a4/t/5602fc01e4b07ebf58d480fb/1443036161782/CyberGrasp_Brochure.pdf, . – Accessed: 2016-01-04
- [SZ94] STURMAN, David J. ; ZELTZER, David: A survey of glove-based input. In: *Computer Graphics and Applications, IEEE* 14 (1994), Nr. 1, S. 30–39

- [Tex03] TEXAS INSTRUMENTS (Hrsg.): *CD74HC4067, CD74HCT4067 - High-Speed CMOS logic 16-Channel Analog Multiplexer/Demultiplexer*. Texas Instruments, 6 2003. (Rev 1)
- [VMSL] VICON MOTION SYSTEMS LTD., UK: *Vicon Vantage Brochure*. <http://www.vicon.com/file/finalvantagebrochure09112015.pdf>, . – Accessed: 2016-01-07
- [WBRF13] WEICHERT, Frank ; BACHMANN, Daniel ; RUDAK, Bartholomäus ; FISSELER, Denis: Analysis of the accuracy and robustness of the leap motion controller. In: *Sensors* 13 (2013), Nr. 5, S. 6380–6393
- [WKTA15] WILHELM, Mathias ; KRAKOWCZYK, Daniel ; TROLLMANN, Frank ; ALBAYRAK, Sahin: eRing: multiple finger gesture recognition with one ring using an electric field. In: *Proceedings of the 2nd international Workshop on Sensor-based Activity Recognition and Interaction ACM*, 2015, S. 7
- [WP09] WANG, Robert Y. ; POPOVIĆ, Jovan: Real-time hand-tracking with a color glove. In: *ACM Transactions on Graphics* 28 (2009), Nr. 3
- [WPC⁺00] WILLIAMS, NW ; PENROSE, JMT ; CADDY, CM ; BARNES, E ; HOSE, DR ; HARLEY, P: A goniometric glove for clinical hand assessment construction, calibration and validation. In: *Journal of Hand Surgery (British and European Volume)* 25 (2000), Nr. 2, S. 200–207
- [YAD13] YUN, Youngmok ; AGARWAL, Prabhakar ; DESHPANDE, Ashish D.: Accurate, robust, and real-time estimation of finger pose with a motion capture system. In: *Intelligent Robots and Systems (IROS), 2013 IEEE/RSJ International Conference on IEEE*, 2013, S. 1626–1631
- [ZCL⁺11] ZHANG, Xu ; CHEN, Xiang ; LI, Yun ; LANTZ, Vuokko ; WANG, Kongqiao ; YANG, Jihai: A framework for hand gesture recognition based on accelerometer and EMG sensors. In: *Systems, Man and Cybernetics, Part A: Systems and Humans, IEEE Transactions on* 41 (2011), Nr. 6, S. 1064–1076
- [ZEI⁺07] ZECCA, Massimiliano ; ENDO, Nobutsuna ; ITOH, Kazuko ; IMANISHI, Kazutaka ; SAITO, Minoru ; NANBA, Nobuhiro ; TAKANOBU, Hideaki ; TAKANISHI, Atsuo: On the development of the bioinstrumentation system WB-1R for the evaluation of human-robot interaction-Head and hands motion capture systems. In: *Advanced intelligent mechatronics, 2007 IEEE/ASME international conference on IEEE*, 2007, S. 1–6
- [Zha12] ZHANG, Zhengyou: Microsoft kinect sensor and its effect. In: *MultiMedia, IEEE* 19 (2012), Nr. 2, S. 4–10
- [Zim85] ZIMMERMAN, Thomas G.: *Optical flex sensor*. September 17 1985. – US Patent 4,542,291